SUOMEN GEODEETTISEN LAITOKSEN JULKAISUJA
VERÖFFENTLICHUNGEN DES FINNISCHEN GEODÄTISCHEN INSTITUTES
PUBLICATIONS OF THE FINNISH GEODETIC INSTITUTE
N:o 140

CALIBRATING DIGITAL PHOTOGRAMMETRIC AIRBORNE IMAGING SYSTEMS USING A TEST FIELD

by

Eija Honkavaara

Dissertation for the degree of Doctor of Science in Technology to be presented with due permission of the Department of Surveying, for public examination and debate in Auditorium M1 at Helsinki University of Technology (Espoo, Finland) on 17th of June, 2008, at 12 o'clock noon.

KIRKKONUMMI 2008

Academic Dissertation in Photogrammetry
Department of Surveying, Helsinki University of Technology

Supervisor

Professor Henrik Haggrén,
Department of Surveying, Helsinki University of Technology

Instructors

Professor Juha Hyyppä
Department of Remote Sensing and Photogrammetry, Finnish Geodetic Institute

Professor Risto Kuittinen
Finnish Geodetic Institute

Dr. Jouni Peltoniemi
Department of Remote Sensing and Photogrammetry, Finnish Geodetic Institute

Pre-examiners

Dr. Michael Cramer
Institute for Photogrammetry, University of Stuttgart

Professor Petri Pellikka
Department of Geography, University of Helsinki

Opponents

PhD Ismael Colomina
Institute of Geomatics, Spain

Professor Petri Pellikka
Department of Geography, University of Helsinki

ISBN: 978-951-711-275-8 (paperback)
ISBN: 978-951-711-276-5 (PDF)
ISSN: 0085-6932

Abstract

Airborne photogrammetry is a fundamental technique for producing reliable, geometrically accurate, high-resolution geospatial information. Passive and active digital imaging is rapidly replacing film imaging in photogrammetric data capture. Optimal use of this new technology enables fast data capture, high accuracy, a high level of automation, and a huge increase in applications.

The reliability, accuracy, and efficiency of airborne photogrammetry are based on calibrated, high-quality sensors and rigorous processing. The calibration processes of the digital photogrammetric airborne imaging systems are under development. Central challenges in the development of the calibration are the extensive variation in digital systems, the need for radiometric calibration, and the necessity for accurate system calibration. Test field calibration is a potential approach for determining the system calibration.

The hypothesis of this study was that system calibration in a test field is necessary for digital photogrammetric airborne imaging systems and that the calibration should involve geometry, spatial resolution, and radiometry. The hypothesis was proven by developing a methodology for the system calibration in a test field and by empirically investigating the need for and feasibility of the system calibration. In the empirical study, data sets from three first-generation commercial digital photogrammetric large-format sensors, Leica Geosystems ADS40, Intergraph DMC, and Microsoft UltraCamD, were used. Theoretical evaluations were performed together with the empirical evaluations.

The Finnish Geodetic Institute's permanent test field in Sjökulla, augmented with some portable targets, is a prototype photogrammetric test field. The results proved that the construction of a test field for geometric, spatial resolution, and radiometric calibration was feasible. A permanent test field can be an efficient, highly automated, and reliable tool for system calibration.

The empirical evaluation showed the great geometric and radiometric potential of the systems, but it also revealed problems. The laboratory calibration of the evaluated systems was either insufficient or invalid in airborne conditions. The test field calibration was necessary to provide the missing or invalid parameters and to assess the measurement capability of the systems. The results also showed that calibration of the systems in a test field was feasible. It appeared that in order to obtain the utmost accuracy, the calibration process of the evaluated systems should include the laboratory, test field, and self-calibration. A product level validation of geometric accuracy also appeared to be necessary to ensure the highest reliability.

This was the first study to model and demonstrate the simultaneous geometric, spatial resolution, and radiometric test field calibration for digital photogrammetric airborne imaging systems. The study had several results: it proved the need for and feasibility of test field calibration and presented new empirical results concerning system performance and test field calibration; it provided recommendations for the calibration process of the systems and for the construction of photogrammetric test fields; and it identified many additional research topics.

Keywords: *Accuracy, airborne, bias, calibration, digital photogrammetric sensor, empirical, geometry, MTF, photogrammetric test field, precision, PSF, radiometry, spatial resolution*

Tiivistelmä

Ilmakuvafotogrammetria on keskeinen menetelmä luotettavan, geometrisesti tarkan ja suuriresoluutioisen tiedon tuottamiseksi elinympäristöstämme. Passiiviset ja aktiiviset digitaaliset kuvausmenetelmät ovat korvaamassa filmikuvauksen fotogrammetrisessa tiedonkeruussa. Optimaalisesti hyödynnettynä uusi tekniikka mahdollistaa nopean tiedonkeruun, suuren tarkkuuden, korkean automaatiotason sekä uudet sovellutukset.

Ilmakuvafotogrammetrian tarkkuus, luotettavuus ja tehokkuus perustuvat korkealaatuisiin, kalibroituihin laitteisiin sekä tarkkaan prosessointiin. Fotogrammetriset prosessit ja kalibrointimenetelmät tulee ajantasaistaa, jotta uutta tekniikkaa voitaisiin optimaalisesti hyödyntää. Kalibrointimenetelmien kehittämisen keskeisiä haasteita ovat kuvauslaitteiden monimuotoisuus, radiometrisen kalibroinnin tarve sekä tarkan systeemikalibroinnin tarve. Testikenttäkalibrointi on potentiaalinen menetelmä systeemikalibroinnin määrittämiseksi.

Tutkimuksen hypoteesi oli, että digitaalisille ilmakuvausjärjestelmille on tarpeen suorittaa systeemikalibrointi testikentällä ja että testikenttäkalibrointiin tulee sisältyä geometrinen, radiometrinen ja spatiaalisen erotuskyvyn kalibrointi. Hypoteesi todistettiin kokeellisesti kehittämällä prototyyppimenetelmä testikenttäkalibrointiin sekä tutkimalla testikenttäkalibroinnin tarvetta ja toteuttamiskelpoisuutta käyttäen testikentällä kerättyjä kuva-aineistoja. Tutkimuksessa käytettiin ensimmäisen sukupolven kaupallisia laajaformaattisia digitaalisia ilmakuvaussensoreita Leica Geosystems ADS40, Intergraph DMC ja Microsoft UltraCamD.

Geodeettisen laitoksen vuonna 1994 perustama Sjökullan pysyvä fotogrammetrinen testikenttä täydennettynä tarpeellisilla siirrettävillä kohteilla on fotogrammetrisen testikentän prototyyppi. Tutkimus todisti geometriseen, radiometriseen ja spatiaalisen resoluution kalibrointiin soveltuvan fotogrammetrisen testikentän toteuttamiskelpoisuuden. Pysyvän testikentän käyttö mahdollistaa tehokkaan, pitkälle automatisoidun ja luotettavan systeemikalibroinnin määrityksen.

Kokeellinen tutkimus osoitti järjestelmien erinomaisen geometrisen ja radiometrisen potentiaalin, mutta myös paljasti puutteita. Laitteiden kalibrointi oli joko pätemätön tai puutteellinen kuvausolosuhteissa. Testikenttäkalibrointi oli tarpeen pätemättömien tai puuttuvien sensorimallien määrittämiseksi sekä järjestelmien suorituskyvyn arvioimiseksi. Tutkimus myös näytti, että järjestelmien kalibrointi testikentällä oli toteuttamiskelpoista. Tulosten perusteella pääteltiin, että suurimman tarkkuuden saavuttamiseksi arvioitujen järjestelmien kalibrointiprosessiin tulisi kuulua kalibrointi laboratoriossa ja testikentällä sekä itsekalibrointi. Geometrisen tarkkuuden arviointi tuotetasolla osoittautui tarpeelliseksi luotettavuuden varmistamiseksi.

Tutkimus mallinsi ja demonstroi ensimmäistä kertaa digitaalisten fotogrammetristen järjestelmien samanaikaisen geometrisen, radiometrisen ja spatiaalisen erotuskyvyn kalibroinnin testikentällä. Tutkimuksella oli monia tuloksia: se todisti testikenttäkalibroinnin tarpeellisuuden ja toteuttamiskelpoisuuden, se antoi uutta tietoa ilmakuvausjärjestelmien ja testikenttäkalibroinnin suorituskyvystä, se tuotti suosituksia ilmakuvausjärjestelmien kalibrointiprosessille ja fotogrammetrisille testikentille sekä osoitti monia tärkeitä tutkimuskohteita.

Asiasanat: *Digitaalinen fotogrammetrinen sensori, fotogrammetrinen testikenttä, geometria, ilmakuva, kalibrointi, kokeellinen, MTF, PSF, radiometria, spatiaalinen erotuskyky, systemaattinen virhe, tarkkuus*

Acknowledgements

This study was carried out at the Finnish Geodetic Institute (FGI), in the Department of Remote Sensing and Photogrammetry. I would like to acknowledge Professor Risto Kuittinen, the Director General of the FGI, for his inspiration, advice, and unfailing support during my entire career. Professor Kuittinen first envisioned the Sjökulla test field; it was due to his farsightedness and persistence that the test field was built and is now maintained. My equally sincere gratitude goes to Professor Juha Hyyppä, who has continued Professor Kuittinen's work as the head of our department. I am grateful to Professor Hyyppä for encouraging me to write my thesis on this important topic and for his instruction and patience in the long months that were needed to finally complete this investigation. I am indebted to Dr. Jouni Peltoniemi as well, for his excellent guidance and the many instructive discussions we shared during this study.

I would like to express sincere gratitude to Professor Henrik Haggrén, the Helsinki University of Technology, Department of Surveying, for his supervision and continuous support during my studies and this project.

Dr. Michael Cramer, of the Institute for Photogrammetry, University of Stuttgart, and Professor Petri Pellikka, of the Department of Geography, University of Helsinki, reviewed this manuscript. I am grateful for their thorough review and many instructive comments that helped me to improve the manuscript.

Many persons from the Department of Remote Sensing and Photogrammetry have made this study possible. My respectful appreciation goes to Juha Jaakkola for his kind and wise guidance and co-operation that started on my first day at the FGI and continued for 15 years, until he retired a year ago. I am extremely grateful to Lauri Markelin for his fluent co-operation and assistance in many parts of this study. Acknowledgements also go to Eero Ahokas and Harri Kaartinen, who took care of the maintenance and building of the Sjökulla test field. I sincerely thank all the employees of the department for many pleasant moments at Sjökulla's annual maintenance parties and for their assistance in organizing the test flights for this study. Now it has been proven, our efforts have been of great importance. The story of Sjökulla continues…

Finally, I would like to thank all my FGI colleagues for their warm camaraderie and gracious working environment.

This study has been carried out in close co-operation with the Finnish photogrammetric industry. Their support in the form of research materials and practical comments has been important and unparalleled. My warmest thanks go to Heikki Luukkonen, Kyösti Laamanen, Pekka Savolainen, and Jan Biström from Blomkartta Oy (formerly FM-Kartta Oy), to Timo Sääski from Finnmap Oy, and to Juha Vilhomaa and Risto Ilves from the Aerial Image Center of the National Land Survey of Finland. This study could not have been conducted without their support. I hope that our co-operation will continue so that we will soon learn how to provide valuable quantitative information about our environment at an affordable price.

The Ministry of Agriculture and Forestry of Finland is acknowledged for their financial support.

My deepest gratitude goes to my dear family: my supportive and understanding husband Jere and our lovely children Iiris, Sakari, and Vuokko. The four of you make my life perfect.

Kirkkonummi, 11 May 2008

Eija Honkavaara

List of publications

The thesis is based on the following scientific papers, referred to in the text by their Roman numerals:

I

Honkavaara, E., J. Peltoniemi, E. Ahokas, R. Kuittinen, J. Hyyppä, J. Jaakkola, H. Kaartinen, L. Markelin, K. Nurminen, J. Suomalainen, 2008. A permanent test field for digital photogrammetric systems. *Photogrammetric Engineering & Remote Sensing*, 74(1): 95-106.

II

Honkavaara, E., E. Ahokas, J. Hyyppä, J. Jaakkola, H. Kaartinen, R. Kuittinen, L. Markelin, K. Nurminen, 2006. Geometric test field calibration of digital photogrammetric sensors. *ISPRS Journal of Photogrammetry & Remote Sensing*, Special Issue on Digital Photogrammetric Cameras, 60(6): 387-399.

III

Honkavaara, E., J. Jaakkola, L. Markelin, K. Nurminen, E. Ahokas, 2006. Theoretical and empirical evaluation of geometric performance of multi-head large format photogrammetric sensors. *International Archives of Photogrammetry, Remote Sensing and Spatial Information Sciences*, 36(A1), unpaginated CD-ROM, 6 pages.

IV

Honkavaara, E., J. Jaakkola, L. Markelin, S. Becker, 2006. Evaluation of resolving power and MTF of DMC. *International Archives of Photogrammetry, Remote Sensing and Spatial Information Sciences*, 36(A1), unpaginated CD-ROM, 6 pages.

V

Markelin, L., E. Honkavaara, J. Peltoniemi, E. Ahokas, R. Kuittinen, J. Hyyppä, J. Suomalainen, A. Kukko. Radiometric calibration and characterization of large-format digital photogrammetric sensors in a test field. *Photogrammetric Engineering & Remote Sensing*, in press.

I, **II**, and **V** are PEER reviewed journal articles, **III** and **IV** are PEER reviewed conference articles.

Author contribution

In Paper **I** I conducted and participated in the recent calibration method development and analysis and wrote the article. Peltoniemi supervised the BRF measurements and processed and analyzed the BRF data. Ahokas is one of the major builders and maintainers of the Sjökulla test field and he has participated in development of methods for testing of analog systems and for radiometric testing of digital systems. Kuittinen invented the Sjökulla test field and the gravel targets, and he has supervised the method development and analysis, particularly during the analog era. Hyyppä has supervised the test field and method development. Jaakkola is the author of the software for the spatial resolution measurement. Kaartinen has maintained and improved the Sjökulla test field. Markelin has performed BRF field measurements, developed methods for radiometric and spatial resolution testing, and performed radiometric analysis. Nurminen has investigated the geometric calibration of oblique images. Suomalainen has participated BRF field measurements.

In Paper **II** I designed the test flights, carried out a large portion of the block measurements, developed the methods, made the calculations, analyzed the results, and wrote the article. Jaakkola, Hyyppä, and Kuittinen supervised the investigation. Ahokas, Kaartien, Markelin, and Nurminen carried out the geodetic measurements and targeting of the ground control points. Markelin performed the image post-processing. Jaakkola provided some graphics.

In Paper **III** I designed the test flights, carried out a large portion of the block measurements, designed and carried out the major development work for the FGIAT software, developed the new methods, performed the calculations, analyzed the results, and wrote the article. Ahokas, Markelin, and Nurminen carried out the geodetic measurements and targeting of the ground control points. Markelin performed the image post-processing. Jaakkola and Markelin provided some graphics.

In Paper **IV** I designed the test flights, supervised the method development, analyzed the results, and wrote the article. Jaakkola created the RESOL software, performed resolution measurements, and participated in analysis of results. Markelin processed the image materials and participated in the development of the resolution measurement method. Becker developed methods for resolution measurement and enhancement.

I and Markelin did mostly the research in Paper **V**. I did major part of the literature research, designed the method on a general level (excluding goniometry), supervised the calculations, analyzed the results to a large extent, and wrote most of the text in the article. Markelin developed the details of the method, carried out the image post-processing and all image measurements, participated in the analysis of results and writing, and provided the tables and graphics. Peltoniemi corresponded the goniometry, and Peltoniemi, Suomalainen, Markelin, and Kukko carried out the field reflectance measurements and calculations. Ahokas participated in the method development in the beginning of the project. Ahokas, Hyyppä, and Kuittinen were supervisors in the study.

Table of contents

List of abbreviations

A/D	Analog-to-digital
AWAR	Area weighted average resolution
BRDF	Bidirectional reflectance distribution function
CIR	Color-infrared
DSNU	Dark signal non-uniformity
EuroSDR	European Spatial Data Research
FGI	Finnish Geodetic Institute
FMC	Forward motion compensation
FOV	Field of view
GCP	Ground control point
GIS	Geographic information system
GPS	Global positioning system
GSD	Ground sample distance
IMU	Inertial measurement unit
MTF	Modulation transfer function
NASA	National Aeronautics and Space Administration
NIR	Near-infrared
NIST	National Institute of Standards and Technology
PRNU	Photo response non-uniformity
PSF	Point spread function
R, G, B	red, green, blue
RMSE	Root-mean-square error
RP	Resolving power
SSC	Stennis Space Center
TDI	Time delay integration
USGS	U. S. Geological Survey
V & V	Verification and validation
3D	3-dimensional

List of symbols

x_0,y_0, c	Principal point and principal distance
$\hat{\sigma}_0$	Standard error of unit weight
σ_{PSF}	Standard deviation of a Gaussian point spread function

1 Introduction

Photogrammetry is defined as the art, science, and technology of obtaining reliable information about physical objects and the environment, through processes of recording, measuring, and interpreting images and patterns of electromagnetic radiant energy and other phenomena (Thompson and Gruner, 1980).

Airborne photogrammetry is a fundamental technique for providing reliable, geometrically accurate, high-resolution geospatial information. Passive and active digital imaging is taking over from conventional film imaging in photogrammetric data capture. New imaging sensors combined with state-of-the-art navigation techniques will make the data capture more efficient and improve the data quality. These advancements improve the automation potential and quality of the airborne photogrammetric applications, such as topographic mapping, orthophotography, digital surface modeling, 3D environmental modeling, forestry, agriculture, environmental research, climate change studies, and disaster management (Heier, 2001; Dold and Flint, 2007). New application areas with a huge growth potential are the Internet-based 3D virtual environments ("platforms") and personal navigation, for which the efficient production of up-to-date high-resolution photorealistic data is crucial (Dold and Flint, 2007; Google Earth, 2008; Microsoft VirtualEarth, 2008). In order to exploit the recent technical developments to optimum effect, thorough revision of the photogrammetric processes is necessary.

A photogrammetric process is a measurement process whose central sub-processes are image acquisition, referencing, and measurement and interpretation (Figure 1). The image acquisition process provides new image data. In the referencing process, the data are georeferenced (Section 2.4), radiometrically corrected (Section 2.6), and sometimes restored (Section 2.5); example outputs of the referencing process are orthophotos, stereomodels, image blocks, reflectance images, and multi- or hyper-spectral 3D point clouds. The image products are utilized in the measurement and interpretation process. The photogrammetric process interacts with the geographical information system (GIS) by utilizing GIS tools and information and by storing the process outputs in it (Wolf and Dewitt, 2000). The sub-processes are presented as overlapping in Figure 1 because they are not necessarily isolated.

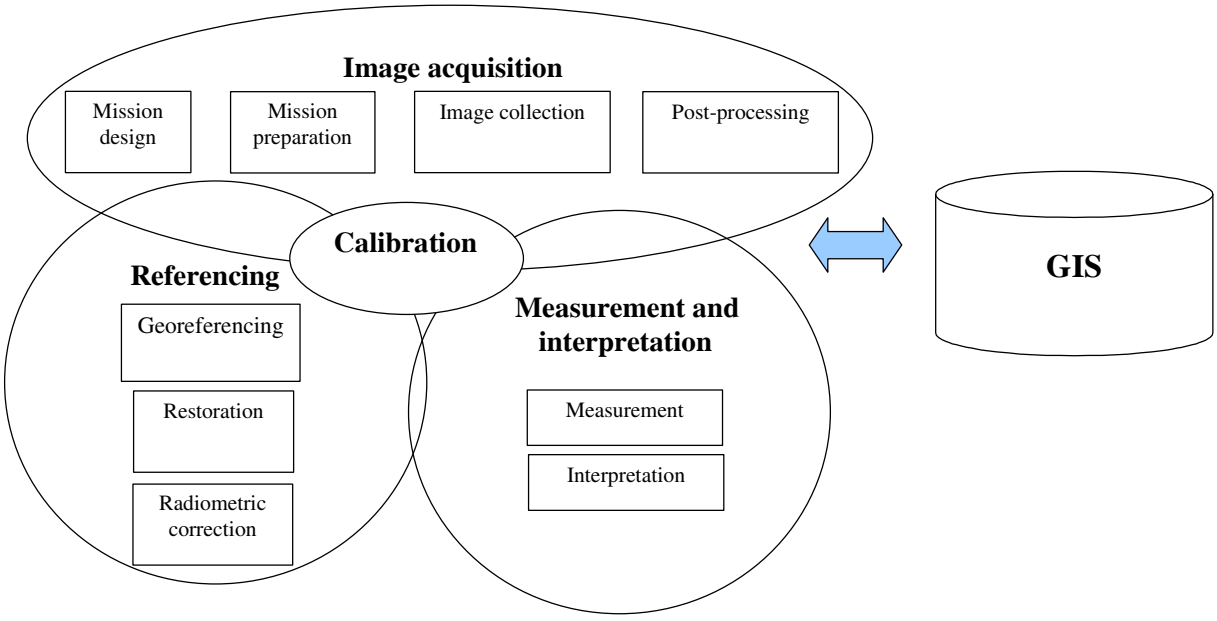

Figure 1. A photogrammetric process and its interaction with a calibration process.

Table 1. Central properties of passive electro-optical imaging systems.

Property	Options
Detector	CCD, CMOS
Image format	Rectangular array (small-, medium-, or large-format), line array
Imaging geometry	Frame, line (pushbroom), panoramic, point (whiskbroom)
Field of view	Narrow, intermediate, wide-angle, etc.
Spectral sensitivity	Monochromatic, color, color-infrared (CIR), thermal, multispectral (4-10 channels), and hyper-spectral (e.g. 200 or even more channels)
Radiometry	Linear, non-linear, calibrated, non-calibrated
Spatial resolution	Ground sample distance potential: cm, dm, and m-classes
Geometry	Metric, non-metric, calibrated, non-calibrated, accuracy potential: cm, dm, and m-classes
Integration	Multiple cameras to provide large-format images; Multiple cameras to provide different multispectral channels; Oblique and vertical cameras to provide different views of the object; Cameras and laser scanners; Imaging systems and GPS/IMU systems

The *digital photogrammetric airborne imaging system* can be defined either as an image acquisition system or as an image product generation system consisting of the image acquisition and referencing systems (Figure 1; Section 2.1). The central component of the imaging system is the imaging sensor. There is extensive variation in sensors that can be used in photogrammetric applications (Mikhail *et al.*, 2001; Petrie, 2003; 2005; 2006). This study emphasizes passive electro-optical imaging sensors, which record the energy emitted or reflected from the scene that originate from sources other than the sensor itself. The central properties of the passive sensors are given in Table 1. There is an increasing tendency to integrate several sensors into a single platform in order to improve functionality or performance in comparison to a single sensor (Hinz, 1997; Leberl and Gruber, 2003; Paparoditis *et al.*, 2006; Petrie, 2006). It is noteworthy that most of these sensor concepts have been available for a long time (e.g. Janza *et al.*, 1975; Slama *et al.*, 1980), but they have only recently begun to enter mainstream operational photogrammetric production. The selection of the imaging system for a certain application should be based on many criteria; in particular, on the quality requirements, cost, and operational issues. In conventional photogrammetric applications, such as topographic mapping, high geometric accuracy and large image format have been the central requirements; the major data providers have been national mapping agencies, military forces, and private mapping companies. It is expected that in the future an increasing number of data providers will supply imagery for the expanding area of photogrammetric applications using a wide variety of sensors.

To fulfil the reliability requirement and to obtain high efficiency, calibrated, high quality instruments and rigorous methods are used in the photogrammetry. *Calibration* is defined as a "process of quantitatively defining the system responses to known, controlled signal inputs" (Morain and Zanoni, 2004). In other words, the calibration determines, in certain conditions, the models and parameters that are needed to transform the system inputs to the outputs, as well as the accuracy of this transformation. The central models to be determined are the geometric (Section 2.4), radiometric (Section 2.6), spectral (Section 2.6), and spatial resolution models (Section 2.5). The four tasks of the digital photogrammetric airborne imaging system calibration are: 1) sensor component calibration (e.g. the lens or CCD), 2) sensor calibration, 3) image acquisition system calibration, and 4) image product generation system calibration. The first two tasks can be carried out in well-controlled conditions in a laboratory. The calibration of the image acquisition system and the image product generation system can only be performed under airborne conditions either using test fields or on a self-calibration basis, whereby the methods characterize the entire measurement system under operational conditions (*in*

situ). Test field and self-calibration concepts originate from geometric calibration (Section 2.4), but they can be generalized to cover spatial resolution and radiometry as follows. The *test field calibration* determines the system calibration using images collected over a *photogrammetric test field*, which is an area with characterized reference targets and measurement devices suitable for calibrating photogrammetric imaging systems (Section 2.7). *Self-calibration* does not require characterized reference targets, and it often determines the system calibration from the data of a certain mapping flight. Calibration can be a separate sub-process in the photogrammetric process, or it can be integrated in different sub-processes, as illustrated in Figure 1.

The calibration methods used for analog photogrammetric instruments (Section 2.4) are not sufficient for digital systems (ASPRS, 2000; Cramer, 2004; 2005; 2006; Stensaas, 2007). As described above, there is extensive variation in digital sensors, each requiring different calibration arrangements and parameters. Existing sensors are improved and new types of sensors enter the market continuously. There is great interest in using off-the-shelf sensors instead of specially constructed photogrammetric sensors. The need for radiometric and spectral calibration is a new issue in photogrammetric calibration. The integrated systems cannot typically be sufficiently calibrated in a laboratory. Furthermore, experience with analog systems indicates that geometric laboratory calibration is not valid in airborne conditions (Section 2.4; Heipke *et al.*, 2002; Honkavaara *et al.*, 2003; Merchant *et al.*, 2004). A general expectation is that test field calibration would be an efficient tool for dealing with the above issues (ASPRS, 2000; Pagnutti *et al.*, 2002; Cramer, 2004; 2005; 2006; Stensaas, 2007), but the performance, need for, and feasibility of test field calibration of digital photogrammetric imaging systems has not been empirically proven.

There are ongoing national and international processes striving for broadly accepted standards for photogrammetric calibration processes (Cramer, 2005; 2006). A comprehensive one is the U.S. Geological Survey (USGS) quality assurance plan for airborne imagery that was established in 2006 (USGS, 2008; Stensaas, 2007). The objectives of the plan are to ensure that high quality standards are used by those involved in the production of digital aerial data and that the data procurers and users use consistent processes and standards; its elements are sensor manufacturer's and data provider's certifications, contracting guidelines and data specifications, and acceptance guidelines for the data users and inspectors. In Europe, the EuroSDR launched in spring 2007 a project for a European camera certification standard entitled "European Digital Airborne Camera Certification – EuroDAC" (Cramer, 2007a; EuroDAC, 2007). This certification aims at covering the whole photogrammetric data generation process. Empirical studies form an important part of the EuroSDR initiative; the geometric study was recently completed (Cramer, 2007b). There is a great need for standardization, and empirical results are needed to enable the development of standards.

1.1 Hypothesis and objectives

The hypothesis of this study was that system calibration in a test field is necessary for digital photogrammetric airborne imaging systems and that the calibration should involve geometry, spatial resolution, and radiometry. The following research objectives were set to prove the hypothesis:

1. To develop a prototype methodology for test field calibration of digital photogrammetric airborne imaging systems.
2. To investigate the need for system calibration by using empirical image materials in order to evaluate the sufficiency and validity of calibration provided by sensor manufacturers.
3. To investigate the feasibility of system calibration in test field empirically by evaluating the feasibility of constructing test fields and calibrating the systems at test fields.

Additional research objectives were the following:

4. To provide information on the performance of digital photogrammetric sensors and test field calibration.

5. To give recommendations for the calibration process of digital photogrammetric systems.
6. To give recommendations for the construction of photogrammetric test fields.
7. To identify central new research topics.

The calibration of the image acquisition subsystem of a photogrammetric data provider (Figure 1) was investigated; the test field is the photogrammetric test field as defined above. In the empirical study, data sets from three first-generation large-format digital photogrammetric sensors, Intergraph DMC, Leica Geosysems ADS40, and Microsoft UltraCamD, were used (Section 2.2). This study did not develop the optimal methodology for test field calibration i.e. detailed, optimal parameters, tolerances, targets, and measurement methods. The optimal procedures should be developed on the basis of international co-operation once sufficient information about imaging systems and test field calibration is available. The rigorous test field calibration laboratory should then take into account the generally accepted standards concerning calibration, imagery, geographic information, etc.

1.2 Structure of the research

This research started in 2003 with trials to perform test flights using large-format digital photogrammetric sensors at the Sjökulla test field of the Finnish Geodetic Institute (FGI). At that time a number of large-format sensors were already in practical use (Section 2.2). The sensor manufacturers promised distortion-free imagery and superior radiometry and geometry compared with film images, but no reliable empirical information on the systems' performance was available. The first test flights were performed in October 2004 using two UltraCamDs. The test flights by the DMC and ADS40 took place in autumn 2005. The preliminary results of the missions were presented by Honkavaara *et al.* (2005; 2006) and Markelin *et al.* (2005; 2006).

The content of this thesis is the following. A calibration methodology for the geometry, radiometry, and spatial resolution, is outlined in **I**. In **II** and **III** the geometric calibration method is presented and the results of geometric evaluation of an analog frame camera, UltraCamD, and DMC are given. **IV** presents the spatial resolution evaluation method and gives empirical results of the evaluation of the DMC. **V** develops the radiometric calibration method and gives results of an empirical evaluation of the ADS40, DMC, and UltraCamD.

The introductory part begins with a review to the current technology in Section 2. The principles of image formation and the entire calibration chains from laboratory to practical mapping applications are covered; the focus is in geometric calibration. The research methods, empirical data sets, and the developed calibration methodology are summarized in Section 3. Central results are given in Section 4 and the findings are discussed in Section 5. Several authors have recently presented empirical results of the geometric performance of the large-format sensors; these results are considered in the discussion part. Topics for the future research are discussed in Section 6. Summary and conclusions in Section 7 summarize the results of this investigation.

1.3 Contribution

Traditionally, the field testing and calibration of geometry, spatial resolution, and radiometry has been performed in separate processes. The photogrammetric community has concentrated on the geometry, and the remote sensing community on the radiometry; spatial resolution has been of interest for all users. The situation is now changing: geometry and radiometry are becoming important for both user groups. The expected great radiometric and geometric accuracy potential of digital photogrammetric sensors led to a vision of a simultaneous calibration of geometry, radiometry, and spatial resolution in a test field, which forms the basis of the hypothesis of this study (Section 1.1).

A common framework for the calibration of geometry, radiometry, and spatial resolution was devised based on a study of the literature (**I**; Section 2). The hypothesis was proven by developing a prototype test field calibration methodology (**I-V**; Section 3) and empirically investigating test field

calibration of digital photogrammetric airborne large-format imaging systems (**II-V**; Section 4). The results proved the hypothesis (Section 5.4). Realization of these steps was the most important and extensive scientific contribution of this study.

The study provided new empirical results concerning the performance of digital photogrammetric systems and test field calibration. The central new results are summarized below.

The most comprehensive analysis focused on geometry. This was the first study to characterize the geometric performance of the UltraCamD. A significant result was the detection of distortions in DMC and UltraCamD images that deformed photogrammetric block (**II**; **III**; Section 4.1). The results showed that the systematic image distortions should be assessed, their influence should be investigated, and they should be reported in the calibration documentation (Section 5.1). The study also indicated that due to the unknown stability of the systems and the unknown accuracy of the models and parameters, system self-calibration and product level validation was necessary to achieve the highest accuracy and reliability (**II**; **III;** Section 5.1). The results were the motivation for the development of a comprehensive method for evaluating a system's geometric performance based on simulations and empirical data (**III**; Section 3.2).

The study provided new, comprehensive information on the spatial resolution of the panchromatic DMC images (**IV**; Section 4.2). Study quantified theoretically the influences of oblique imaging geometry on spatial resolution. Empirical results proved that spatial resolution was significantly dependent on the position in image and on the flying direction. Empirical linear spatial resolution models were developed to predict the resolution of the panchromatic DMC images as a function of the radial distance from the image center, and several resolution estimators were compared (Section 4.2). The conclusion was that the spatial resolution of the evaluated system was significantly lower than the nominal resolution derived from the CCD pixel size (Section 5.1).

New, quantitative information on the radiometric properties of the ADS40, DMC, and UltaCamD were provided. The results proved the linearity of the sensors, provided information about their dynamic range, sensitivity, and absolute calibration, and showed some of the shortcomings of the first generation sensors (**V**; Section 4.3). It was concluded that the missing information about the system radiometric calibration and performance, and non-rigorous processing chains were serious limitations of the systems (Section 5.1).

Special features of this study were parallel empirical and theoretical evaluations, a method recommended to other authors as well. It was concluded that methods for predicting system performance should be included in the system calibration (Section 5.1).

Based on the results, a new, unified parameterization for geometric, spatial resolution, and radiometric test field calibration was presented (Section 5.1). Recommendations for the calibration process of digital photogrammetric systems were given, and the benefits of test field calibration for sensor manufacturers, data providers, and data users were evaluated (Section 5.2). Advantages of permanent test fields were discussed and recommendations for reference targets were presented (Section 5.3). Many research issues were identified (Section 6).

An important result of the simultaneous calibration was that unified approaches could be used in geometric, radiometric, and spatial resolution calibration. Examples of this are the description of calibration and processing chains (Section 2), the analysis of precision, bias, and accuracy of calibration (Section 3.2; 4), and the new parameterization for the calibration (Section 5.1).

Although the study focused on large-format photogrammetric sensors, the structure of the study was designed so that it can be used as a basis for the development of a calibration methodology for all types of photogrammetric imaging sensors (**I-V**; Section 2).

2 Review

Structure of this review is the following. Components of a digital photogrammetric airborne imaging system are presented in Section 2.1 and Section 2.2 gives a short description of the digital large-format photogrammetric sensors. Section 2.3 formulates the parameter determination task. Parameters, methods, and example processes for geometric, spatial resolution, and radiometric calibration are given in Sections 2.4, 2.5, and 2.6, respectively. Finally, test fields and their significance are discussed in Section 2.7. For simplicity, mostly a general term, system calibration, is used, instead of sensor component, sensor, or system calibration.

2.1 A digital photogrammetric airborne imaging system

Section 1 gives two definitions for the digital photogrammetric airborne imaging system: the image acquisition system and the image product generation system (Figure 1). The components of the digital photogrammetric airborne imaging system and the central factors influencing the system outputs are given in Table 2. The central system hardware include the photogrammetric sensor, vehicle, sensor mount, camera port window, and direct orientation system. The essential software components are the image and direct orientation observation post-processing software. The system calibration is considered as a component of the system. If the product generation is considered as part of the image acquisition process, then georeferencing (Section 2.4), restoration (Section 2.5), and radiometric correction (Section 2.6) also become parts of the system. Table 2 groups the conditions for the system

Table 2. Components of a digital photogrammetric airborne imaging system and factors influencing photogrammetric system performance.

System	Sensor	Lens, CCD, filter, beam splitter, shutter
	Other system components	Sensor mount, camera port window, direct orientation system (GPS, IMU), vehicle
	Calibration	Models, parameters, and methods for geometry, spatial resolution and radiometry
	Data post-processing software	Image post-processing, direct orientation post-processing, georeferencing*, restoration*, radiometric correction*
Photogram-metric network	Block structure	Number of flight lines, number of images, side and forward overlaps, relative orientations
	Control	GCPs*, direct orientation observations, GPS base stations, atmospheric observations*, *in situ* reflectance and illumination measurements, reflectance reference targets*, spatial resolution reference targets*
Conditions	System settings	Aperture, exposure time, FMC, in-flight data processing (e.g. compression)
	System environment	Altitude, vibrations and swing, velocity, temperature, pressure, humidity
	Atmosphere	Refraction, Mie and Rayleigh scattering (visibility), absorption, turbulence, clouds, temperature, pressure, humidity
	Illumination	Direct sunlight, diffuse light, solar elevation angle, spectral distribution of light
Object		Structure, contrast, anisotropy, adjacent objects

*) The factors concerning only the image product generation system.

settings, system environment, atmosphere, and illumination. Finally, the object influences the achievable performance.

2.2 Digital photogrammetric large-format airborne imaging sensors

Digital photogrammetric large-format airborne imaging sensors are intended to replace the analog 23 x 23 cm^2 format frame cameras (Read and Graham, 2002). The central properties of these sensors include a calibrated geometry with accuracy potential of up to 1 cm, a ground sample distance (GSD) potential of up to 2 cm, accurate stereoscopic data, an image width of 10,000 pixels or larger, multispectral imagery on the visible to near infrared (NIR) regions of the electromagnetic spectra, and radiometry with linear response, large dynamic range, high resolution, and suitable for visual and quantitative applications (Fricker *et al.*, 1999; Spiller, 1999).

The image width requirement had a fundamental role in directing the technical realizations. The production of sufficiently large CCD arrays is impossible at the moment, so large-format digital sensors are built either as multi-head systems by fusing several smaller CCD arrays and cameras or by using linear CCD arrays (Hinz, 1997; Fricker *et al.*, 1999; Leberl and Gruber, 2003; Figure 2; Figure 3; Figure 4). The properties of the three digital photogrammetric large-format sensors that are currently commercially available, the Leica Geosystems ADS40, Intergraph DMC, and Microsoft UltraCamD, are discussed below. These sensors entered the commercial markets during 2001-2003 and by the end of 2005 more than 100 systems had been taken into operational use world-wide (Cramer 2005; 2006). Several new large-format sensors are expected to enter markets in the near future (Cramer, 2004; Petrie, 2006; Tölg, 2007).

The image post-processing that generates the measurable images from the raw data is an integral part of the image acquisition process for digital airborne sensors. It is a resampling process consisting of geometric and radiometric instrument corrections, which are system dependent and based on laboratory calibration, data collected during the flight mission, and image measuremens (Section 2.4, 2.5, 2.6). The post-processing can overlap different sub-processes of the photogrammetric process, especially the referencing and calibration processes (Figure 1).

The ADS40 (Figure 2) is a pushbroom scanner providing stereo and multispectral data (Eckardt *et al.*, 2000; Sandau *et al.*, 2000; Beisl, 2006a; Leica Geosystems, 2008). ADS40 applies CCD lines, each with 12,000 elements; pixel size is 6.5 µm x 6.5 µm. The geometric quality is based on single-lens geometry, temperature and pressure stabilization of the focal plane, accurate GPS/IMU-processing, and the IMU being mounted rigidly on the focal plane. The radiometric and spectral quality are based on specially designed filters and beam splitter, the temperature and pressure stabilization, a telecentric lens, and accurate calibration. Stereoscopic data is provided by a three-line principle (Figure 2c). The ADS40 provides four spectral channels (blue (B), green (G), red (R), NIR), which are approximately 50 nm in width and non-overlapping (Reulke *et al.*, 2000; **V**). Geometric post-processing applies the sensor calibration information and corrects the impact of the flight dynamics using the exterior orientation information (Section 2.4; Tempelmann *et al.*, 2000). Radiometric correction includes the corrections determined in laboratory and an absolute radiometric correction approach has also been established (Section 2.6; Beisl and Woodhouse, 2004; Beisl, 2006a). The post-processing produces geometrically and radiometrically corrected panchromatic and multispectral image carpets. A second generation ADS40 entered the markets in autumn 2006 (Fricker, 2007). Significant changes in comparison to the first generation ADS40 include an improved beam splitter providing four co-registered multispectral channels, possibility to collect multispectral stereo imagery, a 4 times greater sensitivity, and an improved lens.

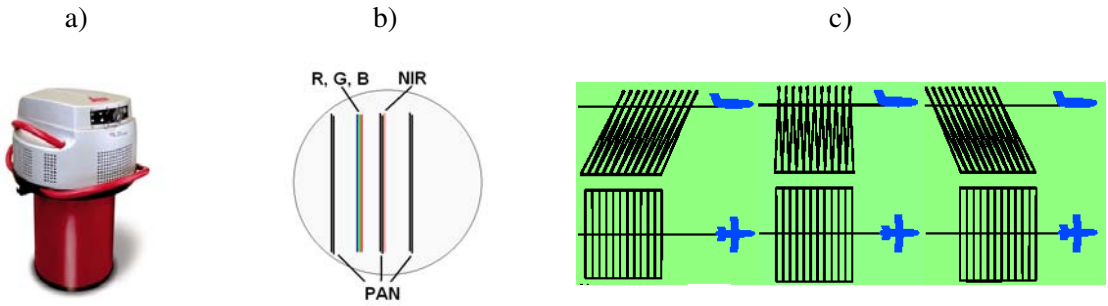

Figure 2. a) ADS40 (© Leica Geosystems). b) An example layout of the focal plane. c) Principle of three-line stereo (Fricker *et al.,* 1999).

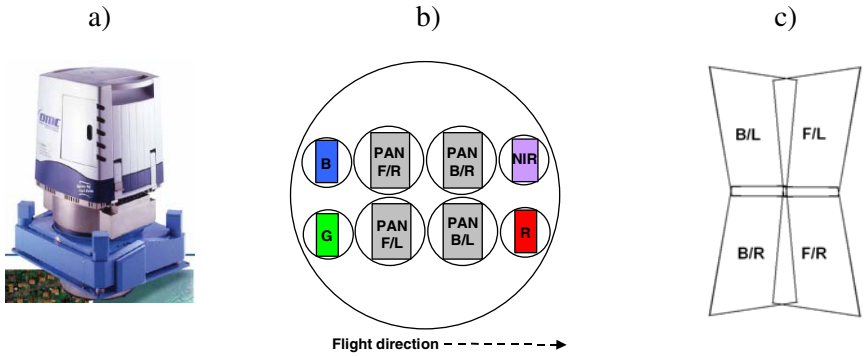

Figure 3. a) DMC (© Intergraph). b) Principle of arrangement of eight camera heads (F, B, R, L indicate forward, backward, right, and left convergence angles, respectively). c) Principle of the formation of the large-format panchromatic image from four oblique images.

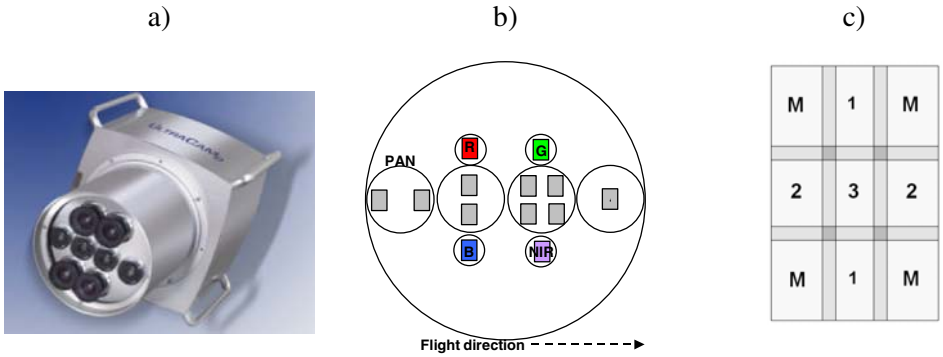

Figure 4. a) UltraCamD (© Microsoft). b) Principle of arrangement of eight camera heads. c) Principle of the formation of the large-format panchromatic image from nine component images.

The DMC (Figure 3) is a multi-head system with eight independent camera cones (Hinz *et al.*, 2000; Tang *et al.*, 2000). The large-format panchromatic image of 13,824 x 7,680 pixels is composed of four medium-format CCD arrays. The component images are collected using four slightly convergent individual cameras (Figure 3b, c; **IV**). Four multispectral channels (red, green, blue, NIR) are collected using four nadir-viewing cameras with medium-format CCD arrays 3,072 x 2,048 pixels in size. The spectral channels are wide (>200 nm) and overlapping (**V**). Pixel size is 12 µm x 12 µm. All the cameras are exposed simultaneously; an electronic time delay integration (TDI) forward motion compensation (FMC) is occupied. Post-processing applies the geometric and radiometric instrument corrections determined in laboratory and by self-calibration (Section 2.4; Section 2.6). It then resamples the panchromatic component images onto the large-format virtual image and processes the multispectral data either to the original color resolution or to a panchromatic resolution using

pansharpening (Diener *et al.*, 2000). The reported developments of the DMC until 2007 have concerned geometric issues and process flow (Hefele, 2006; Dörstel, 2007; Rosengarten, 2007).

The UltraCamD (Figure 4) is a multi-head system consisting of eight independent camera cones (Leberl and Gruber, 2003; Kröpfl *et al.*, 2004). Four cameras create a large-format panchromatic image 11,500 by 7,500 pixels in size by combining 9 medium-format CCD arrays (Figure 4b, c). The cones have parallel optical axes and the same field of view (FOV), and are mounted in a line pointing in the direction of flight. The UltraCamD uses a syntopic imaging principle, which means that each panchromatic camera cone is exposed with a small time delay at the same exposure station. The other set of four cones produces four medium-format multispectral channels (red, green, blue, NIR) 3,680 x 2,400 pixels in size. The spectral channels of the UltraCamD are wide (>200 nm) and overlapping (**V**). Pixel size is 9 µm x 9 µm. An electronic TDI is occupied. The post-processing steps and the system outputs are similar to those of the DMC. A second generation UltraCam (UltraCamX) entered markets in autumn 2006 (Gruber, 2007). The principles of the new system are similar to those of the UltraCamD; the central changes include an increased CCD array size, smaller pixel size, a new lens fitted to the pixel size, and an improved PAN-sharpening ratio.

2.3 Determination of calibration parameters

In this investigation, the calibration parameters are determined by indirect methods. The principle is to rigorously model the functional relationship f between the observations and parameters, with the calibration parameters included, and to solve the values for the unknown parameters using an optimization method. A least squares method formulates the optimization task as follows:

$$\textit{Find such estimate for a parameter vector } \hat{x} \textit{ that } \hat{v}^T C_{ll}^{-1} \hat{v} \textit{ is minimum and } \hat{l} = l + \hat{v} = f(\hat{x}) \qquad (1)$$

The components of the adjustment model are the functional model and a stochastic model C_{ll}, which is the covariance matrix of the observations; l is the vector of observations; $\hat{v}$ is the vector of residuals or corrections. The least squares method provides many attractive properties, including tools for precision and reliability assessment and for functional and stochastic model determination. Properties of the least squares method are thoroughly descried in the photogrammetric literature, for instance, by Mikhail (1976), Förstner (1985), Kraus (1997), Mikhail *et al.* (2001), and Förstner and Wrobel (2004).

Accuracy evaluation is a fundamental phase in the measurement process. The central components of the accuracy are bias (systematic error) and precision. *Accuracy* indicates closeness to the truth. *Precision* indicates the closeness together, i.e. variation around the average value. *Bias* is defined as the difference between the average result of the measurement process and the true value.

The precision estimates (standard deviations) of the adjusted parameters are obtained from the covariance matrix of unknowns (Mikhail, 1976; Förstner and Wrobel, 2004). For instance, the standard deviation estimate for parameter $\hat{x}_u$ is

$$\hat{\sigma}_{\hat{x}_u} = \hat{\sigma}_0 \sqrt{C_{\hat{x}_u \hat{x}_u}}\,, \qquad (2)$$

where $C_{\hat{x}_u \hat{x}_u}$ is the u^{th} diagonal element of the estimated covariance matrix of the unknowns. $\hat{\sigma}_0$ is the estimated standard error of unit weight with a redundancy R:

$$\hat{\sigma}_0^2 = \frac{\hat{v}^t C_{ll}^{-1} \hat{v}}{R}\,. \qquad (3)$$

Empirical estimates for accuracy, precision, and systematic error are obtained by calculating the root-mean-square error (RMSE), standard deviation, and average values of the differences (i.e. errors) between the system outputs and independent reference values of higher accuracy, respectively. In the case of calibration parameters such reference values do not exist but an indication of systematic errors can be obtained indirectly, by analysing systematic distortions in residuals and/or system outputs.

2.4 Geometric calibration

Geometry means the relative positions of objects, which enables the determination of the distances, angles, areas, volumes, elevations, sizes, and shapes of objects.

In an ideal central perspective projection image formation event a bundle of light rays reflected from the object traverses through the atmosphere, intersects at the perspective center, and enters a planar image focal plane, where the intensity of the light rays is recorded using light sensitive media, e.g. CCD array (Figure 5).

A fundamental task in the geometric processing of images is the orientation, i.e. determining the relationship between the image and object coordinates (imaging model). The rigorous physical imaging model is based on the central perspective projection model, a collinearity model, assuming that the ray between the object point, perspective center, and image point is linear (Figure 5). The major phenomenon invalidating the linearity in airborne conditions are atmospheric refraction and system distortions. For the atmospheric refraction, correction terms are available (e.g. Mugnier *et al.*, 2004). The nonlinearities caused by the sensor are mainly due to lens distortions, geometric inaccuracies of a CCD array (e.g. non-flatness), and errors in the platform calibration in the case of multi-head systems (Fraser, 1997; Fiete *et al.*, 2004; Kruck *et al.*, 2004; Dörstel, 2007). The filter, beam splitter, and camera port window also influence the light rays (Table 2). Furthermore, the above influences can be dependent on the environmental conditions, such as temperature, pressure, and humidity (Meier, 1975; Worton, 1977; Merchant *et al.*, 2004). The linear imaging model can be supplemented by appropriate additional parameters to model the distortions caused by the system. The complete imaging model thus includes the exterior orientation (perspective center coordinates and rotations of the image), interior orientation (principal point and principal distance), and the system distortion parameters, and the corrections for the atmospheric refraction. The imaging model is discussed in details in the photogrammetric literature, e.g. by Torlegård (1989), Fraser (1997), Kraus (1997), Mikhail *et al.* (2001), and Förstner *et al.* (2004).

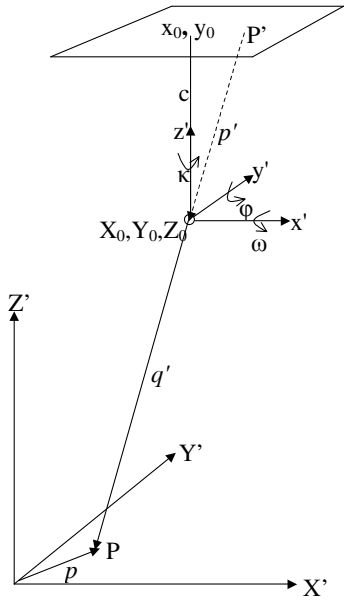

Figure 5. Central perspective geometry for a rectangular image. (X_0,Y_0,Z_0) is perspective center, (ω,φ,κ) are image rotations, (x_0,y_0) is principal point, c is principal distance, P is object point, and P' is image point. Vectors *p'* and *q'* are collinear.

Direct and indirect approaches can be used for orientation (Schwarz *et al.*, 1993; Cramer, 2001; Heipke *et al.*, 2002a). The *direct method* determines the exterior orientations utilizing GPS and inertial (IMU) observations measured during the image collection and relies on existing sensor calibration data. The *indirect method*, aerial triangulation, utilizes tie point observations between images and ground control point (GCP) and/or direct exterior orientation observations between images and object. The

optimal values for the unknown parameters are determined by *bundle block adjustment*, which is based on the least squares method (Section 2.3); the imaging model is the primary functional model. Block adjustment is called *self-calibrating* when parameters describing the system calibration are determined in the adjustment. The orientation methods are described in details in the photogrammetric literature, e.g. by Kraus (1993), Fraser (2001), Grün and Beyer (2001), Mikhail *et al.*, (2001), and Förstner *et al.* (2004).

After the orientation process, georeferencing takes place (Wolf and Dewitt, 2000). In the georeferencing process, the images are rectified to the object coordinate system; typical outputs are the orthophotos, stereomodels, and image blocks.

The geometric calibration methods currently in use are based for the most part on the work by Brown (1966, 1972, 1976). Extensive overviews of the geometric calibration methodology are given by Livingston *et al.* (1980), Clarke and Fryer (1998), Boland *et al.* (2004), Cramer (2004), and Remondino and Fraser (2006). In the following the most feasible methods for the photogrammetric airborne imaging system calibration are briefly discussed.

Geometric system calibration parameters

Geometric calibration determines the geometric characteristics of an imaging system. The fundamental parameters are the interior orientation and the factors distorting the linearity of the imaging ray within the system. The distortion models can be classified as mathematical, physical, and mixed models (e.g. Brown, 1976; Ebner, 1976; Kilpelä, 1981; Förstner *et al.*, 2004). An appropriate distortion model in many situations, and especially for the digital cameras, is the *10-parameter physical model* with its principal distance, principal point, radial distortions, decentering distortions, and in-plane distortions (Brown, 1966; Brown, 1972; Fraser, 1997; Förstner *et al.*, 2004; **II**). The optimum distortion model is dependent on the sensor and system properties; examples from a few types of sensors are discussed below.

For integrated systems, e.g. integrated camera, GPS, and IMU or multi-head cameras, the positional and angular misalignments of the sub-systems are determined (Dörstel *et al.*, 2003; Honkavaara, 2003; 2004; Kröpfl *et al.*, 2004).

Central geometric quality indicators include the estimates of the precision of the calibration parameters, model correctness, and of the system output (e.g. block, stereo model, and orthophoto) accuracy.

Geometric calibration methods

Two fundamental geometric calibration approaches are triangulation methods utilizing point measurements and goniometer methods utilizing angular measurements (Mikhail et al., 2001; Boland *et al.*, 2004; Cramer, 2004). The calibration can be determined in a laboratory, in a test field, and by self-calibration.

The triangulation-based methods are most commonly used and these methods are also suitable for test field calibration (Brown, 1972). A single image or a block made up of more than one image is captured from an array of targets with known positions, and appropriate parameters are determined using the self-calibrating bundle block adjustment.

The laboratory calibration of analog frame cameras is based on multicollimators or goniometers (Livingston *et al.*, 1980; Light, 1992; Pacey *et al.*, 1999; Cramer, 2004). Calibration frame (gage) methods, based on 2 or 3-dimensional control point fields, are frequently used with close-range systems and increasingly used also for digital airborne systems (e.g. Fraser, 2001; Grün and Beyer, 2001; Cramer, 2004; Kröpfl *et al.*, 2004; Mostafa and Hutton, 2005).

The airborne *in-situ* system calibration is determined in the real operating condition either by test field calibration or self-calibration. For *test field calibration*, a block of images is collected over a test

field with GCPs and the system calibration is determined utilizing the GCPs and optional tie point and exterior orientation observations (Section 2.7). *Self-calibration* does not necessarily require GCPs and it often determines the system calibration from the data of a certain mapping flight.

Bundle block adjustment provides estimates of the calibration parameter precisions (standard deviations) and reliability (Section 2.3). Analysis of residuals of various observations gives empirical indication about the correctness of the system model. The object point and exterior orientation precision estimates given by the bundle block adjustment are often used as the indicators of block precision. Empirical point determination accuracy is obtained by comparing the system output coordinates with reference checkpoint coordinates.

An efficient method for the prediction of the geometric performance of a photogrammetric system is simulation. Important parameters in the simulations are the sensor geometry, the block geometry, image distortions, and distribution and accuracy of tie point, GCP, and exterior orientation observations (Ebner, 1972; Ackermann, 1992; Fraser, 1997; Burman, 2000; Honkavaara, 2000; 2003; Mikhail *et al.*, 2001; Nilsen, 2002b). Simulation results correspond to the empirical results if the simulation conditions correspond to the empirical conditions. The contradiction between the simulated and empirical results will therefore indicate errors in the functional or stochastic models.

Example geometric calibration processes

In the following, three types of calibration processes are presented. The process of an analog frame camera exemplifies calibration process of top-quality metric cameras. The process of a close-range camera is an example of a calibration process of off-the-shelf cameras, which are increasingly used in the airborne applications as well (Petrie, 2006). The calibration is an integral part of the system geometric processing chain in both cases and the processes can be regarded to be on a mature state (Remondino and Fraser, 2006). Each digital photogrammetric large-format sensor is calibrated using different methodology and calibration chains are still under development. The first information from the DMC and UltraCamD manufacturers was that the post-processed images were geometrically distortion free and that self-calibration was not necessary (Heier *et al.*, 2002; Cramer, 2004; Kröpfl *et al.*, 2004); the correctness of this claim is evaluated in Section 5.1.

The calibration of analog frame cameras is based exclusively on the laboratory calibration (Table 3; Livingston *et al.*, 1980). Three types of camera with similar geometric principles dominated the markets, and all these systems can be calibrated with similar methodology (Read and Graham, 2002; Cramer, 2004). The lenses are optimized for metric applications; they are stable and distortions are symmetrical and small, less than 3 μm in modern lenses (Light, 1992). The laboratory calibration is typically repeated over 2-3-year intervals. Self-calibration is routinely applied on production blocks, because image distortions (e.g. due to film deformations) appear in airborne operational conditions (Brown, 1976; Ebner, 1976; Kilpelä, 1981). In conventional mapping blocks, the inaccuracies in the interior orientation parameters are compensated for due to high correlations with the exterior orientation parameters but the use of directly measured orientations has revealed that the laboratory calibration is not valid in airborne conditions (Cramer, 2001; Heipke *et al.*, 2002b; Wegmann and Jacobsen, 2002; Honkavaara *et al.*, 2003; Merchant *et al.*, 2004). Laboratory calibration determines the interior orientations and radial distortions with a 5 μm accuracy (Tayman, 1984). The state of statistical control has been achieved for film-based processes and the empirical results correspond normally to theoretical expectations. Simulation-based accuracy models are widely utilized in practical work (Ebner, 1972; Ackermann, 1992; Burman, 2000).

Terrestrial (close-range) applications often apply off-the-shelf cameras. Lenses of off-the-shelf cameras are not optimized for metric purposes, for instance, the principal point can be instable and the lens can have large irregular and instable symmetric and non-symmetric distortions. Possible causes of the instability include the movement of the CCD sensor or lens with respect to the camera body and

Table 3. Summary of geometric calibration methods.

System	Parameters	Method
Analog frame camera	Various principal points, focal length, fiducial mark coordinates, radial and tangential distortions, resolving power, shutter, filter parallelism, magazine platen, and stereo model flatness	Laboratory: multicollimators or goniometers, 2-3 years interval
	Physical, mathematical, mixed additional parameters	Self-calibration during production
Close range	10-parameter physical model	Laboratory: 2D or 3D calibration frames
camera	10-parameter physical model	Self-calibration during production
ADS40	x_0, y_0, c, radial symmetric distortion, tangential distortion, flatness and height of CCD lines, positions of pixels, locations of CCD lines*	Laboratory: Vertical goniometer, code target
	Boresight, x_0, y_0, c, radial symmetric distortion (6^{th} order polynomial)	Self-calibration using cross-shaped blocks collected from two altitudes.
DMC	Single-head calibration: 10-parameter physical model	Laboratory: two rotation tables
	Platform calibration: rotations of 3 camera heads, three focal lengths, and projection centre offset with respect to single reference camera head	
	Platform calibration, system testing	Elchingen test field
	Platform calibration for every image	Image post-processing (self-calibration)
UltraCamD	Single-head calibration:	Laboratory: A 3D calibration frame
	For each cone: x_0, y_0, c, radial lens distortion, and look-up table of remaining image distortions	
	For each CCD: shift, scale, shear, and perspective distortions	
	Shutter and sensor electronics	
	Platform calibration: Approximate projective transformation between camera cones	
	Platform calibration for every image	Image post-processing (self-calibration)

*) All these parameters are discussed in the literature but the effective parameters are not given

differential movements of the lens elements (Fraser 1997; Shortis and Robson, 1998). For these cameras, the 10-parameter physical model has been considered appropriate (Table 3; Fraser, 1997). The calibration process can involve laboratory calibration (Fraser, 2001; Grün and Beyer, 2001; Cramer, 2004) but the self-calibration is routinely applied during production work because of the stability problems; for these systems the state of the statistical control is obtained typically on the measurement process basis.

The geometric laboratory calibration of the ADS40 involves a lens cone, focal plane, and digital sensor calibration (Table 3; Pacey *et al.*, 1999; Schuster and Braunecker, 2000). Laboratory calibration is completed using airborne self-calibration (Tempelmann *et al.*, 2003). The designed geometric accuracy is 1/3 pixel (Eckardt *et al*, 2000). The calibration flights have provided $\hat{\sigma}_0$ of 2.5-2.9 μm (Tempelmann *et al.*, 2003). New geometric calibration parameters have been developed for the second generation ADS40 and its calibration is relying on *in situ* calibration (Fricker, 2007).

DMC geometric calibration involves a single-head calibration and a platform calibration (Table 3; Heier *et al.*, 2002; Dörstel *et al.*, 2003; Hefele, 2006; **III**). In the single-head calibration each camera head is calibrated in laboratory. Platform calibration is determined approximately at the

sensor-manufacturing phase in laboratory, improved by test field calibration, and determined accurately for every image in the post-processing phase of photo flights on self-calibration basis utilizing tie points between the overlapping component images. Laboratory calibration has provided 2-8 μm precisions for the interior orientation parameters of individual camera cones and $\hat{\sigma}_0$ of approximately 0.5 μm (Hefele, 2006). $\hat{\sigma}_0$ of the platform calibration has been 1/12 to 1/6 pixel (Dörstel *et al.*, 2003). Recent geometric improvements of the DMC have concerned the improvement of the laboratory calibration processes (Hefele, 2006) and the treatment of the image distortions (Dörstel, 2007) (Section 5.1).

Similar the DMC calibration, UltraCamD calibration also involves the single-head and platform calibration (Table 3; Kröpfl *et al.,* 2004; **II**). The single-head laboratory calibration is based on methods used with close-range cameras. In the image post-processing the laboratory-determined platform calibration parameters are improved on self-calibration basis. Laboratory calibration provides better than 2 μm precision for the interior orientation parameters and the remaining image distortions are less than 2 μm; $\hat{\sigma}_0$ of the calibration has been 1-1.5 μm and the estimated precision of the control point measurement is 1.3 μm (0.14 pixel) (Kröpfl *et al.*, 2004).

2.5 Spatial resolution calibration

Spatial resolution indicates a system's ability to capture the fine detail found in the original scene (ISO 12233).

An optical system blurs the input signal. The blur can be characterized by a point-spread function (PSF), which is the system response to a point source. The measured signal is the convolution of the signal entering the system and the PSF (Gonzales and Wintz, 1987). The PSF of the sensor is dependent on the nature of the detector, diffraction, and lens aberrations. Image motion, defocusing of the optics, vibration, and atmosphere cause further blur in airborne conditions. The Nyquist sampling theorem states that the maximum frequency that can be distinguished from a sampled signal is 1/(2 times sampling interval) (Graham and Koh, 2002; Thomson, 2004). According to the Rayleigh's criterion, the resolution of an ideal aberration-free lens is limited by the effects of diffraction, and it is directly proportional to the wavelength of incoming radiation and the relative aperture (Slater, 1975; Fiete *et al.*, 2004). The lens resolution for a CCD camera should be adjusted to the CCD resolution in order to avoid aliasing and diffraction effects (Boland *et al.*, 2004; Thomson, 2004). The resolution of an image typically decreases when the distance from the image center increases (distance from the image center is often characterized by a field angle, which is the angle between the optical axis and the image ray); this is due to lens properties and the atmospheric influences (Slater, 1975; Fiete *et al.*, 2004). The lens resolution is different in radial and tangential directions (Slater, 1975; Fiete *et al.*, 2004). The image motion causes differences in resolution in the flight and cross-flight directions; the amount of image motion blur is dependent on exposure time and flight speed, but it can be compensated for by using FMC (Hinz, 1999). The angular motion caused by vibrations and swing can be compensated for by using a gyro-stabilized camera mount (Abdullah *et al.*, 2004). The blur caused by the atmosphere, mainly due to turbulence and haze, is influenced by variable atmospheric conditions (Slater, 1975; Boland *et al.*, 2004). Various image processing, such as resampling, compressing, and enhancement, cause further decrease of the spatial resolution.

Typical spatial resolution processing steps of the digital photogrammetric airborne imaging systems include resampling, restoration, and pansharpening. The image post-processing is a resampling process (Section 2.2). If the system PSF is known, an appropriate deconvolution filter for the image blur compensation can be defined (Pagnutti *et al.*, 2003; Boland *et al.*, 2004; Becker *et al.*, 2005; 2006; Reulke *et al.*, 2006). Pansharpening is commonly applied in systems that provide

multispectral images with a lower resolution than panchromatic images (Diener *et al.*, 2000; Gruber *et al.*, 2004; Becker *et al.*, 2006).

Spatial resolution calibration parameters

The ISO standard (ISO 12233) defines resolving power (RP), limiting resolution, spatial frequency response (edge response), modulation transfer function (MTF), and optical transfer function (OTF) as the resolution measures. RP, MTF, and PSF are discussed below briefly.

RP is the ability of an imaging system to reproduce closely separated lines or other elements (Read and Graham, 2002). It is determined by calculating how many lines or line pairs can be solved per millimeter. The limitation of RP is that it does not take the loss of the contrast in the lower frequencies into account and thus does not measure the edge sharpness (Read and Graham, 2002; Kölbl, 2005).

MTF characterizes the loss of contrast as the function of the spatial frequency (Read and Graham, 2002; **IV**). Various quality indicators can be derived from the MTF, such as the PSF (Becker *et al.*, 2005; 2006; Reulke *et al.*, 2006), full width of half maximum (Ryan *et al.*, 2003), MTF at Nyquist frequency (Pagnutti *et al*., 2002), and 10% MTF (often used as an estimate of the RP; Kölbl, 2005). Relationship between the PSF and the MTF is as follows: the Fourier transform of the PSF is the OTF and the modulus of the OTF is the MTF. Typically, the PSF is modeled using a Gaussian function and then also the MTF is a Gaussian (Equation 4; Reulke *et al.*, 2006). The system MTF and PSF are feasible spatial resolution (or response) models of the system.

It is necessary to measure resolution for various field angles, for radial and tangential directions, and for flight and cross-flight directions. In order to characterize the resolution using a single measure, indicators averaged over the entire image are used, e.g. area weighted average resolution (AWAR) (Read and Graham, 2002).

Spatial resolution calibration methods

To evaluate the resolution, an image of a suitable reference target is captured with the system that is being tested. This target should include patterns with sufficiently fine detail (ISO 12233). Popular targets are resolution bar, edge, and Siemens star targets (Figure 7; ISO 12233; Slater, 1975; Hakkarainen, 1986; Read and Graham, 2002; Blonski *et al.*, 2002; Becker *et al.*, 2005; **I**; **IV**). The spatial resolution can be determined in a laboratory on a component or a sensor basis or the spatial resolution of the entire imaging system can be determined in airborne *in situ* conditions (Section 2.7; Slater, 1975; Read and Graham, 2002; Fiete *et al.*, 2004).

The spatial resolution of the entire imaging system can be predicted by combining resolution estimates of individual factors. For instance, the system MTF can be obtained by using a cascade of component MTFs (Boland *et al.*, 2004) and the system RP can be estimated by summing RPs of various components of the system (Fiete *et al.*, 2004).

Spatial resolution calibration of digital photogrammetric sensors

The resolution calibration methods used for the digital photogrammetric sensors are only briefly described or not described at all in the literature. For the ADS40, the lens MTF is determined simultaneously during the geometric calibration for various field angles in flight and cross-flight directions (Pacey *et al.*, 1999; Schuster and Braunecker, 2000). The UltraCamD calibration protocol gives the MTF at radial and tangential directions as the function of the image height for various apertures (UltraCamD, 2004). The information of the DMC resolution is that MTF of individual lenses is homogeneous and flat and fitted to the CCD pixel size (Hinz *et al*., 2000).

2.6 Radiometric calibration

Radiometry means the measurement of radiance. A digital sensor stores the result of the radiance measurement as a digital number (DN). Airborne images provide different DN at different parts of a single image and in different images for the same object. This is caused by the variability of the radiance entering the system (*at-sensor radiance*) and by the system properties. Image radiometry is typically modeled in two phases, the radiance transfer from object to the system and the at-sensor radiance transfer to DNs inside the system.

The at-sensor radiance has many components, as illustrated in Figure 6 (Beisl, 2001; Beisl and Woodhouse, 2004). An irradiance at the object is composed of direct sunlight (A), the skylight (B), the multiple scattering (D), and the light reflected from adjacent objects (F). Objects typically have anisotropic reflectance properties, i.e. the observed reflectance is dependent on illumination and observation geometry (mathematically modelled using the Bidirectional Reflectance Distribution Function (BRDF)) (Lillesand and Kiefer, 2000; Beisl, 2001). Additional variable radiance components entering the system are the path-scattered radiance (C) and the radiance from the adjacent objects (E). In good weather conditions components A, B, and C are of importance. Atmospheric influences are caused mainly by gaseous absorption and Mie and Rayleigh scattering processes; these influences are also dependent on the observation geometry (Pellikka, 1998; Lillesand and Kiefer, 2000; Beisl, 2001).

The radiometric model of the system describes the transformation from the radiance entering the system to DNs; this issue is discussed below. The central system factors influencing the output DN are the system properties (e.g. optics transmittance, spectral filters, PSF, gain and offset parameters, and dynamic range of the A/D conversion) and system settings (e.g. aperture and exposure time). The system environment (Table 2) influences the system performance as well; in high-end systems these influences are compensated for (Section 2.2; Diener et al., 2000; Beisl, 2006a).

Radiometric correction eliminates distracting radiation components from the images. The first step in the radiometric processing chain is to apply the instrument corrections that are typically determined in the laboratory calibration. Optimum radiometric processing is dependent on the application, which can be roughly divided into visual and quantitative. For the quantitative applications the objective is to obtain either the absolute reflectance information of the scene elements or to obtain correct relative magnitudes of the reflectance of scene elements in a single channel, in different channels, in different images taken in one mission, or in images taken at different times. Correction methods have been developed for satellite and airborne remote sensing systems (e.g. Schowengerdt, 1997; Pellikka, 1998; Atcor, 2008); methods for photogrammetric systems are under development (Paparoditis *et al.*, 2006; Beisl, 2006a; 2006b; Fricker, 2007). For the visual applications the objective is usually to obtain natural colors. Additional radiometric manipulations, mainly used for visual applications, include gamma corrections, tonal transformations, transformations from the 16 bit to 8 bit domain, pansharpening, and image enhancement and restoration (Lillesand and Kiefer, 2000; Diener *et al.*, 2000; Becker *et al.*, 2005; 2006). Image resampling and compression cause further radiometric degradation.

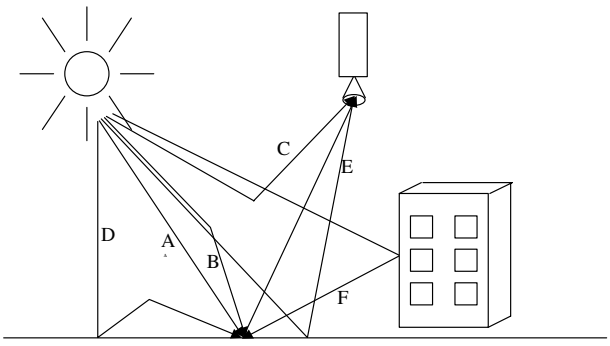

Figure 6. Radiation components (adopted from Beisl 2001).

Radiometric calibration parameters

Radiometric calibration determines the radiometric characteristics of an individual imaging system. The radiometric calibration approaches can be classified into absolute and relative (Dianguirard and Slater, 1999). *Absolute calibration* determines the models and parameters that are needed to transform the DNs

into the units of radiance (W/(m^{2}sr nm)), i.e. an absolute radiometric response and a spectral response. *Relative calibration* normalizes the outputs of the detectors so that all the detectors give the same output when the focal plane of the sensor is irradiated with a uniform radiance field. The complete radiometric model thus consists of the absolute calibration parameters and relative calibration corrections.

The absolute radiometric response model of a digital sensor can be typically simplified to a linear equation with gain and offset parameters (Equation 5; Schowengerdt, 1997; **V**). The spectral response calibration determines the system's response as a function of wavelength for various channels; the parameters are typically the central wavelength and bandwidth. (Vane *et al.*, 1993; Cocks *et al.*, 1998; Chrien *et al.*, 2001; Morain and Zanoni, 2004; Beisl, 2006a; Bruegge *et al.*, 2007)

The relative radiometric calibration of a single band determines the nonuniformities of the system radiometric response (Pellikka, 1998; Diener *et al.*, 2000; Schuster and Braunecker, 2000; Boland *et al.*, 2004; Beisl, 2006a; Hefele, 2006; **V**). Corrections are determined for the sensitivity differences of individual cells of a CCD array (Photo Response Non-uniformity; PRNU), defect pixels, light falloff, and dark signal (Dark Signal Non-uniformity; DSNU).

Important radiometric quality indicators include the absolute radiometric accuracy (difference between input and output radiance of the sensor), relative radiometric accuracy (for a constant input radiance, the difference between measured radiometric values from pixel-to-pixel, band-to-band, and/or image-to-image), linearity (fit of the calibration model), sensitivity, signal-to-noise ratio, and dynamic range (noise and saturation) (Morain and Zanoni, 2004; **V**).

Radiometric calibration methods

The principle of radiometric calibration is to capture images of a flat radiance field at various intensity levels, using the system and by evaluating the system's DN response to this radiance field to determine the radiometric calibration parameters. The comprehensive radiometric calibration of spaceborne and airborne imaging systems consists of three phases: preflight calibration in a laboratory, on-board calibration, and vicarious calibration (Vane *et al.*, 1993; Dianguirard and Slater, 1999; Chrien *et al.*, 2001; Green and Pavri, 2001; Bruegge *et al.*, 2007; **V**).

Rigorous radiometric laboratory calibration is performed by measuring a system's response to light sources (e.g. integrating spheres or hemispheres) that are traceable to the international radiance standards (Lowe *et al.*, 1975; Vane *et al.*, 1993; Cocks *et al.*, 1998; Dianguirard and Slater, 1999; Chrien *et al.*, 2001; Beisl, 2006a; Hefele, 2006; Bruegge *et al.*, 2007; **V**).

Typical on-board calibrators are lamps or diffuse panels reflecting solar light, and they are used to obtain checks of system calibration during image collection (Vane *et al.,* 1993; Dianguirard and Slater, 1999; Bruegge *et al.*, 2007). The disadvantage of these devices is that they are subject to degradation. For satellite sensors natural light sources (the Sun, the Moon) can also be used (Dianguirard and Slater, 1999).

Vicarious methods determine radiometric calibration in airborne conditions. Radiance- or reflectance-based methods can be used (Biggar *et al.*, 1994; Dianguirard and Slater, 1999; Green and Pavri, 2001; Pagnutti *et al.*, 2002; 2003; Bruegge *et al.*, 2007). The *radiance-based method* determines the at-sensor radiance by using a calibrated radiometer. The *reflectance-based method* predicts the at-sensor radiance by measuring the reflectance of a ground target, modeling the atmosphere using a radiative transport code (e.g. MODTRAN; Berk *et al.*, 2003), and then propagating the ground target radiance through the modeled atmosphere. The reflectance based vicarious method (reflectance based test field calibration) is further discussed in Sections 2.7 and 3.2 and in **V**.

The absolute calibration accuracy of a specific system is dependent on the reference at-sensor radiance accuracy and the system performance. Chrien *et al*. (2001) reported about 1.6% uncertainty of the absolute radiometric calibration at laboratory. For the reflectance based vicarious methods the

Table 4. Summary of the radiometric calibration methods used by manufacturers.

System	Parameters	Method
ADS40	PRNU, light falloff, DSNU, gain, offset	Laboratory: Ulbricht sphere (NIST-traceable)
	Spectral response	Laboratory: monochromatic light source (NIST-traceable), goniometer
	DSNU	In-flight
DMC	PRNU, defect pixels, light falloff, influence of aperture and filter for each aperture, temperature and TDI settings	Laboratory: Ulbricht sphere
	Color balancing, brightness difference compensation	Self-calibration
UltraCamD	PRNU, defect pixels, and light falloff for various aperture settings	Laboratory: 60 flat field images provided by two normal light lamps with known spectral illumination curves

most influential factors are the accuracy of the target reflectance and atmospheric modelling. The accuracy of the atmospheric modelling is typically 3-4% for satellite systems (Biggar *et al.,* 1994). Vicarious calibration experiments have shown an at-sensor radiance prediction accuracy of 2-10% (Biggar *et al.,* 1994; Dianguirard and Slater, 1999; Pagnutti *et al*., 2003; Bruegge *et al.*, 2007). The accuracy is lower for low reflectance objects, and radiance-based methods are in general more accurate than reflectance-based methods. The radiometric accuracy of digital photogrammetric sensors is a research issue.

Radiometric calibration of digital photogrammetric sensors

The radiometric calibration approaches of the large-format photogrammetric sensors are briefly described in the following and a summary of the methods is given in Table 4. The calibration process of the ADS40 is described in details in the literature while the DMC and UltraCamD calibration methods are described only briefly.

The laboratory calibration of the ADS40 involves both absolute and relative calibration (Table 4; Beisl, 2006a; 2006b; **V**). The spectral calibration is performed using a spectral measurement unit applying a National Institute of Standards and Technology (NIST) traceable light source. The relative and absolute radiometric calibrations are determined using an Ulbricht sphere providing NIST traceable radiances. The linear absolute calibration model is sufficient; the accuracy of the gain factor is 5% (Beisl, 2006b). The DSNU correction is determined partially at the laboratory and partially in flight. A processing chain from raw images to reflectance images has been presented but no empirical results have been published (Beisl and Woodhouse, 2004; Beisl, 2006a; 2006b; Fricker, 2007).

The laboratory calibration of the DMC involves the relative calibration (Table 4; Diener *et al.*, 2000; **V**). In the post-processing of the imagery (Section 2.2), the colors of multispectral channels are balanced by using an object with similar reflectivity in each band (e.g. asphalt) and the possible brightness differences of the panchromatic component images are compensated for (Diener *et al.*, 2000; Heier *et al.*, 2002; Hefele, 2006; **V**).

The laboratory calibration of the UltraCamD occupies relative radiometric calibration (Table 4; UltraCamD, 2004; **V**).

2.7 Test fields

In general, photogrammetric test fields can be classified into permanent and temporal. The most relevant types of reference targets are artificial targets that can be permanent or portable and natural targets that can be permanent or temporal. Central requirements for permanent test fields and targets are that they should exist over a long period of time and be available year-around (**I**).

A test field can contain reference targets for calibrating one or more of the system properties. Two permanent photogrammetric test fields with reference targets for geometric, spatial resolution, and radiometric calibration have been established in the literature: the Stennis Space Center Verification and Validation (SSC V&V) test field of the National Aeronautics and Space Administration (NASA) in USA (Pagnutti *et al.*, 2002) and the Sjökulla test field of the FGI in Finland (Kuittinen *et al.*, 1994; Ahokas *et al.*, 2000; **I**). Several test fields exist for the calibration of some of the system properties, and especially for geometric calibration.

In this section, reference targets for geometric, spatial resolution, and radiometric calibration are discussed, examples of existing test fields are given, and significance of field-testing and calibration are considered.

Test fields for geometric calibration

Important parameters of the test fields for geometric calibration are the size, distribution, positional accuracy, and number of reference targets, and the type of the landscape, especially the height differences (**I**, **II**). The reference targets are normally the targeted GCPs, but also natural objects can be used as GCPs or tie points; in practice the entire object contributes the geometric calibration. Accurate elevation models are also increasingly used as reference targets (Pagnutti *et al*., 2002; Alamús *et al*., 2006). To enable direct measuremet of exterior orientations, a GPS base station should be available at the test field to collect reference data during the flight missions.

In order to achieve good determinability and accuracy from the self-calibrating bundle block adjustment (Section 2.4), a calibration set-up with highly convergent imaging configuration, orthogonal sensor angles around height axis, four or more images, and an object point field well distributed in three dimensions should be used (Fraser 1997; Fraser 2001; Grün and Beyer, 2001). In the airborne conditions the calibration set-up does not typically fulfill these recommendations. The target is flat compared with the object distance and the images have typically parallel optical axes; this results in strong correlations between the interior orientation parameters and the perspective center coordinates. Possible ways for carrying out interior orientation determination are the application of GPS or GPS/IMU observations of the perspective center coordinates (Wegmann and Jacobsen, 2002; Honkavaara, 2003; Merchant *et al*., 2004; **II**), the use of a test field with large height differences (Merchant, 1974), and the use of an image block with vertical and oblique images (Merchant and Tudhope, 1989).

Several permanent test fields for geometric calibration are currently in operation over the world. Well-known test fields are Vaihningen/Enz in Germany (Cramer, 2005), Fredrikstad in Norway (Nilsen, 2002a), Pavia in Italy (Casella and Franzini, 2005), Sjökulla in Finland (Section 3.2; **I**), USGS SSC (Pagnutti *et al.*, 2002), and USGS/OSU Madison (Merchant *et al.,* 2004); the USGS has recently established several test fields for geometric calibration (Stensaas, 2007; USGS, 2008). The photogrammetric sensor manufacturers also have test fields for geometric calibration: e.g. Elchingen (Dörstel, 2003; Hefele, 2006) and Herbrugg (Tempelmann *et al.,* 2003). The Fredrikstad, Sjökulla, and Vaihningen/Enz have been in operation already more than 10 years. The sizes of the test fields vary between 1 x 1 km^2 to 10 x 10 km^2. Numbers of GCPs vary between 30 and 200 and their accuracy is 1 cm or worse.

Empirical geometric evaluations have played a considerable role in the development of photogrammetric methods and sensors, taking the new methods into operational use, and assessing the

state of statistical control for photogrammetric processes. In the 1970s to the 1980s, geometric test fields were used for the performance analysis of film cameras (e.g. Salmenperä, 1972; Merchant, 1974; Kupfer, 1975; Brown, 1976; Kilpelä, 1981; Waldhäusl, 1986). Results from these tests and other similar tests form the basis for the modern self-calibration methods. International investigations on digital aerial triangulation (Jaakkola and Sarjakoski, 1996), automatic tie point extraction (Heipke and Eder, 1998), and GPS/IMU aerial triangulation (Heipke *et al.*, 2002b) were of great practical importance. The first EuroSDR investigation on geometric calibration aspects of digital photogrammetric sensors was completed in 2007 (Cramer, 2004; 2006; 2007b).

There exist already some examples of test field calibration as a part of photogrammetric production process. In Finland, the Finnish airborne remote sensing data producers use Sjökulla test field regularly for geometric system calibration (**I**). The National Land Survey determines the boresight misalignment parameters and improved interior orientation parameters of their analog camera/GPS/IMU systems at FGI test fields once or twice a year. Private companies operating large-format analog and digital photogrammetric sensors test field calibrate their systems at Sjökulla as well. Data providers using smaller format sensors also perform test-flights at Sjökulla in order to characterize and validate their systems and products. System calibration at the test field has also been a central part of the digital photogrammetric sensor purchasing process of Finnish mapping companies; the test flights reported in this work are part of extensive empirical tests that were carried out to evaluate the quality and technical performance of the sensors (Section 3.1). In USA, USGS is encouraging the data providers for the system calibration in test fields (Merchant *et al.*, 2004; Stensaas, 2007). Their current investigations concern the development of simple methods for geometric test field calibration and sensor stability evaluation.

Test fields for spatial resolution calibration

Popular artificial resolution targets in field testing are resolution bar targets, edge targets, and the Siemens star target (Section 2.5; Figure 7). The portable artificial targets are typically painted on plywood or hardboard (Hakkarainen, 1986) or on tarpaulin (Kuittinen *et al*., 1996; **I**), or they can be constructed using appropriate fabrics (**I**). Permanent artificial targets can be painted on a concrete slab or, for instance, gravel targets (Kuittinen *et al.,* 1994, Pagnutti *et al.*, 2002; **I**). Frequently used natural targets are sharp-edged lines with high contrast (border of roof and shadow, road, ditch in field, etc.). Central parameters of the resolution targets are their reflectance properties (especially contrast, uniformity, and spectral and multi-angular properties), size, direction, and the density of lines on the resolution bar targets (Pagnutti *et al.*, 2002; Ryan *et al.*, 2003; **I**).

Examples of resolution test fields can be found from the literature. In the 1970s and 1980s Hakkarainen (1986) established several portable resolution test fields painted on hardboard. For instance, a test field for RP and MTF calibration, suitable for flying altitudes from 600 m to 5 km, was 21 m x 22 m in size and its total weight was 1,600 kg. The USGS developed a permanent resolution test field in 1980s (Salamonowicz, 1982). The targets, a 43 m diameter Siemens star and two perpendicular resolution bar targets 6 m by 30 m, were painted on the roof of a building. Experience gained during one year of operation showed that the paints did fade rapidly. At the SSC V&V test field, edge targets are used to characterize spatial response; GSDs up to 1 m can be tested (Pagnutti *et al.*, 2002). The individual reflectance targets forming the edge target are 10 m x 20 m or 20 m x 20 m in size and they are painted on a concrete slab and tarpaulins. In the Sjökulla test field central resolution targets are permanent resolution bar targets constructed from gravel and a portable Siemens star constructed from light and dark fabrics (Figure 7; Section 3.2; **I**).

Airborne resolution tests were performed frequently in the 1970s and 1980s for characterizing the spatial resolution of the photogrammetric film cameras. Central research issues were the lens and film resolution and the influence of the FMC, camera mount, and environmental factors (Hakkarainen,

1986; Jaakkola *et al.*, 1985; Read and Graham, 2002). These tests had a significant role in the development of high-quality photogrammetric cameras. The satellite image spatial resolution is characterized using test fields. For instance, the NASA validates the satellite images used in the scientific work using edge response analysis (Blonski *et al.*, 2002; Ryan *et al.*, 2003).

Test fields for radiometric calibration

For the reflectance based vicarious radiometric calibration reflectance reference targets are needed. Portable artificial reflectance targets are typically painted on tarpaulin (e.g. Moran *et al.*, 1999; Pagnutti *et al.*, 2002; **I**; **V**). Permanent artificial targets can be painted on a concrete slab (Pagnutti *et al.*, 2002) or, for instance, constructed out of gravel (Kuittinen *et al.*, 1994; **V**). Possible natural targets are concrete parking lots, asphalt, dry lakebeds, deserts, water, and dense spruce forests (Dianguirard and Slater, 1999; Green and Pavri, 2001; Pagnutti *et al.*, 2002; Bruegge *et al.*, 2007). The central parameters of the reflectance targets are size and reflectance properties (Pagnutti *et al.*, 2002; **I**; **V**). In order to be able to determine accurate at-sensor radiances for the reflectance based calibration, the test site should contain devices for the measurement of the reflectance of the ground target, illumination at target, and properties of the atmosphere when a scene is imaged (Section 2.6; Dianguirard and Slater, 1999; Pagnutti *et al.*, 2002; **I**, **V**).

The test sites for vicarious radiometric calibration of satellite instruments typically have high probability of having clear skies, low aerosol loading, flat level terrain, uniform, high surface reflectance, and near lambertian reflectance characteristics for view angles slightly off nadir (e.g. alkali flats and dry lakebeds) (Dianguirard and Slater, 1999). At the SSC V&V test site the edge response targets described above, a portion of a concrete parking lot, and a relatively uniform grass field are used as reflectance reference targets (Pagnutti *et al.*, 2002; 2003). The site contains several spectroradiometers, solar radiometers, and a radiosonde weather balloon for *in situ* measurements. At Sjökulla, permanent gravel targets and a portable 8-step gray-scale can be used for the radiometric studies (Figure 7; **I**; **V**).

The vicarious methods are crucial for satellite systems because of the changes that take place and/or the inaccuracy of laboratory and on-board calibration (e.g. Schowengerdt, 1997; Dianguirard and Slater, 1999; Pagnutti, *et al.*, 2003; Bruegge *et al.*, 2007). Vicarious calibration is also used routinely for the verification of the airborne multispectral and hyperspectral sensors (Vane *et al.*, 1993; Cocks *et al.*, 1998; Chrien *et al.*, 2001; Green and Pavri, 2001). The vicarious radiometric calibration is a new issue for digital phtogrammetric large-format imaging systems.

Table 5. Research objectives and methods used in this study

1. To develop a prototype methodology for test field calibration
Designing a general calibration framework. (**I**; Section 2)
Summarizing properties of the Sjökulla test field and evaluating its usability for digital photogrammetric airborne imaging systems. (**I**; Section 3.2)
Developing necessary methods and software. (**I-V**; Section 3.2)
2. To investigate the need for test field calibration
Design and realization of comprehensive calibration flights in Sjökulla (several sensors, several flying heights, repetitive blocks). (**I-V**; Section 3.1)
Geometry (**II**; **III**; Section 3.2; 4.1; 5.1)
Developing a comprehensive simulation method. A simulation study on geometric potential of DMC, UltraCamD, and wide-angle analog frame camera.
Self-calibrating bundle block adjustments of DMC, UltraCamD, and analog frame camera blocks. Analysing parameters and residuals. Determining theoretical and empirical point determination accuracy.
Comparing simulated, theoretical, and empirical results.
Spatial resolution (**IV**; Section 3.2; 4.2; 5.1)
Quantifying influence of the oblique imaging geometry of the DMC
Panchromatic DMC images: Measuring RP and MTF. Analysing resolution as a function of radial distance from image center using linear regression. Investigating influence of flying direction and altitude. Evaluating performance of different resolution prediction methods.
Multispectral DMC images: Measuring MTF. Analysing influence of position and flying direction.
Radiometry (**V**; Section 3.2; 4.3; 5.1)
Investigating linearity, sensitivity, dynamic range, and absolute calibration of ADS40, DMC, and UltraCamD using a reflectance based vicarious calibration method.
3. To investigate the feasibility of system calibration in test field
Geometry (**I**; **II**; **III**; Section 2.7; 4.1; 5.1)
Considering feasibility to construct test fields for geometry. Evaluating geometric modeling, precision of parameters, theoretical expectations, and empirical point determination accuracy.
Spatial resolution (**I**; **IV**; Section 2.7; 4.2; 5.1)
Considering feasibility to construct test fields for spatial resolution. Evaluating spatial resolution modeling, precision of parameters, theoretical expectations, and spatial resolution of DMC.
Radiometry (**I**; **V**; Section 2.7; 4.3; 5.1)
Considering feasibility to construct test fields for radiometry. Evaluating radiometric model, precision of parameters, accuracy of absolute radiometric calibration, and radiometric quality.
4. To provide information on the performance of digital photogrammetric sensors and test field calibration
All the methods listed in 2.
5. To give recommendations for the calibration process of digital photogrammetric systems
Considering parameters that are needed and that can be determined in a laboratory and in a test field. Considering precision of parameters, stability of systems, and empirical accuracy. (**I-V**; Section 2; 4; 5.1; 5.2)
6. To give recommendations for the construction of photogrammetric test fields
Considering literature and experiences from Sjökulla. Considering the geometric, spatial resolution, and radiometric performance of sensors to be tested based on the obtained results. (**I**; Section 2; 3.2; 4; 5.1; 5.3)
7. To identify central new research topics
All the methods listed in 1-6; Section 6.

3 Materials and methods

The research objectives (Section 1.1) and methods are summarized in Table 5. Section 3.1 gives an overview of the materials used in this study. In Section 3.2, the developed prototype test field calibration methodology is briefly outlined, and some details of the research methods are given. More details on the study are given in **I**-**V**.

3.1 Empirical image materials (Papers II-V)

The digital image materials were collected using four UltraCamDs, one DMC, and one ADS40 over the period 2004-2006 (Table 6). The complete system calibration was performed only for the DMC. Older scanned film imagery collected using an analog frame camera (Leica Geosystems RC20) were used as reference materials in geometric studies. During the DMC mission, reflectance reference targets were measured using a goniospectrometer in field; these data were used to validate the laboratory reflectance measurements.

Most of the calibration flights were performed at the FGI Sjökulla test field (Section 3.2; **I**). The target of the missions was to evaluate system stability by collecting images from several altitudes and by making repetitive blocks with similar GSD and block structure. The disadvantage of the ADS40 was that, due to the integration time requirements, it was not possible to collect images with a smaller than 15 cm GSD with the high-speed aircraft used in the study. The analysis concentrated on images with small GSDs (8 cm or smaller), for which accurate reference targets were available. Details of the materials are given in the papers indicated in Table 6.

3.2 Calibration methodology (Papers I-V)

I presents a prototype methodology for test field calibration of digital photogrammetric airborne imaging systems. The components of the methodology are a test field with appropriate reference targets and measurement devices, software for data processing, measurement, and analysis, and a specified sequence of operations. **I** provides also recommendations for reference targets and calibration processes. The test field, process flow, and analysis methods are briefly discussed in the following.

Table 6. Empirical image materials. Analysed properties: G: geometry, SR: spatial resolution, R: radiometry.

Sensors	Date	GSD [cm]	Property	Paper
UltraCamD	11.10.2004	4	G	**II**
UltraCamD	14-15.10.2004	4, 8, 25, 50	G	**II**, **III**
UltraCamD	14.5.2005	4	G	**II**, **III**
DMC + goniospectrometer	1-2.9.2005	5, 8	G, SR, R	**III**, **IV**, **V**
ADS40	26-27.9.2005	15, 25	R	**V**
UltraCamD	1.7., 5.7. 2006	4, 8	R	**V**
RC20	24.4.2002	6.6	G	**II, III**
RC20	25.4.2002	8	G	**II, III**
RC20	9.9.2004	62	G	**II**

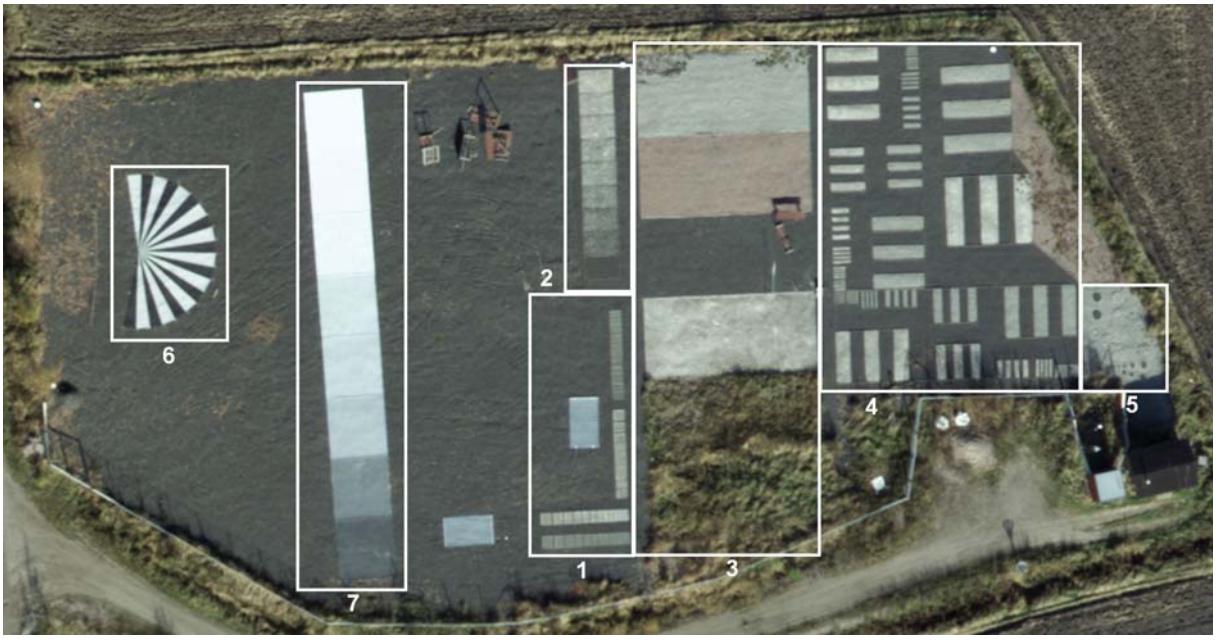

Figure 7. The Sjökulla image quality test field: 1) permanent dense resolution bar target, 2) permanent gray scale, 3) permanent reflectance targets, 4) sparse resolution bar target, 5) permanent circular targets, 6) portable Siemens star, and 7) portable gray scale.

Test field

The permanent Sjökulla test field together with some supplementary portable targets is a prototype photogrammetric test field (**I**). It was established in 1994. The Sjökulla test field consists of an image quality test field for radiometric and spatial resolution calibration (Figure 7) and networks of targeted benchmarks for geometric calibration at large, medium, and small imaging scales.

Permanent spatial resolution and reflectance targets made of gravel are special features of the Sjökulla test field. The gravel, combined with a proper substructure, forms a durable, weather-resistant concept for constructing spectrally, radiometrically, and geometrically well-behaving permanent reference targets; this has been proven with repetitive field measurements by a spectrogoniometer (**I**; Peltoniemi *et al.*, 2007). To complete the analysis of the gravel materials in **I**, the uniformity of the targets in images was analyzed based on standard deviations of DNs (Appendix 1). The standard deviations were 2.5-7% for DMC images with 5 cm to 38 cm GSD; as was expected, the standard deviation decreased when the GSD increased. With these targets a sufficiently accurate reference reflectance value, e.g. 1%, can be obtained by using an average value calculated over an appropriate object space window.

The Sjökulla test field is kept continuously in operation. The necessary maintenance actions are:

- GCPs: repairing, remeasurement of points on the soil, mowing the grass 1-2 times a summer.
- Gravel targets: cleaning out once a year, measurement of spectral properties once a year, changing the gravel materials every 3-10 years.
- Portable targets: installation and reinstallation for each mission, cleaning.
- In situ measurements during calibration flights (Figure 8).

Calibration process flow

The process flow for test field calibration in Sjökulla is shown in Figure 8. The process is divided into image data collection, reference data collection, and analysis sub-processes.

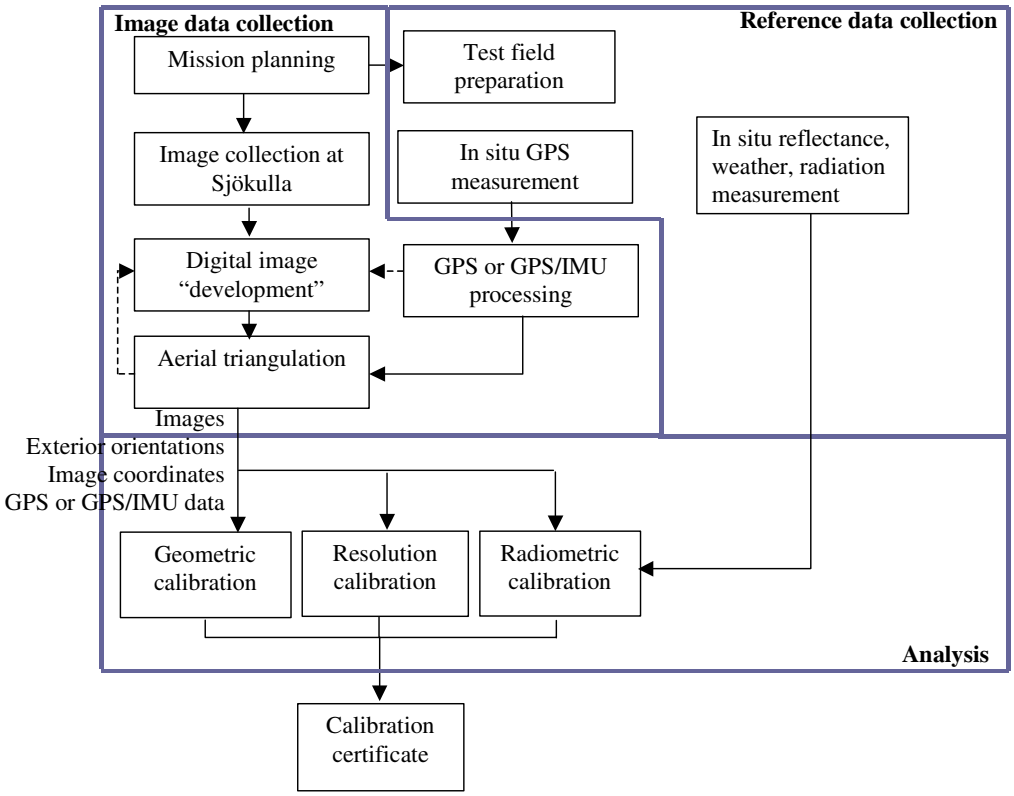

Figure 8. Process flow for the test field calibration.

The image data collection process begins with mission planning; important tasks are to specify the system, photogrammetric network, and conditions for the calibration flight (Table 2; **I**). During the mission, information about the conditions should be collected in order to be able to specify the conditions in which the calibration was determined. After the mission, the image data and GPS or GPS/IMU data are post-processed. The process ends with aerial triangulation.

The reference data collection sub-process ensures that the necessary reference targets are installed at the test field. During the mission, GPS reference data are collected, and the measurements for the reflectance-based radiometric calibration method are carried out (**I**; **V**).

The test field calibration process ends with the analysis process (**I-V**); the methods are briefly described below.

The calibration process can be automated to a considerable extent by implementing permanent targets and measurement devices on the test field and by using automatic methods for the measurement and analysis. In the Sjökulla prototype process, many of the steps require interaction. In the reference data generation phase, time-consuming and logistically difficult tasks include the installation of the portable targets and carrying out the necessary measurements during the image data collection. Interactive measurement of the GCPs in images is also laborious and probably not as accurate as automatic measurement could be. At Sjökulla, the automation of GCP measurement is difficult because of the relatively small size of the targets and the shadows and obstructions caused by the surrounding objects.

Calibration accuracy

Calibration is a refined form of measurement (Eisenhart, 1963). In principle, the general factors influencing the output of the digital photogrammetric imaging system also affect the calibration result (Table 2). The central components of the calibration system influencing calibration accuracy are the photogrammetric network and the measurement and calculation methods. To minimize the influences of environmental conditions, the calibration flight should be performed in a setting where there is a

clear atmosphere, good visibility, high solar elevation angle, and low turbulence. The performance of the Sjökulla prototype methodology is evaluated in this study (Section 4; 5).

Geometric calibration

Geometric calibration is based on self-calibrating bundle block adjustment (Section 2.4). The test fields for geometric calibration at Sjökulla are described in **I** and the calibration method and parameters are presented in **II**.

The empirical results in **II** were the motivation for developing a comprehensive four-step method for analysing the geometric performance of imaging systems in **III**. The steps are the following:

1. The theoretical geometric performance of the system is evaluated in the absence of systematic errors by means of simulation. Because of geometric differences, the accuracy models developed for film cameras are not valid for digital systems, and different digital systems require different accuracy models. Accuracy models can be determined for different photogrammetric products, such as image blocks, stereo models, or orthophotos.
2. The sufficiency of the geometric system model is evaluated empirically by analysing systematic distortions. In this study, systematic image distortions were assessed by evaluating averages of image residuals (**II**, **III**). The averaged residuals significantly different from 0 indicate non-modeled distortions but do not show the exact magnitude of the distortions (Förstner and Wrobel, 2004).
3. If systematic distortions appear, their influences on end products are evaluated by simulation. In order to perform this evaluation accurately, the distortion model should be known, which was not the case in this study.
4. Finally, the empirical results and theoretical expectations are compared. The theoretical expectations can be assessed e.g. by simulation or by utilizing the block adjustment statistics.

The limitation of the flight missions was that accurate exterior orientation information was not collected. The data were not suitable for interior orientation determination because the Sjökulla test field is flat (terrain heights in the area used for geometric calibration of large-scale imagery are 35 to 60 m; **I**) and the blocks were optimized for the calibration with GPS/IMU support (no convergent images). Due to these limitations, the analysis concentrated on the accuracy assessment.

Mainly the 10-parameter physical model without principal distance was used for self-calibration (Section 2.4; **II**). For the most part, FGI FGIAT software was used in the analysis (Honkavaara, 2003; 2004; **II**, **III**). In the FGIAT, the additional parameters can be assigned to each panchromatic camera head of the DMC and UltraCamD. The FGIAT contains also efficient tools for simulation.

Various estimates were used to evaluate the accuracy of a photogrammetric block:

- *Standard error of unit weight,* $\hat{\sigma}_0$ (Equation 3), characterizes the tie point accuracy; it consists mainly of the tie point measurement precision and systematic image distortions.
- *Theoretical accuracy:* standard deviations of the adjusted object coordinates given by the block adjustment (Equation 2).
- *Simulated accuracy*: accuracy of the object coordinates given by simulations.
- *Empirical accuracy*: differences of the adjusted and reference coordinates of checkpoints.

In practice, the theoretical and simulated accuracy show how precise the tie point coordinates are, because the majority of the adjusted points are tie points. The empirical accuracy shows how accurate well-defined targeted points are. RMSEs, minimums, maximums, averages, standard deviations, and error vector plots were evaluated.

Spatial resolution calibration

The spatial resolution targets and calibration methods are described in **I** and **IV**.

The RP was obtained from the dense resolution bar target (Figure 7) using an automatic method (Kuittinen *et al.*, 1996; Ahokas *et al.*, 2000; **IV**). The MTF was obtained from the Siemens star (Figure 7; **IV**) using a method based on the method developed by Reulke *et al.* (2006) and Becker *et al.* (2005; 2006). The MTF was modeled using the Gaussian shape function:

$$scale \cdot MTF(K) = e^{-2\pi^2 \sigma_{PSF}^2 K^2}, \tag{4}$$

where K is the frequency as cycles/pixel, σ_{PSF} is the standard deviation of a Gaussian point spread function, and *scale* is a scaling parameter (**IV**). The adjustment was performed using a numerical method, and thus no precision estimates were obtained for the parameters; $\hat{\sigma}_0$ (Equation 3 with C_{ll} = I) is used as the precision indicator.

The influence of the distance from the image center on the resolution was analysed using the ordinary least squares regression (Pindyck and Rubinfeld, 1991). The significance of the regression parameters was evaluated using t-test, and the significance of differences between various regressions was evaluated using F-test, both with a 95% confidence level.

The RP of the DMC panchromatic images was predicted with five methods: 1) based on sampling (84 lines/mm), 2) based on sampling and the convergent image geometry (84 lines/mm at image center, 53-60 lines/mm at image corner; Section 4.2; **IV**), 3) based on sampling, image tilt, and a uniform lens resolution of 84 lines/mm (59 lines/mm at image center, 45-49 lines/mm at image corner), 4) 1.5 times RP based on sampling (56 lines/mm; a rule of thumb for digital systems; Graham and Koh 2002), and 5) the empirical model determined at the test field (Section 4.2). Approaches 1-4 are based on technical information of the DMC. In 2, 3, and 5, a linear dependence on the radial distance from the image center is assumed.

Radiometric calibration

The reflectance reference targets and a method for radiometric calibration are presented in **I** and **V**.

The 8-step gray scale of the FGI was used as the reflectance reference target (Figure 7). The system absolute radiometric response was modeled using a linear model:

$$L_{tb} = cal\_gain_b DN_{tb} / time_b + cal\_offset_b \tag{5}$$

where $time_b$ is the integration (exposure) time in ms; cal_gain_b and cal_offset_b are the parameters of the linear model; L_{tb} and DN_{tb} are an average at-sensor radiance and average DN calculated in a small target t window in band b, respectively. The parameters were obtained by the ordinary linear least squares regression.

The limitations of the missions were that the atmospheric and illumination data were not collected during the test flights and that the reference targets had not been calibrated comprehensively. The laboratory-determined target spectral reflectance at nadir and the MODTRAN 4 default atmospheric models were used (Berk et al., 2003; **V**). Due to these limitations, the calibration could only be performed partially (**V**). The results of the linearity and dynamic range evaluations can be considered reliable, while the sensitivity and absolute calibration results should be considered indicative. The relative empirical accuracy of absolute calibration was evaluated by determining the calibration using subsets of the reference targets and evaluating the accuracy with the remaining targets. This accuracy evaluation is considered to be relative, because the accuracy of the atmospheric correction was not known.

4 Results

Results of the geometric, radiometric, and spatial resolution calibration are given in **II**-**V**; in this section the central results are summarized. Combining the results of various properties provided additional insight to the accuracy analysis and prediction of spatial resolution and radiometry; because of this some extended results are given in Sections 4.2 and 4.3.

4.1 Geometric calibration (Papers II and III)

The geometry of three technically similar UltraCamDs and one DMC was calibrated; three Leica RC20 blocks were used as reference (Table 6). In one of the UltraCamD missions, blocks were collected with a 4 cm, 8 cm, 25 cm, and 50 cm GSD, and three repetitive blocks with an 8 cm GSD were collected during two days; for the other two UltraCamDs, only single blocks with a 4 cm GSD were available (**II**). The DMC was calibrated using blocks with 5 cm and 8 cm GSD; repetitive blocks with an 8 cm GSD were collected on two consecutive days (**III**).

In **III** the ideal geometric performance of the DMC, UltraCamD, and an analog wide-angle frame camera was evaluated using the simulation method (Section 3.2). The important results were point determination accuracy models (coefficients) for various block structures, sensors, and control configurations. Variables of the models include scale factor and pointing accuracy (image point precision) as fractions of the pixel size (*pixel size/n*). Due to the differences in FOV, and especially in the base-to-height ratio (B/Z ratio), the theoretical accuracy estimates were the best for the wide-angle analog camera and the worst for the UltraCamD (**III**: Table 3). For instance, the expected point determination accuracy (RMSE) of normal mapping blocks with 60% forward overlap and 20% side overlap is approximately *GSD/n* in horizontal coordinates and *GSD/(n/3.5)* for the DMC and *GSD/(n/4)* for the UltraCamD in height. Experience in automatic tie point measurement has shown that presenting the image point precision as fractions of pixel size is a feasible approach (Förstner, 1995; Heipke and Eder, 1998). Analysis of $\hat{\sigma}_0$ of empirical Sjökulla blocks indicated that the best tie point measurement precision for the DMC and UltraCamD was approximately *pixel size/6* (*n=6*) (**II**; **III**).

The presumption was that the large-format multi-head images of UltraCamD and DMC were geometrically correct and distortion free (Section 2.4), but the analysis of the image residuals showed that the images contained multi-head distortions (**II**, **III**). The available software did not have additional parameter models for these distortions. An option was added to the FGIAT software so that the available additional parameters could be assigned to each camera head (Section 3.2). In many cases the multi-head parameters reduced the multi-head distortions, but the optimum parameters were not investigated in this study (**II**, **III**).

Typically, most of the parameters of the physical additional parameter model were significant. This distortion model was not optimal, but a better description of the data was obtained with it than without additional parameters. For instance, the principal point corrections were 1-64 µm for the UltraCamD (**II**). These values are not reliable due to correlation with the perspective center coordinates. What are more interesting are the precision estimates, which were 2-5 µm. Calibration parameters obtained from various blocks showed similar trends, but some variations also appeared. Further evaluations of the parameters were not performed because the models were not correct and the data were not optimal for the model determination (Section 3.2).

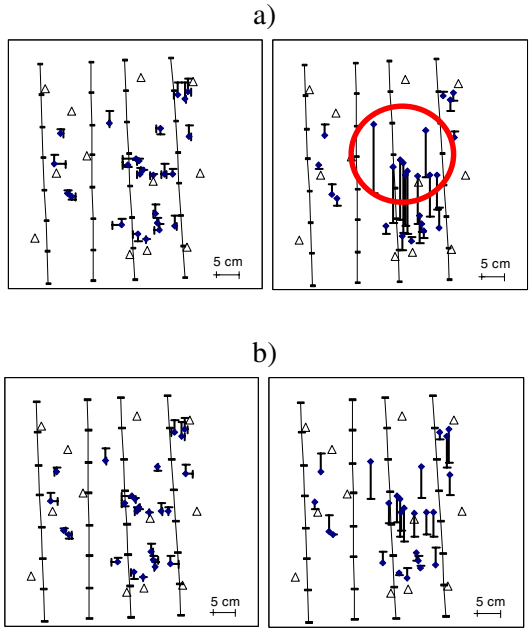

Figure 9. UltraCamD, GSD=4 cm, errors at independent checkpoints in horizontal (left) and height (right) coordinates; the flight lines and perspective centers are given; GCPs are marked as triangles. a) No self-calibration and b) self-calibration using single-head physical parameters.

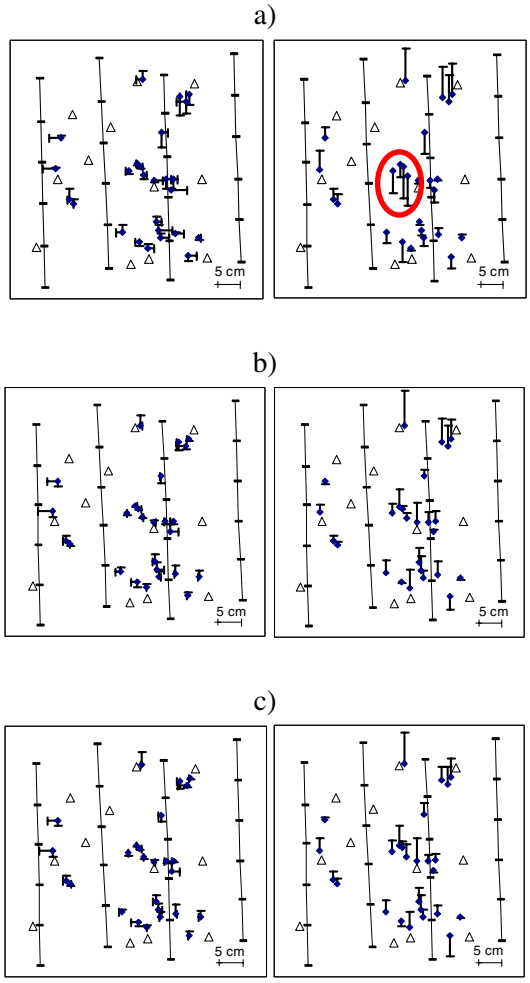

Figure 10. DMC, GSD=5 cm, errors at independent checkpoints in horizontal (left) and height (right) coordinates; the flight lines and perspective centers are given; GCPs are marked as triangles. a) No self-calibration, b) self-calibration using single-head physical parameters, and c) self-calibration using multi-head physical parameters.

The errors at the checkpoints for the UltraCamD and the DMC blocks with four image strips, 60% forward and side overlaps, and 12 GCPs are shown in Figure 9 and Figure 10. Systematic block deformations appeared with both systems, especially in the height coordinate. The deformations were more serious when self-calibration was not performed (Figure 9a, Figure 10a), but self-calibration did not eliminate the deformations entirely (Figure 9b, Figure 10b,c). Block height deformations in the central area of the block were estimated by calculating averages and standard deviations in the deformed area (marked by a circle in Figure 9a and Figure 10a). The averages and standard deviations were -10.3 cm and 2.2 cm for the UltraCamD, and -4.5 cm and 1.6 cm for the DMC when self-calibration was not performed. With self-calibration (single-head physical model) the corresponding values were -5.2 cm and 1.3 cm for the UltraCamD and 2.0 cm and 1.2 cm for the DMC, respectively. For the DMC, the multi-head parameters compensated for the multi-head systematic residuals at image coordinates more efficiently than the single-head parameters, but both parameter sets provided similar empirical accuracy (Figure 10b,c; Figure 11; **III**). The sparse checkpoint distribution did not enable detailed analysis of the distribution of the block deformations. The height deformations were apparent also in the block statistics (averages, RMSEs, and standard deviations of the errors) (**II**; **III**).

The simulated, theoretical, and empirical point determination RMSEs (Section 3.2) for a block with four strips, 60% forward and side overlaps, and 12 GCPs are shown in Figure 11. In simulations, the value σ_0=3 µm was used as a pointing accuracy for the analog camera to obtain the accuracy of targeted points. Two values were used for the digital systems: σ_0=*pixel size/6* corresponding to the

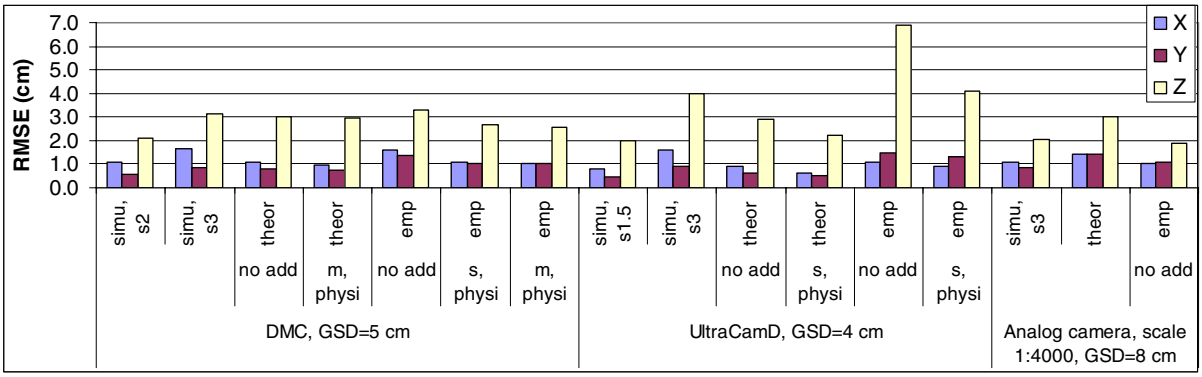

Figure 11. Simulated (simu; the number after s shows the σ_0), theoretical (theor), and empirical (emp) point determination RMSE for the example blocks (details are given in the text).

pointing accuracy of tie points and σ_0=3 μm corresponding to the pointing accuracy of targeted points at film images. The simulated accuracy for digital images with σ_0=*pixel size/6* was better than the empirical accuracy. The simulation with σ_0=3 μm provided the best correspondence with the empirical accuracy for the UltraCamD, while the simulation with σ_0=2 μm provided the best correspondence for the DMC. Theoretical accuracy was often better than empirical accuracy for the digital systems, while for the analog camera the opposite was true (Figure 11; **II**; **III**).

The empirical results of the example blocks above indicated relatively high geometric accuracy potential (Figure 11). With the best calibration models, the empirical accuracy of the DMC was 0.2 GSD in X and Y and 0.5 GSD (0.05‰ of the object distance, H) in height. The corresponding values for the UltraCamD were 0.2-0.3 GSD and 1.0 GSD (0.09‰ H). The systematic height deformations in the central areas of the example blocks were for the UltraCamD 2.5 times and for the DMC less than 1 times the theoretical height determination accuracy when self-calibration was performed (Figure 9, Figure 10, Figure 11). Without self-calibration, the values were 4.5 and 1.5, respectively.

In most cases the accuracy was poorer especially in the height coordinate if self-calibration was not performed. In the case of DMC, the self-calibration improved the height RMSE up to by a factor of 1.3 in comparison to the adjustments without self-calibration (**III**). For the UltraCamD, the maximum height RMSE improvement factor was 3.4 (**II**). Increasing the image overlaps in the block typically improved the accuracy (**II**, **III**). Simulations in **III** indicated that the block deformations caused by the image distortions could be reduced by using GPS/IMU support and by increasing block overlaps.

The images of all three UltraCamDs contained multi-head distortions, but the distortion pattern varied (**II**). One of the tested UltraCamDs did not function correctly, which appeared in the form of exceptionally bad point determination accuracy, poor $\hat{\sigma}_0$, and large systematic distortions (**II**). In the case of two repeated DMC blocks, the second day block provided a slightly better $\hat{\sigma}_0$ (2.28 vs. 2.12) and empirical height accuracy (2.5 cm vs. 2.0 cm) and smaller block height deformations than the first day block (**III**). With both DMC and UltraCamD, the repeated blocks showed some similarities (e.g. similar distortion patterns and self-calibration parameters in many cases). This indicated some level of stability, also with respect to altitude, but some unexplained instability appeared as well (**II**, **III**).

The estimated accuracy of the GCPs at the Sjökulla large-scale test field is 1.0 cm in horizontal coordinates and 2.0 cm in height (**I**). The best empirical RMSE was 1.0 cm in horizontal coordinates and 1.2 cm for height. These values were obtained for the DMC block with 5 cm GSD, 12 GCPs, 8 flight lines, and multi-head physical additional parameters. These results indicated that GCP accuracy could be better than the estimated accuracy, at least for the height coordinate. It is likely that the

limited accuracy of checkpoints made the empirical accuracy estimates slightly pessimistic when accuracy was high, but it did not influence the analysis of the height deformations.

4.2 Spatial resolution calibration (Paper IV)

In the empirical spatial resolution calibration study, DMC images with 5 cm GSD (block d1_g5) and 8 cm GSD (blocks d1_g8a, d1_g8b) were used; two blocks with an 8 cm GSD were collected over consecutive days (Table 6; **IV**). The effect of the distance from the image center, the altitude (500 m and 800 m), and the flying direction were evaluated. In this section, the central empirical results are summarized, and extended analysis concerning the empirical modeling and prediction of the spatial resolution is presented.

The MTFs of the high-resolution panchromatic images and the low-resolution multispectral images were determined using the Siemens star. The Gaussian fitted well with the observations (**IV**); $\hat{\sigma}_0$ of the adjustment of the MTF observations to the Gaussian was less than 3.5%, and the RMSEs were 1.8-2.8% (Appendix 2). The undulations of the MTF observations caused by the topographic variations of the Siemens star were considered insignificant. In the case of multispectral images, it is possible that the dimensions of the reference target caused optimistic bias (**IV**). The RPs of the panchromatic images with 4 cm and 8 cm GSDs were determined using the dense 4-bar target. It appeared that the line width range (3-12 cm) was not adequate for reliable RP determination from images with an 8 cm GSD. Lines wider than 1.5 times GSD cannot be measured with this target, which caused optimistic bias (Figure 12).

Panchromatic images

The resolution of the panchromatic images weakened as the distance from image center increased; the resolution reduction factor from the image center to the image corner was up to 2 (Figure 12; **IV**). One important reason for this behavior in the case of the DMC is the oblique construction of the system. Theoretical evaluation showed that the resolution reduction factors from the nominal 12 µm pixel size, caused by the image tilt, are at their maximum 1.6 in the cross-flight direction and 1.4 in the flight direction in the corners of the image (**IV**).

The effect of position on spatial resolution was modeled using a linear model as the function of the radial distance from the image center. The intercept indicates the resolution at the image center, and the slope indicates the resolution decrease with the increasing distance from the image center. In the case of DMC, the rigorous approach is to model the resolution as a function of the x and y coordinates (**IV**). The difference of the simplified and rigorous approaches is less than 6 lines/mm in RP (RMSE is less than 2 lines/mm), and the simplified approach is slightly optimistic at image center. The regression statistics for the RP, 10% MTF, and σ_{PSF} are given in Table 7 (corresponding to Figure 12 and **IV**; the RP statistics of the images with an 8 cm GSD are not given due to the optimistic bias). The statistics indicated a significant linear fit at a 5% confidence level, excluding σ_{PSF} in the cross-flight direction with the imagery with a 5 cm GSD. The imagery with a 5 cm GSD gave a lower slope in the cross-flight direction than in the flight direction; the slopes of the imagery with an 8 cm GSD were similar in flight and cross-flight directions; the slopes in the flight direction were similar for all evaluated image blocks. The non-optimal distribution of observations (only one observation close to image center) or some physical phenomenon could explain the lower slope of the images with a 5 cm GSD. $\hat{\sigma}_0$ of the RP and 10% MTF regression was 4 to 8 lines/mm. The linear regression models in Table 7 are empirical spatial resolution models of the panchromatic DMC images.

Due to the image tilt, the resolution should be better in the flight direction than in the cross-flight direction. The empirical results showed the opposite (Figure 12; **IV**).

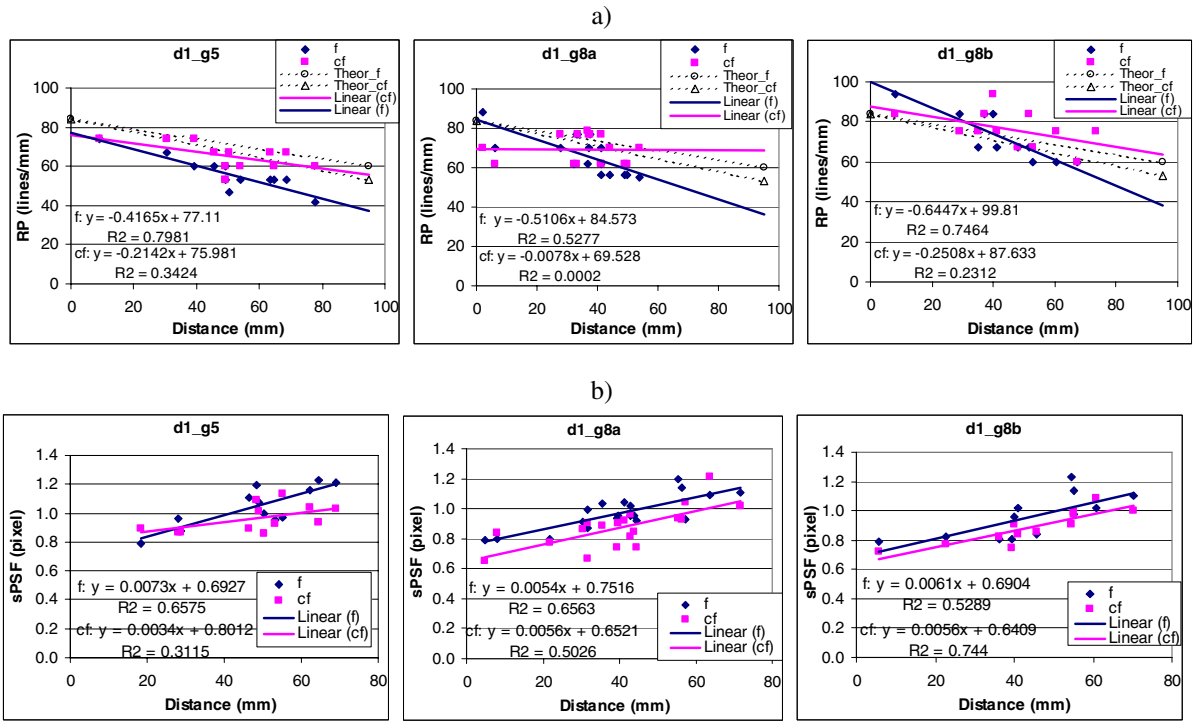

Figure 12. Resolution as a function of the distance from the image center: a) RP and b) σ_{PSF}. Blocks from left: d1_g5, d1_g8a, and d1_g8b; f: resolution in flight direction, cf: resolution in cross-flight direction. The dashed lines in a) show the expected resolution based on the sampling and image tilt. Regression statistics are given also in Table 7.

Table 7. Statistics of the spatial resolution regression. $\hat{a}$: slope, $\hat{b}$: intercept, $\hat{\sigma}_{\hat{a}}$, $\hat{\sigma}_{\hat{b}}$: standard deviations of slope and intercept, R^2 coefficient of determination, $\hat{\sigma}_0$: standard error of unit weight in lines/mm or in pixels, f: flight direction, cf: cross-flight direction. The results with significant slope parameters are shaded.

Block	Measure	cf						f					
		$\hat{a}$	$\hat{b}$	$\hat{\sigma}_{\hat{a}}$	$\hat{\sigma}_{\hat{b}}$	R^2	$\hat{\sigma}_0$	$\hat{a}$	$\hat{b}$	$\hat{\sigma}_{\hat{a}}$	$\hat{\sigma}_{\hat{b}}$	R^2	$\hat{\sigma}_0$
d1_g5	RP	-0.21	75.98	0.09	4.99	0.3	5.75	-0.42	77.11	0.07	3.52	0.8	4.05
d1_g5	10% MTF	-0.22	70.27	0.09	4.69	0.3	4.82	-0.43	76.25	0.09	4.61	0.7	4.74
d1_g8a	10% MTF	-0.43	83.99	0.11	4.64	0.5	7.75	-0.36	74.05	0.06	2.43	0.7	4.06
d1_g8b	10% MTF	-0.42	84.16	0.07	3.39	0.8	4.18	-0.40	78.49	0.11	5.01	0.6	6.19
d1_g5	σ_{PSF}	0.003	0.80	0.002	0.08	0.3	0.08	0.007	0.69	0.002	0.08	0.7	0.09
d1_g8a	σ_{PSF}	0.006	0.65	0.001	0.06	0.5	0.10	0.005	0.75	0.001	0.04	0.7	0.07
d1_g8b	σ_{PSF}	0.006	0.64	0.001	0.05	0.7	0.06	0.006	0.69	0.002	0.09	0.5	0.11

It appeared that two blocks with an 8 cm GSD yielded quite similar results and that the imagery with an 8 cm GSD provided slightly better resolution than the imagery with a 5 cm GSD (**IV**). The F-test indicated that only the regressions of the block with a 5 cm GSD and the second day block with an 8 cm GSD were significantly different in the cross-flight direction. Comparison of two blocks with an 8 cm GSD indicated that the first day block provided slightly worse resolution than the second day block, but that difference was not significant with a 95% confidence level.

The empirical RP for the imagery with a 5 cm GSD was between 40 and 80 lines/mm (Figure 12). The RP and 10% MTF were similar in the flight direction; RP was approx. 2 lines/mm (3%) higher than 10% MTF. In the cross-flight direction the RP and 10% MTF were slightly different, the RP was approximately 6 lines/mm (9%) higher than the 10% MTF.

The σ_{PSF} was between 0.7 and 1.2 pixels (Figure 12b). Examples of the worst (σ_{PSF} = 1.2 pixels), best (σ_{PSF} = 0.7 pixel), and average (σ_{PSF} = 1 pixel) Gaussian PSFs are shown in Figure 13. In the worst case, the point spread was approximately ±4 pixels.

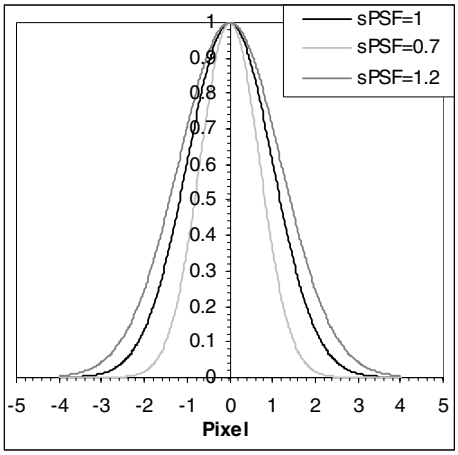

Figure 13. Examples of the Gaussian point spread function with different σ_{PSF} values.

The accuracy of prediction methods (Section 3.2) was assessed by calculating RMSEs of prediction errors at each observation. The RP estimates based on technical information were evaluated using the RP measurements of the block with a 5 cm GSD and the 10% MTF measurements in the flight direction (Figure 14a, b). The empirical regression model (the 10% MTF model based on the first day block with an 8 cm GSD) was evaluated using the 10% MTF measurements of other two blocks (Figure 14b). The empirical model provided the best results; the RMSE was 4-7 lines/mm, and estimates were not seriously biased (this was an expected result due to the similarity of the regressions). The RP prediction based on the sampling and image tilt was more accurate in the cross-flight direction (RMSE ≈ 7 lines/mm) than in the flight direction (RMSE 13-16 lines/mm). The RP predictions based on sampling and on sampling and tilt were optimistic, while the RP predictions based on sampling, tilt, and lens, and on the 1.5 RP-rule were pessimistic.

The average true GSD for the panchromatic images, derived from the AWAR of 10% MTF, was approximately 1.4-1.5 GSD for the images with a 5 cm GSD and 1.3-1.5 GSD for the images with an 8 cm GSD (**IV**).

Multispectral images

The distance from the image center did not significantly influence the MTFs of the DMC low-resolution multispectral images (GSD = 22 cm) (**IV**). The AWAR values (based on 10% MTF) were approximately 80 lines/mm for red and NIR channels and 84 lines/mm for blue and green channels, which corresponds approximately to the RP derived from the sampling interval.

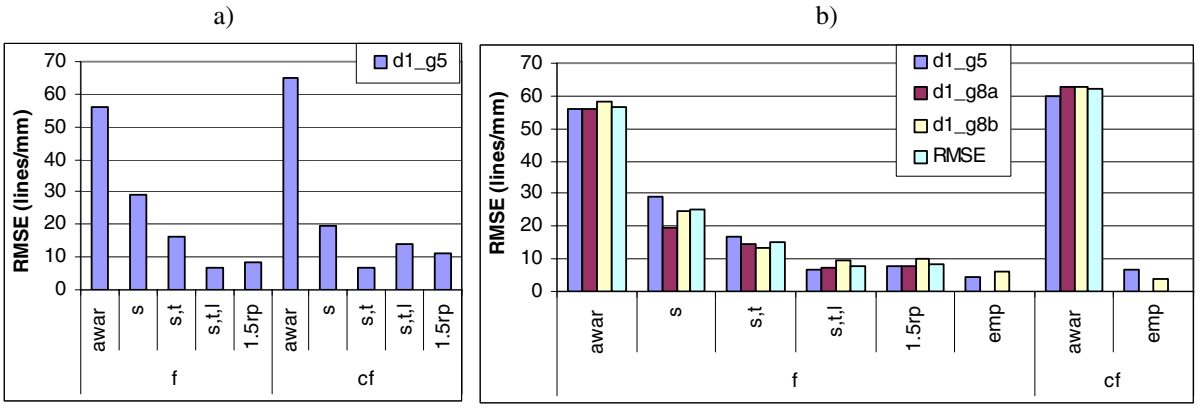

Figure 14. RMSEs of different prediction methods using a) RP measurements and b) 10% MTF measurements as reference (awar: AWAR; s: sampling; t: image tilt; l: lens; 1.5rp: 1.5 RP rule; emp: empirical regression model; f: flight direction; cf: cross-flight direction; blocks: d1_g5, d1_g8a, d1_g8b).

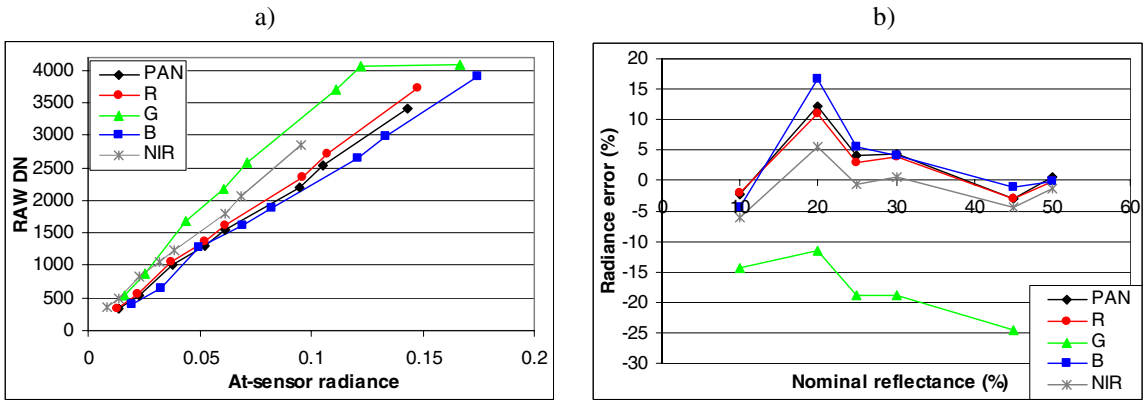

Figure 15. DMC radiometry evaluation, GSD=5 cm. a) DNs plotted as the function of at-sensor radiance. b) Absolute calibration residuals as a % of radiance, 5% and 70% targets were used as a reference (5% and 50% for the green channel).

Case	Model	Calibration targets	Check targets
8	Gain, offset	All	All (no 20%)
8g	Gain	All	All (no 20%)
4	Gain, offset	5, 25, 45, 70	10, 50
2	Gain, offset	5, 70	10, 25, 30, 45, 50
1	Gain	30	5, 10, 25, 45, 50, 70

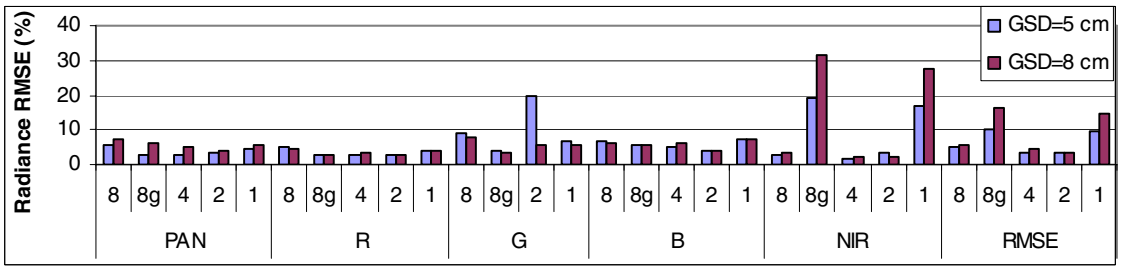

Figure 16. RMSE of absolute radiometric calibration in % of the radiance for the DMC images with 5 and 8 cm GSD. The numbers below the bars refer to the table above showing the calibration model and the calibration and check targets used. For the green channel the 50% target was the brightest target used.

4.3 Radiometric calibration (Paper V)

The ADS40, UltraCamD, and DMC were radiometrically test field calibrated (**V**). For each sensor two different altitudes were used. In the following, the analysis in **V** is completed with the evaluation of the accuracy of the absolute calibration.

The systems were linear in response (**V**). As an example, radiometric response plot of one DMC image is shown in Figure 15a. In some cases, however, nonlinearity appeared. Some of the channels of the DMC and UltraCamD were saturated in some images at bright reflectance values, which appeared as non-linearity (for instance, the green channel in Figure 15a). Nonlinearity appeared also with the 20% reflectance target because of the inaccuracy of the reference value (see below).

The A/D-conversion is made with 12 bits for the DMC and with 14 bits for the UltraCamD and ADS40. The DMC used the 12-bit dynamic range entirely, while UltraCamD and ADS40 panchromatic channel indicated a close to 13-bit dynamic range (**V**). The dynamic range of the ADS40 multispectral channels was as low as 9-10 bits. This evaluation did not take the system noise into account, which makes the dynamic range estimates slightly optimistic (the expected noise is < 1%). Differences in the sensitivity of various channels was the smallest for the DMC and the largest for the

ADS40 (**V**). The solar elevation angle was approximately 28˚ for the ADS40, 35˚ for the DMC and 50˚ for the UltraCamD.

The absolute radiometric calibration was determined for the DMC and ADS40 (**V**). Either the linear model with gain and offset parameters or with the gain parameter on its own was appropriate for absolute calibration. The precision of the gain parameters was 1-2% for the DMC (4-8 targets) and 3-5% for the ADS40 (5 targets).

The errors in the check reflectance targets are given for one DMC image with a 5 cm GSD in Figure 15b; the darkest and brightest targets were used for the calibration. The errors were clearly greater for the 20% target than for other targets, which indicated outlier. The errors in the green channel were clearly larger than the errors in other channels; this was caused by the saturation of the green channel at greater than 45% reflectance. The saturation is an outlier, which caused bias to the calibration parameters and deterioration of accuracy. The errors were less than 6%, excluding the green channel and the 20% target.

The absolute radiometric calibration RMSEs for the DMC with single and two-parameter models and 1-8 reference targets are given in Figure 16 (single images with 5 cm and 8 cm GSD). The single and two-parameter models provided similar accuracy, excluding the NIR channel, which had a significant offset parameter. The single-parameter model gave better RMSE than the two-parameter model for PAN, red, and green channels when all eight targets were used for calibration; the erroneous 20% target caused this unexpected performance. The average RMSEs for the red, blue, NIR, and PAN channels were 3.3-4.5% when the 20% target was not included in the evaluation, 2-4 reference targets, and the best fitting models were used. The green channel was not saturated at images with 8 cm GSD, and its performance was similar to other channels. The major error source in this analysis is the reference reflectance error, which was estimated at 5-10% (**V**).

5 Discussion

Based on the results of this study, conclusions about the performance of the digital photogrammetric imaging systems are made (Section 5.1), recommendations for the calibration process of the systems are presented (Section 5.2), and recommendations for photogrammetric test fields are given (Section 5.3). The proof for the hypothesis is derived in Section 5.4.

5.1 Performance of digital photogrammetric airborne imaging systems

Geometry

The geometric calibration investigation concentrated on the accuracy assessment. A fundamental empirical result was the detection of the distortions in the multi-head images, which caused block deformations. The sensor manufacturers did not provide information on these distortions, nor did they provide tools for compensating for them (Section 2.4). The self-calibration with single and multi-head additional parameters partially compensated for the distortions and improved the point determination accuracy. With self-calibration, the systems could be considered high quality photogrammetric instruments (Kraus, 1993). Without self-calibration substantial systematic height deformations appeared, 1-5 times the theoretical accuracy expectations; this is intolerable in many photogrammetric applications. The empirical blocks were optimized for calibration and had high side-overlap percentages. The simulations indicated that larger height deformations could be expected for the typical mapping blocks, e.g. with 20% side overlaps.

Empirical, simulated, and theoretical point determination accuracy were compared. The point determination accuracy predicted by the model based on simulation appeared to be consistent with the empirical RMSE. However, in order to provide realistic accuracy estimates for particular objects by simulation, their measurement precision should be known. For instance, the pointing accuracy of targeted points in digital images is not accurately known. The experience with analog systems is that if systematic image distortions do not distort results, the empirical accuracy, obtained with targeted checkpoints, is better than the theoretical point determination accuracy, which corresponds accuracy of natural tie points (Section 3.2). This is mainly caused by the inferior pointing accuracy of natural tie points. Contrary to these beliefs, however, the empirical accuracy of the digital images was in many cases worse in this study than the theoretical accuracy; the image distortions and the possible higher precision of the automatic tie point measurement than the interactive GCP measurement in digital images could possibly explain this behavior. Despite the agreement of the various estimates, the theoretical estimates were not representative in all cases because of systematic block deformations.

The geometric performance of the DMC and UltraCamD did not quite fulfill expectations. The digital systems provided similar or worse empirical accuracy (RMSE) than analog cameras. Also, the simulations indicated that the wide-angle analog camera provided better height accuracy for well-defined objects than the digital systems. The conclusion could be different for different objects; for example, it is expected that the pointing precision of indistinct natural objects could be much better for digital sensors than for analog sensors due to the better radiometry. For instance, Perko *et al.* (2004) has demonstrated the superior matching accuracy and success rate of digital systems. It is also important to notice that the use of larger forward overlaps is a feasible approach for improving the height accuracy in the case of digital sensors (**II**). But again it should be emphasized that in order to obtain the full accuracy potential from digital systems, image distortions should be sufficiently compensated for.

Realistic and reliable predictions of the output product accuracy (especially the bias) could not be provided by test field calibrating the image acquisition system only. Thus, the calibration (or validation) of the output products is necessary to assess the image product generation system performance accurately. When the system is stable and the distortion model and pointing precision is known, a significant part of the empirical testing could be replaced with the simulation technique described in Section 3.2. Of course, it is possible to use large confidence intervals; inaccurate information of the sensor performance would then be sufficient, but this would lead to non-optimal utilization of the sensors.

The above discussion indicated the consequences of insufficient system modeling. In order to reliably and optimally use the systems, the systematic image distortions should be assessed, their influence should be investigated, and they should be reported in the calibration documentation. It was concluded that the most convenient way to deal with the distortions would be to compensate them using appropriate sensor models in the image data post-processing (**II**).

The empirical results are consistent with other recently published results. Alamús *et al.* (2006), Büyüksalih and Jacobsen (2006), Kruck (2006), and Baz *et al.* (2007) detected similar multi-head distortions in the DMC and UltraCamD images. Results of the EuroSDR empirical test also showed multi-head image distortions (Cramer, 2007b). In these studies, improvements in accuracy were obtained by using single or multi-head additional parameters. Approaches taking into account the multi-head distortions involved either using standard parameters for each sensor head (Alamus *et al.*, 2006) or using sensor specific parameters (Büyüksalih and Jacobsen, 2006; Kruck, 2006; Baz *et al.* 2007). Some stability analysis has also been done. Alamús *et al*. (2006) showed that the systematic residual pattern of the DMC was quite stable over a 3-month period. Büyüksalih and Jacobsen (2006) analyzed the stability of UltraCamD by determining the distortions with one data set and using these parameters for other image blocks; the best results were obtained by self-calibrating each block. Spreckels *et al.* (2007) evaluated deformations of the stereomodels provided by DMC, UltraCamD, and an analog frame camera. Their conclusion was that the deformations appeared for all the sensors, but in the cases of digital sensors, if self-calibration was not applied, they were not acceptable. Empirical investigations with the ADS40 have also indicated that there are advantages to *in situ* calibration (Cramer, 2006; 2007b; Kocaman *et al.*, 2007). Alamús *et al*. (2006) and later Cramer (2007b) showed that the effects of multi-head distortions could also be compensated for by decreasing the weighting of the image observations in the block adjustment. Honkavaara (2000) drew similar conclusions in the analysis of the accuracy of automatic tie point measurement. Modeling the systematic distortions as random errors is not an optimal way to treat the image distortions, but it can be a functional approach if rigorous modeling is not possible.

A significant consequence of the empirical investigations has been that camera manufacturers have started to take action to eliminate distortions. Dörstel (2007) concluded that the most likely reason for the distortions of the DMC large-format panchromatic images was the remaining lens-chip distortions. To compensate for the distortions, the laboratory calibration methodology has been improved (Hefele, 2006), and a method based on correction grids has been developed. The correction grid can be determined in a test field for individual sensor heads by using an image block with large overlap percentages (Dörstel, 2007). For the UltraCamD, a new step in the geometric processing is temperature-dependent correction; the remaining distortions can be determined by self-calibration (Gruber, 2007). Independent empirical results about the performance of the improved digital systems have not been presented to date.

There are still many questions concerning the sufficiency of test field calibration, including what the important parameters are, how accurately they can be determined, and how stable the systems are. For instance, the precision estimates of the principal points (2-5μm) give some indication of the accuracy obtainable. These precision values are consistent with the results obtained with analog cameras at Sjökulla (Honkavaara *et al.*, 2003) and only slightly worse than the precision estimates of

the laboratory calibration (Section 2.4). These values are quite poor in comparison with the estimated image point precision (1.5 μm for the UltraCamD, 2 μm for the DMC). The stability of the systems has not been verified yet. As long as the sensor stability or the adequacy of the accuracy of the parameters is questionable, self-calibration is recommended to obtain the highest accuracy.

Spatial resolution

The empirical spatial resolution study analysed comprehensively the DMC panchromatic images. The study revealed that their resolution was significantly lower than the nominal resolution based on the Nyquist sampling theorem. First of all, the resolution was up to 2 times lower in the image corner than at the image center. It was shown that this was for the most part due the convergent image geometry; the influences of atmosphere and lens could be additional causes for the resolution decrease towards image border. It also appeared that the resolution was significantly worse in the flight direction than in the cross-flight direction; an insufficiency in the FMC could be reason this behavior. Furthermore, the MTF appeared to improve slightly when the GSD increased. A possible explanation for this is that the relative image motion is smaller with a greater GSD, and the blur caused by image motion is therefore smaller. The sensor manufacturer did not provide information about the above behavior. It is possible that the selection of the flight parameters using the nominal resolution values would not lead into acceptable image quality in some applications.

The resolution of the multispectral images appeared to be close to the Nyquist limit and slightly different for various channels; this issue should be investigated further.

The comprehensive calibration blocks enabled the determination of empirical linear spatial resolution models for the DMC panchromatic images. The resolution was predicted as a function of the radial distance from the image center. A similar approach could also be used for the resolution self-calibration in practical mapping applications: a linear model could be estimated for σ_{PSF} using sharp edges appearing in the scene. Resolution estimates based on technical information of the DMC (sampling, image tilt, and lens) were biased and less accurate than the empirical estimates; the insufficient information about the lens MTF and the blur caused by the image motion, resampling, and atmosphere that were not included in the analysis are possible reasons for the prediction inaccuracy. However, the DMC occupies FMC, and the missions were performed in excellent weather conditions at a low altitude, so the atmosphere and image motion should have minimal influence. The averaged resolution estimates (e.g. AWAR) are not realistic for the DMC because of the dependence of the resolution on the position in image. In this study, AWAR values indicated a true GSD of 1.3-1.5 GSD, which is close to the expected correspondence, 1.5 GSD, given by Graham and Koh (2002).

The similarity of the results of various image blocks indicated stability of the system. However, a small difference appeared in the resolution of two similar blocks with an 8 cm GSD. Also, the geometric accuracy analysis indicated that the block with better resolution provided slightly better geometric accuracy (Section 4.1; **III**). Unfortunately, the possible influence of mission conditions (e.g. differences in the flight speed, temperature) could not be evaluated, because the mission log was not available for the other block.

Only a few empirical spatial resolution results for digital photogrammetric systems have been presented in the literature. Results of Kölbl (2005) indicated also that the resolution of the DMC images was worse in the image border than in the image center, but the observed factors were different from those found in this study. The difference could be due to the differences in system, GSD, image processing, and evaluation methodology. Reulke *et al.* (2006) and Becker *et al.* (2005; 2006) have especially concentrated on the spatial resolution processing chains by investigating restoration and pansharpening methods; investigation of these issues should be continued, and the results obtained in this study should be taken into account in the processing chains.

Radiometry

The evaluation of the radiometry of the ADS40, DMC, and UltraCamD proved the attractive radiometric properties of the systems. The linear radiometric response is an expected performance of the CCD arrays tested (Hinz *et al.*, 2000; Beisl, 2006b; Dalsa, 2008), but this research proved this empirically for the first time. A practical consequence of the linearity is that the absolute calibration can be determined by relatively simple means. The large dynamic range (up to 12 bit for the DMC and 13 bit for the ADS40 and UltraCamD) and the capability to measure in most cases at least the 5%-70% reflectance range are advantageous for the measurement processes; for instance, they will enable accurate measurements in shadows and in bright areas. High radiometric quality, calibration, and the possibility of collecting multi-angular and multispectral imagery will enable the use of the images in various interpretation applications (e.g. Zepedin *et al.,* 2006).

Sensitivity of the color channels appeared to be a serious limitation for the first generation ADS40 in limited illumination conditions (solar elevation angle less than 30˚). The large sensitivity differences of the different channels of the ADS40 are partially caused by the widths of the bands and the filtering principle (Section 2.2; **V**). Furthermore, it was not possible to collect multispectral imagery with smaller than 15 cm GSD by the system tested (Section 3.1; **V**). It was concluded that the first generation ADS40, when combined with a relatively high-speed aircraft, was not the optimum sensor to illumination conditions in high latitudes, where solar elevation angles are low even in the summer time. The flying speed and illumination conditions did not cause noticeable problems for the DMC and UltraCamD because the exposure time could be increased with the help of TDI. However, it appeared that for the UltraCamD and DMC, the exposure and aperture settings were critical parameters causing a risk of over-exposure. Moreover, the spatial resolution analysis of the DMC indicated influences of improper FMC; this problem may be emphasized in poor illumination conditions if long exposure times and high flying speeds are used. It can be expected that for the first generation ADS40 the conventional solar elevation angle requirements (approx. 30˚ above horizon) are still necessary. The conclusion could be different for the second generation ADS40, for which the manufacturer has announced a four-fold improvement in sensitivity (Fricker, 2007), theoretically providing an 11-bit or greater dynamic range for the color channels of the test materials. For the DMC and UltraCamD the solar elevation angle requirements could probably be decreased. The possibility to extend the operational imaging time would be a significant advantage for the photogrammetric processes; this should be verified empirically for different systems and applications by taking the radiometric, geometric, and spatial resolution aspects into account.

The accuracy of the vicarious calibration was promising. The relative errors of the absolute calibration were less than 6%, and the RMSEs were 3.3-4.5%. The major source of error was the calibration inaccuracy and non-uniformity of the reference targets. Assuming an atmospheric error of 3-4% (Section 2.6), approximately 6% absolute radiometric accuracy can be expected. This accuracy is similar to values obtained for the remote sensing systems (Section 2.6), and it could be further improved by improving the reference target uniformity and calibration.

Several authors in the literature have discussed the radiometric restrictions of various sensors, but they have not been quantitatively measured. For the multi-head systems, the color artefacts of the PAN-sharpened images, possible influences of the electronic TDI on radiometric values, and wide spectral filters have been criticized (Fricker and Rohrbach 2005; Pacey and Fricker 2005; Souchon *et al*. 2006). Color artefacts caused by the lens quality have been reported for the UltraCamD (Souchon *et al.* 2006). The reported shortcomings for the ADS40 (1st generation) include the limitations in the dynamic range due to short integration times, unrealistic colorimetric content caused by the separate spectral channels, displacement of one of the multispectral channels from other three channels causing registration problems, and BRDF data only for the panchromatic channel (Leberl and Gruber 2005; Souchon *et al.* 2006). This investigation verified the limitations in the dynamic range of the ADS40.

Table 8. Central calibration parameters. Parameters that can be determined only at laboratory are indicated by Lab and only in flight conditions by *in situ*.

Geometry

Single head sensor
- Interior orientation
- CCD
- Distortion model
- Remaining image distortions

Multi head sensor
- Relative orientation
- Interior orientation
- Distortion model
- Remaining image distortions

GPS/IMU or GPS
- Lever arms (*in situ*)
- Boresight (*in situ*)

Performance assessment
- Point determination
- Back projection
- Perspective center observations (*in situ*)
- Image rotation observations (*in situ*)

Spatial resolution

Model for RP, MTF, σ_{PSF}

Radiometry

Relative calibration
- PRNU (Lab)
- DSNU
- Defect pixels (Lab)
- Light falloff

Absolute calibration
- Spectral response (Lab)
- Radiometric response

Performance assessment
- Absolute radiometric accuracy
- Relative radiometric accuracy
  - Pixel-to-pixel (uniformity)
  - Band-to-band (sensitivity)
  - Image-to-image (stability)
- Dynamic range (saturation, noise)

The radiometry of photogrammetric sensors has not been extensively empirically studied in literature, and a gray scale has not been used in any investigation. Martinez *et al.* (2007) recently presented a radiance-based absolute calibration method, which integrates DMC and a calibrated hyper-spectral scanner into the same platform. They also performed colorimetric calibration of the DMC. Their conclusion was that the DMC was appropriate for the radiometric calibration.

The conclusion of the radiometric study was that the systems had the potential to provide high-quality radiometric information. The insufficient manufacturer calibration and information on the system performance, and the non-rigorous radiometric processing chains were serious shortcomings of the systems (**V**). Rigorous processing of the radiometry is challenging, but the experiences with remote sensing systems show that functional processing chains could be developed (Section 2.6).

A parameterization for the system calibration

Paper **II** presented a comprehensive parameterization for the geometric test field calibration. This parameterization can be generalized for geometry, spatial resolution and radiometry as follows:

- System model and its parameters
- Accuracy of the system model (precisions of parameters, $\hat{\sigma}_0$, residuals, bias)
- Empirical accuracy of output products (RMSE, precision, and bias assessed by using independent check observations)
- Performance prediction method and its accuracy (RMSE, precision, and bias by using independent check observations)

The parameterization is given on a general level; some details of the parameters are given in **I**-**V**, Section 2, and Table 8. The exact parameters are system dependent.

The parameters in **II** were extended with the performance prediction method. The capability to predict system performance is often advantageous, because it allows versatile use of the system without a need for validating every output product. In the case of the analog frame cameras the prediction is possible; theoretical models are applied in practical applications to determine appropriate flight parameters (Section 2.4). The evaluation of the performance of different spatial resolution prediction methods (Section 4.2) demonstrated the quantitative prediction accuracy assessment.

5.2 Calibration process for digital photogrammetric airborne imaging systems

The empirical results in Section 4 and the analysis of the calibration parameters (Section 2.4, 2.5, 2.6) showed that the digital photogrammetric data acquisition system should be calibrated at three levels: the laboratory calibration, the test field system calibration, and the system self-calibration, if a high accuracy is required. There appeared also a need for the geometric calibration or validation of the system outputs. The central calibration parameters, which are related to the imaging models and system performance, are summarized in Table 8. Most of the parameters can be determined using both laboratory and *in situ* calibration methods.

Laboratory calibration is the cornerstone of the photogrammetric system calibration and quality verification. The major reasons for this are that it is the most accurate calibration method, it enables sensor component and sensor calibration in a controlled way in varying conditions (e.g. different apertures, temperature), and all necessary parameters cannot be determined in airborne conditions (Table 8). It appeared that the laboratory calibration was necessary especially for the radiometry (**V**).

The strength of test field calibration is that the entire system is calibrated in the operational environment. For the sensor manufacturer test field calibration before delivering the sensor to the user is an important part of the quality control system. When various instances of the same sensor are calibrated under similar conditions, it is possible to detect abnormal behavior immediately. The manufacturers of photogrammetric instruments already perform this kind of operation regarding geometry (Tempelmann *et al.*, 2003; Dörstel, 2003; 2007; Fricker, 2007; Gruber, 2007). For the image provider, test field calibration is necessary to determine consistent calibration parameters, to ensure that the system functions correctly, and to assess the system's measurement potential. *In situ* calibration (in a test field or by self-calibration) is advantageous for integrated camera/GPS/IMU-systems in particular (Section 2.4). When the geometric, spatial resolution, and radiometric properties of the system are known, it is possible to optimize the flight parameters for particular mapping tasks. The expectation is that digital sensors provide stable geometry and radiometry. Thus if the system is properly calibrated, the imagery can be used in highly direct means enabling efficient data production. A further advantage of the test field calibration for the data provider is that if the appropriate test field infrastructure is available, the systems can be calibrated and tested in test fields for the most part with little effort, without a need for shipping the system to the laboratory of the system manufacturer. If the system performance cannot be predicted based on the system parameters, test field calibration is needed to characterize different products. (**I-V**)

In addition to the data providers and sensor manufacturers, test fields provide important information for data users. When the sensor parameters and performance information are available, users can evaluate the appropriateness of various sensors on their applications. Furthermore, various organizations are increasingly applying quality systems. Test fields are valuable tools for sensor manufacturers and data providers in the quality assurance of their products. Quality systems of data users also require reliable quality management from data providers. For example, Honkavaara *et al.* (2004) presented a quality system for the national orthophoto production process. A convenient way to enable the use of different sensors (e.g. new sensors entering market, medium-format mapping sensors, off-the-self sensors) in this process would be to require acceptable test field calibration.

The practical experiences with analog aerial cameras and remote sensing instruments have shown the importance of test field calibration (Section 2.7). Test field calibration of geometry and spatial resolution has been prerequisite for obtaining the maturity for the analog photogrammetric sensors and processes. There exist examples of the geometric test field calibration as a part of the photogrammetric production process. In the case of satellite and airborne multispectral instruments, test fields are necessary for radiometric recalibration of the systems and for assessing the system performance. The importance of the test field calibration has been also realized with new digital photogrammetric sensors; they have already been improved based on the results obtained from test fields (Section 5.1).

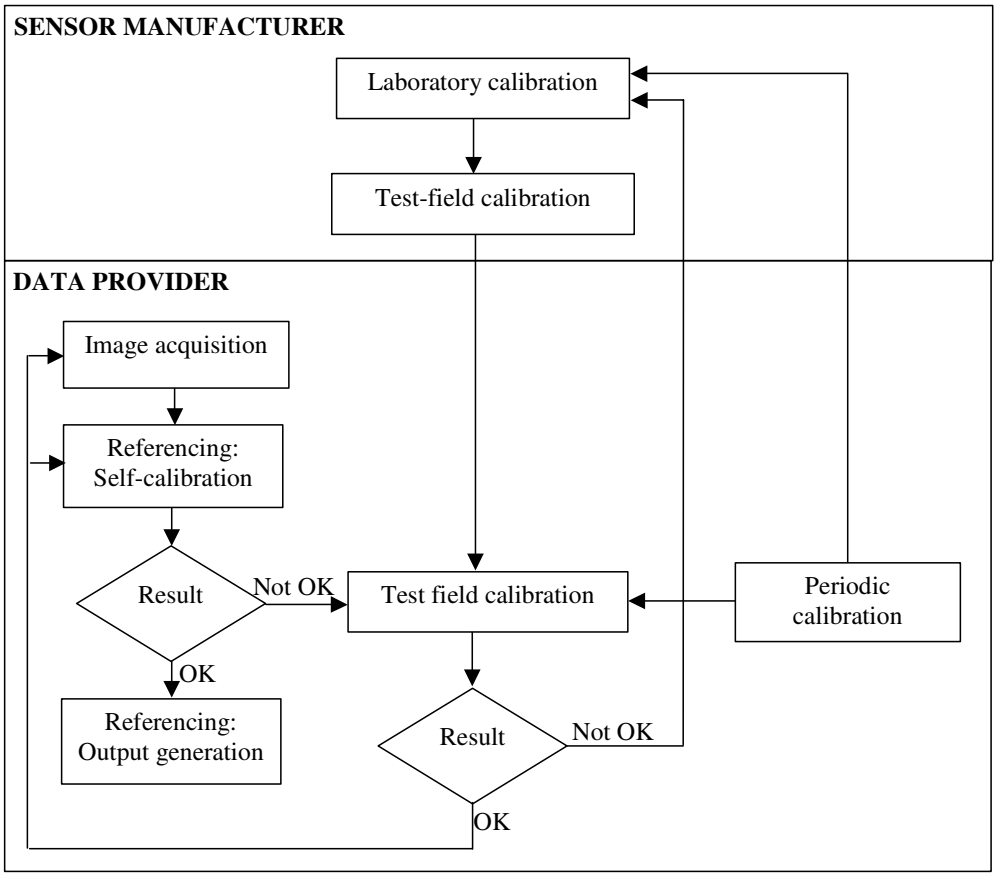

Figure 17. Calibration of digital photogrammetric airborne imaging systems.

System stability and calibration model and parameter accuracy determine the sufficiency of test field calibration. The stability should be assessed for various systems under various operational conditions, e.g. pressure, temperature, humidity, aperture, and flight speed (Table 2; Section 2.1; **I; II; V**). It is expected that various systems have different stability due to differences in technical properties (Section 2.2). Because the stability of the systems and accuracy of the models and parameters have not been proven, self-calibration is necessary to obtain the highest accuracy and reliability (Section 5.1). Self-calibration of the geometry is a well-known method in photogrammetry, but self-calibration methods for the spatial resolution and radiometry should be investigated. Spatial resolution self-calibration methods could be developed on the basis of the results in Section 4.2.

A flow chart of a recommended calibration process for the digital photogrammetric airborne imaging systems is presented in Figure 17 (**I**). The first steps in the calibration processing are the laboratory and test field calibration by the sensor manufacturer. It is reasonable for the sensor manufacturer to perform the laboratory calibration of the large-format systems, because of the complexity of the systems. After the sensor is installed in the operating environment, the system should be calibrated in a test field. The first calibration is the reference for future calibrations. Test field calibration should be repeated occasionally (e.g. annually) to update parameters and for quality control purposes, and it is especially important to test the sensor after suspected damage. If the result shows that system is not in condition, it can be sent to the sensor manufacturer for repair and calibration. As discussed above, the self-calibration of the mapping blocks is necessary to obtain the most accurate and reliable results. It is important for the results of the various calibrations to be stored and analyzed so that information about the stability and quality of the systems can be obtained and the

Table 9. Recommended targets for a photogrammetric test field (GSD range: GSD_{min} to GSD_{max}). The suggested minimum configuration for the photogrammetric test field is shaded.

Property	Target	Recommendation
Geometry	GCPs	Number: 30-100 clusters with 2-3 points each Accuracy: X,Y: GSD_{min}/18, Z: GSD_{min}/6
	Dense elevation model	Accuracy: Z: GSD_{min}/6
Spatial resolution	Edge target	Reflectance: 5%, 50% (Pagnutti *et al.*, 2002) Size: 20 GSD_{max} x 20 GSD_{max} (Pagnutti *et al.*, 2002) Alignment: flight and cross-flight directions
	Resolution bar target	3-bar target Bar width: GSD_{min} to 3 GSD_{max}; $\sqrt[6]{2}$ width increment (**I**) Alignment: flight and cross-flight directions Material: gravel
	Siemens star	Semicircle (**I**) Maximum sector: 10 GSD_{max}, 10-degree sectors (**I**)
Radiometry	Grayscale	Painted on e.g. tarpaulin or concrete (**I**) 8 steps, 5-70% reflectance range, approx. 10% reflectance interval Target size: 11 GSD_{max} x 11 GSD_{max}
	Reflectance targets	Reflectance: 5%, 50%, (etc.) Target size: 11 GSD_{max} x 11 GSD_{max} (or same as the edge target)

changes of the systems can be recognized. This performance data is an important part of the process-level quality assurance (Eisenhart, 1963).

5.3 Recommendations for photogrammetric test fields

This section gives recommendations for photogrammetric test fields from the perspectives of the test field provider and user. Some recommendations for photogrammetric test fields were given in **I** and **V** and the literature research (Section 2) and empirical investigation (Section 4) provided further information; the recommendations are summarized in Table 9 and discussed below.

From the test field providers' point of view, the important factors are the required reference targets and their properties, such as size, material, and quality. On the one hand, accurate reference targets have to be provided, while on the other, the construction and maintenance costs should be minimized.

For the geometric calibration, accurate reference points are needed. A common requirement for the reference points is that their accuracy should be better than one third of the accuracy of the products to be tested (**I**). Results suggested that in good conditions, such as in the Sjökulla test field, the accuracy of the reference points should be at least GSD/18 in horizontal coordinates and GSD/6 in height (Section 4.1; 5.1; **II; III**). In the existing test fields, the point accuracy is typically 1-2 cm (Section 2.7; **I**), which is suitable for the calibration of imagery with 18-36 cm GSD in horizontal coordinates and 6-12 cm in height coordinates. Lower accuracy, e.g. the expected point determination accuracy, could be sufficient to observe block deformations. The calibration and output product evaluation aspects should be taken into account when designing the reference point distributions (**I**). In general, a large number of reference points is necessary for precise accuracy assessment of output products, but for the determination of the system model, a smaller number of points is sufficient if tie points are utilized. A dense image point distribution is needed to model the distortions of the multi-head sensors; this can be achieved efficiently by using large image overlaps and densely distributed tie

points (**II**, **III;** Alamús *et al.*, 2006; Dörstel, 2007). A possible approach for minimizing the object-related factors from the calibration results could be to apply a fixed set of tie points. The optimal block and point configurations can be determined for instance by using the simulation technique presented by Honkavaara (2003) when appropriate system models are available. In this study, the checkpoints were sufficient for detecting block height deformations but did not enable the accurate analysis of the distortions (Figure 9, Figure 10). For these blocks 12 GCPs and one checkpoint in the center of each stereomodel would lead to 32 to 40 reference points; the use of point clusters with 2 or more points would improve reliability. Dense reference point configurations, up to 200 points, are available in some test fields (e.g. Pagnutti *et al.*, 2002; Cramer, 2005). Airborne laser scanning is an efficient method for providing dense height reference information (Section 2.7); Alamús *et al.* (2006) demonstrated the efficiency of this approach.

Results of the spatial resolution analysis provided information for the designing of the resolution bar targets and Siemens star (Section 4.2; 5.1; **IV**). The RP results indicated that the bar width range of a resolution bar target should extend from the minimum GSD to more than twice the maximum GSD to be tested (Section 4.2); the measurement method also influences this requirement. Gravel appeared to be a functional material for the resolution bar target. In the case of MTF targets (e.g. Siemens star), in order to use the target itself for the object modulation determination a point spread of ±3-4 pixels should be taken into account. In Table 9, a border area 4 pixels wide and two data pixels are used to specify the maximum sector width of the Siemens star (Section 3.2; 4.2; **I**; **IV**). The Siemens star, made of a poly-acrylic fabric, was difficult to install evenly on gravel (Section 4.2; **IV**); stiffer material and/or more uniform ground could improve the accuracy of the MTF measurement. The recommendations for the edge target in Table 9 are based on Pagnutti *et al.* (2002); the suggested reflectance range and target size appeared to be appropriate for the systems evaluated (Section 4.3; 5.1; **V**). The targets should enable the resolution evaluation of all the available channels in the flight and cross-flight directions. The evaluation of the spatial resolution in different parts of the image could be carried out by utilizing appropriate image blocks, as was demonstrated in this study.

For the reflectance based radiometric calibration, a few reflectance targets or a gray scale can be used (Section 5.1; **I; V**). The linear absolute radiometric calibration model with two (gain, offset) or one (gain) parameters was appropriate for the tested systems. The cost of the absolute calibration can be minimized by scarifying the reliability and using the minimum number of reference targets (1-2). Larger numbers of targets improve the precision and reliability and enable precision estimation. For the absolute radiometric calibration, the reflectance range 5-50% appeared to be appropriate, in order to avoid biased calibration parameters due to possible saturation of the bright targets (Section 4.3). For the characterization of the sensor radiometric response, a wider reflectance range and more targets are needed. The FGI's gray scale, with a 5-70% reflectance range and 8 steps, appeared to be appropriate for linearity evaluation and for giving important information about the dynamic range (Section 4.3; **V**). The size of the target should be selected so that it contains a sufficient border area and data pixels; in Table 9, a square target with a border area 4 pixels wide and 3 times 3 data pixels is used (Section 3.2; 4.2).

The fundamental challenges for the photogrammetric test fields are 1) the accuracy and distribution requirements of the reference points (**I**; see above), 2) the requirements for the size and reflectance properties of the reflectance and spatial resolution targets (Section 2.7; Pagnutti *et al.*, 2002; **I; V**), and 3) the demands for the *in situ* measurements in the radiometric calibration (Pagnutti *et al.*, 2002; **I; V**). When concerning the durability and weather-resistance, the gravel is an attractive material for the resolution and reflectance targets; the limitations of gravel are the restricted reflectance range and uniformity (Section 3.2; **I**). The GSD range to be tested is a central parameter in the specifications. Typical GSD range in photogrammetric applications is 3 - 50 cm but the influence of GSD (or flying altitude) on the calibration result is still a research issue (**I-V**). An important design

aspect is the possibility to automate the target measurements; the automation improves the objectivity, efficiency, and often also accuracy of the calibration.

The minimum reference target configuration for a photogrammetric test field, allowing geometric, radiometric, and spatial resolution calibration, is a set of reference points, and 5% and 50% reflectance reference targets arranged so that they can be simultaneously used as edge response targets (Table 9). This kind of set-up has been realized at the SSC (Pagunutti *et al*., 2002).

In principle, any area containing appropriate reference targets and measurement equipment can be considered a photogrammetric test field, but permanent test fields have several advantages in comparison with temporal test fields. The use of permanent targets and measurement equipment will minimize the need for interaction and thus increase the automation level (Section 3.2). When calibration is performed in the same environment under acceptable conditions, object-dependent and condition-dependent variations can be minimized, and unexpected results can be directly addressed as problems of the system. It is particularly important to be able to build permanent test fields for geometric calibration because numerous reference points are needed and the entire object contributes to the result. Permanent resolution and reflectance targets are also preferable, but the results showed that portable targets can also be functional. It is feasible to develop optimal procedures and automated calibration methods for permanent test fields. If systems are calibrated in several test fields, the differences of various test fields should be assessed in order to be able to detect changes in systems. This is feasible for permanent test fields. Finally, the accreditation that is in general required for testing and calibration laboratories is practical mainly for permanent test fields. This investigation confirmed this by pointing out the high quality requirements of the reference targets, the efficiency of the permanent test field in revealing abnormal performance of systems, and the feasibility of permanent targets and measurement devices.

For the users of the test fields, operational and financial issues are of importance (**I**). The test fields should be easily accessible. Of great practical importance is the maximum probability of appropriate atmospheric conditions for photogrammetric data collection flights. Reference targets and automatic calibration methods should be standardized so that the processing can be highly automated and objective. The test field should also be suitable for multipurpose product validation (e.g. point determination, digital elevation models, feature extraction, classification, and orthophotos).

5.4 On the need for and feasibility of system calibration in test field

The results that proved the hypothesis of this study (Section 1.1) are summarized below. Many further advantages of the test field calibration are presented in Section 5.2.

1. Test field calibration is needed

The test field calibration of the geometry of the DMC and UltraCamD was needed because the calibration, provided by the sensor manufacturer, was not valid in airborne conditions and system performance, especially the systematic height deformations, could not be predicted on the basis of the information available (**II**; **III**; Section 4.1; 5.1). The test field calibration of the spatial resolution of the DMC panchromatic images was needed to determine missing parameters and to assess system performance (**IV**; Section 4.2; 5.1). The test field calibration of the radiometry of the ADS40, DMC, and UltraCamD was needed to determine missing radiometric parameters and to assess system performance (**V**; Section 4.3; 5.1). A methodology that could have replaced the test field calibration was not available for the evaluated systems.

Currently, the most fundamental reason for the test field calibration is the performance assessment, which is a crucial task in the establishment of a measurement process (Eisenhart, 1963).

2. Test field calibration of the systems is feasible

Evaluation of the geometric performance of the systems was feasible in the test field; the empirical results proved that test field calibration was a powerful tool for determining the precision and bias of the system model and output products (**II**; **III**; Section 4.1). The calibration blocks did not enable the determination of the geometric system calibration model. However, current literature and experiences with analog frame cameras indicate that appropriate parameters could be determined in a test field (Section 2.7).

Spatial resolution of the DMC panchromatic images could be calibrated in the test field (**IV**; Section 4.2). The comprehensive calibration blocks enabled the development of empirical models for spatial resolution which outperformed the resolution estimates based on the technical information of the system (Section 4.2).

The radiometric study showed that the radiometric response of the ADS40, DMC, and UltraCamD was linear (**V**; Section 4.3). Calibrating this model in the test field is feasible. The expected calibration accuracy corresponds to results from remote sensing systems. The radiometric data provided by the sensors are applicable to quantitative use, thus radiometric calibration is advantageous.

The extent to which the parameters determined in the test field can be utilized in subsequent mapping processes is dependent on the development of models that are accurate and on the stability of the systems (**I; II; V**; Section 5.2). If self-calibration is necessary, the test fields are feasible tools for developing and testing self-calibration methods.

3. Construction of a test field for geometry, spatial resolution, and radiometry is feasible

This study showed that permanent test fields are feasible for operational reasons and for obtaining the best possible potential from the test field calibration process (Section 5.3). Permanent test fields for geometric calibration have proven their feasibility over the years (**I**; Section 2.7). The results further showed that construction of a permanent test field for spatial resolution and radiometric calibration was also feasible. Many years of experience at Sjökulla have shown that gravel is a durable material for permanent reference targets (**I**; Section 3.2). Sometimes non-permanent targets are necessary; then the test field can be designed so that the non-permanent targets can be utilized in the calibration process as they were permanent. The use of the portable gray scale and Siemens star demonstrated the feasibility of this approach (**I**; **IV**; **V**; Section 4.2; 4.3).

4. On generalization of the results

The results of this study proved that system calibration in a test field was necessary and feasible for the evaluated systems. The conclusion and recommendation of this study is that, for the time being at least, those properties of digital photogrammetric airborne imaging systems that are quantitatively used should be calibrated in a test field.

6 Future research

This work can be seen as one of the first steps in the extensive updating of the photogrammetric processes and calibration methods for the digital era. The central research issues identified in this study are summarized below.

The first generation prototype methodology that was developed here can be improved in many ways. The reference targets could be improved to fulfill the recommendations in Section 5.3 enabling calibration in a larger scale range, improving the accuracy of the calibration, and raising the automation level (Section 3.2; 5.3). The optimum block structures should be determined and finally, the accuracy of the improved calibration procedures should be thoroughly assessed. In order to fully support the needs, reference targets for the validation of various photogrammetric products (e.g. 3D environmental models, orthophotos, classification) should be developed.

The foundation of this study was to explore the calibration using existing sensors and calibration methods. The sensor manufacturers should consider whether it is possible to take calibration aspects into account in sensor construction. The possibility of developing simple calibration devices (e.g. flat fields that could be used by the data providers for operational quality control) should be investigated. The prototype methodology developed utilized conventional reference targets; in the future, other possibilities should be considered such as carrying out geometric calibration in a built environment utilizing straight lines, or using natural targets for spatial resolution and radiometric calibration.

The eventual objective of calibration is to optimize the efficiency and reliability of photogrammetric processes. It is necessary to continue the development of the laboratory, test field, and self-calibration methods and ultimately to integrate the calibration processes closely into the photogrammetric process (Figure 1). Existing sensors and new sensors entering the market should be repetitively evaluated in controlled conditions. Temporal stability of the systems as well as influence of the conditions (Table 2) on geometry, spatial resolution, and radiometry in different systems should be investigated. The sensor manufacturers should provide more detailed calibration information so that the *in situ* calibration results could be compared with them. Important data for the evaluation of the system stability are the self-calibration results of practical mapping blocks. The advantages of the simultaneous calibration of geometry, radiometry, and spatial resolution, and their correlations should be further studied.

Specific matters to consider when discussing the test field calibration of geometry are the appropriate calibration models, optimum block structures, and accuracy potential. Optimal procedures for the determination of the physically relevant parameters of various systems should be developed. The most efficient way of obtaining the accurate system calibration is probably the exploitation of direct exterior orientation observations. In the case of multi-head systems, the potential of calibrating each component camera *in situ* should be investigated. This study developed a comprehensive method for predicting the geometric accuracy of the photogrammetric end products (**III**; Section 3.2). In the future, more appropriate image distortion models should be used to evaluate the effects of distortions in various products, and the performance of the method should be assessed. To provide realistic accuracy estimates for certain objects and measurement methods by simulation, their measurement precision should be assessed. Realistic methods for predicting spatial resolution and radiometric performance should be also developed.

This study thoroughly characterized the spatial resolution of the panchromatic DMC images, but the resolution of the multispectral images should be further studied. It is also important to evaluate the performance of other systems. The usefulness of empirical spatial resolution models should be investigated in practical applications. Methods for the spatial resolution self-calibration as well as

operational spatial resolution processing chains should be developed on the basis of system performance; for instance, in the case of the DMC the results in Section 4.2 and **IV** should be taken into account. For spatial resolution prediction, the approach based on a cascade of MTFs is appealing (Section 2.5); in order to use this method, information about the various component MTFs is needed.

Radiometric properties are the special advantage of digital photogrammetric sensors. Studies on the vicarious radiometric calibration of different systems should be continued; this study only scratched the surface of a broad research area. In order to optimally utilize the image radiometry, functional radiometric processing chains should be developed to provide accurate relative and absolute radiometric information, and visually attractive tones; performance of these methods should be thoroughly assessed using test fields. Atmospheric correction is a difficult task, and an interesting approach is to apply the photogrammetric block and national GPS networks to determine the correction. Studies should be carried out to utilize image radiometry in geometric applications (3D object models, feature extraction, automatic tie point measurement, etc.) and in automated image interpretation applications (classification, change detection, etc.). Digital photogrammetric systems already provide large amounts of data, e.g. the orthophotos collected over the country every few years as a repeat cycle. These data sets provide elementary sources for future environmental studies, but in order to fully utilize image radiometry, the traceability of the DNs to the object reflectance should be ensured.

This investigation focused on digital photogrammetric large-format systems. However, for similar reasons, all kinds of airborne imaging systems should be test field calibrated. The calibration aspects of different types of sensors should be investigated using the methodology developed.

A large number of research issues remain. Theoretical evaluations, rigorous empirical investigations in well-controlled conditions, and support from sensor manufacturers are needed to answer many of these questions. International co-operation is important to collect empirical data extensively and to develop widely accepted procedures for digital photogrammetric airborne imaging system calibration; this work has already started (Cramer, 2007a; EuroDAC, 2007; Stensaas, 2007).

7 Summary and conclusions

Digital imaging by passive and active systems is replacing conventional film imaging in photogrammetric data capture. Digital imaging combined with modern navigation techniques makes the data capture more efficient, raises the automation potential and quality of photogrammetric processes, and generates new applications. The photogrammetric processes should be thoroughly revised in order to optimally utilize the new technology.

The reliability, accuracy, and efficiency of photogrammetry are based on calibrated, high quality instruments and rigorous processing. Calibration processes for the digital systems are under development. Central challenges in the development of calibration are the extensive variation in digital systems, the need for radiometric calibration, and the necessity for accurate system calibration. Test field calibration is a potential approach for determining the system calibration.

The hypothesis of this study was that system calibration in a test field is necessary for digital photogrammetric airborne imaging systems and that the calibration should involve geometry, spatial resolution, and radiometry. The hypothesis was proven by developing a methodology for photogrammetric system calibration in a test field and by empirically investigating the need for and feasibility of system calibration. The need for calibration was studied by evaluating the sufficiency of the system calibration provided by the manufacturer and by investigating the possibility to predict the system performance. The feasibility analysis was carried out on the feasibility of constructing test fields for photogrammetric systems and calibrating the systems in the test fields. In the empirical investigation, data sets from three first generation commercial digital photogrammetric large-format sensors, Leica Geosystems ADS40, Intergraph DMC, and Microsoft UltraCamD, were used. The calibration of an image acquisition system of a data provider was concerned.

The permanent Sjökulla test field of the Finnish Geodetic Institute, augmented with some portable targets, is a prototype test field for photogrammetric systems. Targeted ground control points exist for geometric calibration in various imaging scales. Spatial resolution calibration is performed using permanent resolution bar targets made of gravel and a portable Siemens star. Radiometric calibration is performed using a portable, calibrated gray scale. The calibration process can be automated to a high degree.

The most comprehensive analysis focused on geometric calibration. Empirical investigation showed that the laboratory calibration of the DMC and UltraCamD was not valid in airborne conditions. The images contained distortions which deformed the photogrammetric block, especially in the height coordinate, and decreased the geometric accuracy of the end products. These distortions were not taken into account in the systems at the time the tests were performed, but recently sensor manufacturers have developed tools for their compensation. The results indicated the high accuracy potential of the systems and, at best, a geometric accuracy comparable to analog frame cameras. In practice, the full accuracy potential was not always obtained because of the systematic deformations. To support geometric calibration, a method utilizing simulation and empirical results was developed for sensor evaluation and photogrammetric product quality prediction. Theoretical evaluations were performed together with the empirical investigation. The set-up in this study did not allow detailed analysis of geometric system calibration models.

The empirical analysis showed that the spatial resolution of the DMC panchromatic images was below the Nyquist limit and dependent on the position in image, on the direction of flight, and slightly also on altitude. It was determined that due to oblique imaging geometry, the resolution of the panchromatic images is in theory 1.4-1.6 times lower in the image corner than in the image center; empirical results indicated a resolution up to two times lower in the image corner than in the image

center. Empirical linear spatial resolution models were developed to predict the resolution of the panchromatic DMC images as a function of the radial distance from the image center; these models yielded more realistic resolution estimates than the technical information of the sensor. Insufficient information on the sensor caused problems for the predicting of the system resolution.

The radiometric properties are the special advantage of digital photogrammetric systems in comparison to film-based systems. The radiometric calibration of the ADS40, DMC, and UltraCamD proved the attractive properties of the sensors, which included linear radiometric response, large dynamic range, a high radiometric resolution, and the potential for the absolute radiometric calibration. Detected limitations included the low sensitivity of the multispectral channels of the first generation ADS40 and the saturation of some channels of the DMC and UltraCamD at bright reflectance values in some cases. The missing information on the absolute calibration and radiometric performance and inadequate radiometric processing chains are serious limitations hindering the quantitative use of the image radiometry.

The results proved the hypothesis. Test field calibration was necessary for the three most high-end calibrated photogrammetric sensors to determine the invalid or missing system calibration parameters and to assess system measurement capability. The evaluated high-quality photogrammetric instruments were feasible for calibration, and test field calibration was a feasible method for determining system calibration. The evaluations indicated that permanent test fields are especially feasible for operational system calibration. Experiences from the Sjökulla test field since 1994 have shown that the construction of permanent test fields for geometric, spatial resolution, and radiometric calibration is feasible.

The investigation concluded that the central calibration parameters were the geometric, spatial resolution, and radiometric models of the system, the accuracy (precision and bias) of the models, the empirical accuracy of the output products, and the performance prediction method. The analysis showed that a comprehensive calibration process should include all of the following: laboratory calibration, test field calibration, self-calibration, and product level validation.

The importance of field testing has already been realized with conventional analog imaging systems and with satellite and airborne remote sensing systems. The eventual objective of calibration is to optimize the efficiency and accuracy of photogrammetric processes; the results showed that the test field calibration was necessary to achieve this objective with the evaluated systems. It is expected that in the rapidly developing, versatile digital photogrammetric environment, the significance of test field calibration will soon be widely recognized. The recommendation is that, for the time being at least, those properties of digital photogrammetric airborne imaging systems that are quantitatively used should be calibrated in a test field. International co-operation is important for developing widely accepted calibration procedures.

This work demonstrated for the first time the simultaneous geometric, spatial resolution, and radiometric system calibration of digital photogrammetric airborne imaging systems in a test field. The study provided several new results concerning digital photogrammetric system performance and test field calibration, including recommendations for the calibration process of digital photogrammetric airborne imaging systems and for the construction of photogrammetric test fields. It also identified many important research topics.

References

Abdullah, Q.A., J. Collins, K. Edmundson, J. Grodecki, H. Heier, J. Hutton, D. Liddle, M. Mostafa, C. Mondello, K. Novak, R. Pacey, B. Scherzinger, 2004. Photogrammetric platforms, *ASPRS Manual of Photogrammetry, 5th Edition,* (McGlone, J.C., E. Mikhail, J. Bethel, Eds.), American Society for Photogrammetry and Remote Sensing, pp. 677-730.

Ackermann, F., 1992. Operational rules and accuracy models for GPS-aerotriangulation, *International Archives of Photogrammetry and Remote Sensing*, 29(B3): 691-700.

Ahokas, E., R. Kuittinen, J. Jaakkola, 2000. A system to control the spatial quality of analogue and digital aerial images, *International Archives of Photogrammetry and Remote Sensing*, 33(B1): 45-52.

Alamús, R., W. Kornus, J. Talaya, 2006. Studies on DMC geometry, *ISPRS Journal of Photogrammetry & Remote Sensing*, 60(6): 375-386.

ASPRS, 2000. ASPRS Camera calibration panel report, http://www.asprs.org/news/archive/final_report.html (Last date accessed 29 April 2008).

Atcor, 2008. http://www.rese.ch/atcor/index.html (Last date accessed 29 April 2008).

Baz, I., G. Büyüksalih, K. Jacobsen, 2007. Bundle block adjustment with high resolution UltraCamD images, *Proceedings of the ISPRS Hannover Workshop 2007: High-Resolution Earth Imaging for Geospatial Imaging*, unpaginated CD-ROM, 6 p.

Becker, S., N. Haala, R. Reulke, 2005. Determination and improvement of spatial resolution for digital aerial images, *Poceedings of ISPRS Hannover Workshop 2005: High-Resolution Earth Imaging for Geospatial Information,* unpaginated CD-ROM, 6 p.

Becker, S., N. Haala, E. Honkavaara, L. Markelin, 2006. Image restoration for resolution improvement of digital aerial images: a comparison of large format digital cameras, *International Archives of Photogrammetry, Remote Sensing and Spatial Information Sciences*, 36(A1), unpaginated CD-ROM, 6 p.

Beisl, U., 2001. Correction of bidirectional effects in imaging spectrometer data, *Remote Sensing Series 37*, Remote Sensing Laboratories, Department of Geography, University of Zurich, 2001, 188 p.

Beisl, U., N. Woodhouse, 2004. Radiometric processing sheme for multispectral ADS40 data for mapping purposes, *International Archives of Photogrammetry, Remote Sensing, and Spatial Information Sciences*, 35(B7), unpaginated CD-ROM, 5 p.

Beisl, U., 2006a. Absolute spectroradiometric calibration of the ADS40 sensor, *International Archives of Photogrammetry, Remote Sensing, and Spatial Information Sciences*, 36(B1), unpaginated CD-ROM, 5 p.

Beisl, U., 2006b. Absolute spectroradiometric calibration of the ADS40 sensor, Presentation given at ISPRS Comm. I Symposium in Paris, July 2006, 21 p.

Berk, A., G. Anderson, P. Acharya, M. Hoke, J. Chetwynd, L. Bernstein, E. Shettle, M. Matthew, S. Alder-Golden, 2003. *MODTRAN4 Version 3 Revision 1 User's Manual*, Air Force Research Laboratory, Space Vehicles Directorate, Hanscom Air Force Base, Ma 01731-3010, 101 p.

Biggar, S.F., P.N. Slater, D.I. Gellman, 1994. Uncertainties in the in-flight calibration of sensors with reference to measured ground sites in the 0.4-1.1 μm range, *Remote Sensing of Environment*, 48(1994): 245-252.

Blonski, S., M. Pagnutti, R.E. Ryan, V. Zanoni, 2002. In-flight edge response measurements for high-spatial-resolution remote sensing systems, *Proceedings of SPIE, Vol. 4814*, pp. 317-326.

Boland, J., T. Ager, E. Edwards, E. Frey, P. Jones, R.K. Jungquiet, A.G. Lareau, J. Lebarron, C.S. King, K. Komazaki, C. Toth, S. Walker, E. Whittaker, P. Zavattero, H. Zuegge, 2004. Cameras and

sensing systems, *ASPRS Manual of Photogrammetry, 5th Edition,* (McGlone, J.C., E. Mikhail, J. Bethel, Eds.), American Society for Photogrammetry and Remote Sensing, pp. 581-676.

Brown, D.C., 1966. Decentering distortions of lens, *Journal of Photogrammetric Engingeering and Remote Sensing*, 32(3): 444-462.

Brown, D.C., 1972. Calibration of close range cameras, Presented at the XII Congress of the International Society of Photogrammetric Engineering, Ottawa, Canada, July 23 through August 5, 1972, 25 p.

Brown, D.C., 1976. The bundle adjustment – progress and prospects, *International Archives of Photogrammetry*, Vol. 21, Invited Papers, Commission 3, 33 p.

Bruegge, C.J., D.J. Diner, R.A. Kahn, N. Chrien, M.C. Helmlinger, B.J. Gaitley, W.A. Abdou, 2007. The MISR radiometric calibration process, *Remote Sensing of Environment,* 107(2007): 2-11.

Büyüksalih, G., K. Jacobsen, 2006. Bundle block adjustment with UltraCamD images, *International Archives of Photogrammetry, Remote Sensing and Spatial Information Sciences*, 36(B1), unpaginated CD-ROM, 8 p.

Burman, H., 2000. Calibration and orientation of airborne image and laser scanner data using GPS and INS, *Fotogrammetriska Meddelanden, Photogrammetric Reports,* No 69, 111 p.

Casella, V., M. Franzini, 2005. Experiences in GPS/IMU calibration. Rigorous and independent cross-validation of results, *Proceedings of ISPRS Hannover Workshop 2005, High-Resolution Earth Imaging for Geospatial Information,* unpaginated CD-ROM, 6 p.

Chrien, N.L, C.J. Bruegge, B.J. Gaitley, 2001. AirMISR laboratory calibration and in-flight performance results, *Remote Sensing of Environment*, 77(2001): 328-337.

Clarke, T.A, J.F. Fryer, 1998. The development of camera calibration methods and models, *Photogrammetric Record*, 16(9): 51-66.

Cocks, T., R. Jensen, A. Stewart, I. Wilson, T. Shields. The HYMAP™ airborne hyperspectral sensor: the system, calibration and performance, *1st EARSEL Workshop on Imaging Spectroscopy, Zurich, October, 1998*, http://www.aigllc.com/pdf/EARSEL98_HyMap.pdf, (Last date accessed 29 April 2008), 6 p.

Cramer, M, 2001. Performance of GPS/Inertial solutions in photogrammetry, *Photogrammetric Week 2001, (Fritsch, D., R. Spiller, Eds.)*, Wichmann Verlag, pp. 29-62.

Cramer, M., 2004. EuroSDR network on Digital Camera Calibration, Report Phase I (Status Oct 26, 2004). http://www.ifp.uni-stuttgart.de/eurosdr/EuroSDR-Phase1-Report.pdf, (Last date accessed 29 April 2008), 54 p.

Cramer, M., 2005. Digital airborne cameras - Status and future, *Proceedings of ISPRS Hannover Workshop 2005: High-Resolution Earth Imaging for Geospatial Information*, unpaginated CD-ROM, 8 p.

Cramer, M., 2006. Calibration and validation of digital airborne cameras, *International Archives of Photogrammetry, Remote Sensing and Spatial Information Sciences*, 36(B1), unpaginated CD-ROM, 6 p.

Cramer, M., 2007a. European digital airborne camera certification – EuroDAC, www.eurosdr.net (Last date accessed 29 April 2008).

Cramer, M., 2007b. The EuroSDR performance test for digital aerial camera systems, *Photogrammetric Week 2007, (Fritsch, D., Ed.)*, Wichmann Verlag, pp. 107-116.

Dalsa, 2008. Dalsa Professional Imaging, http://www.dalsa.com/pi/index.asp (Last date accessed 29 April 2008).

Dianguirard, M., P.N. Slater, 1999. Calibration of space-multispectral imaging sensors: A Review, *Remote Sensing of Environment*, 68(3): 194-205.

Diener, S., M. Kiefner, C. Dörstel, 2000. Radiometric normalisation and colour composite generation of the DMC, *International Archives of Photogrammetry and Remote Sensing*, 33(B1): 82-88.

Dold, J., D. Flint, 2007. Leica Geosystems photogrammetric sensor and workflow developments, *Photogrammetric Week 2007,* (Fritsch D., Ed.), Wichmann Verlag, pp. 3-14.

Dörstel, C., K. Jacobsen, D. Stallmann, 2003. DMC – photogrammetric accuracy – calibration aspects and generation of synthetic DMC images, *Proceedings on Optical 3-D measurement techniques VI*, (Grün/Kahmen, Eds.), Zürich, Swizerland, pp. 74-82.

Dörstel, C., 2003. DMC – Practical experiences and photogrammetric system performance, *Photogrammetric Week 2003*, (Fritsch, D., Ed.), Wichmann Verlag, pp. 59-65.

Dörstel, C., 2007. DMC – (R)evolution on geometric accuracy, *Photogrammetric Week 2007*, (Fritsch, D., Ed.), Wichmann Verlag, pp. 81-88.

Ebner, H., 1972. Theoretical accuracy models for block triangulation, *BUL*, 40(5): 214-221.

Ebner, H., 1976. Self calibrating block adjustment, *International Archives of Photogrammetry*, Vol. 21, Invited Papers, Commission 3, 17 p.

Eckardt, A., B. Braunecker, R. Sandau, 2000. Performance of the imaging system in the LH Systems ADS40 airborne digital sensor, *International Archives of Photogrammetry, Remote Sensing and Spatial Information Sciences*, 33(B1): 104-109.

Eisenhart, C. (1963). Realistic evaluation of the precision and accuracy of instrument calibration systems, *Journal of Research, National Bureau of Standards*, 67C(2): 161-187.

EuroDAC, 2007. European airborne digital camera certification: http://www.ifp.uni-stuttgart.de/eurosdr/index.html (Last date accessed 29 April 2008)

Fiete, R.R., J.G. Baker, J.A. Lebaron, A.A. Magill, W.P. Tayman, K. Pestrecov, F.E. Washer, 2004. Elements of photogrammetric optics, *ASPRS Manual of Photogrammetry, 5th Edition,* (McGlone, J.C., E. Mikhail, J. Bethel, Eds.), American Society for Photogrammetry and Remote Sensing, pp. 317-398.

Fraser, C.S., 1997. Digital camera self-calibration, *ISPRS Journal of Photogrammetry & Remote Sensing*, 52 (1997): 149-159.

Fraser, C.S., 2001. Photogrammetric camera component calibration: A review of analytical techniques, *In: Calibration and Orientation of Cameras in Computer Vision, (*A. Gruen, T.S. Huang Eds.), Springler-Verlag Berlin, Heidelberg, pp. 95-121.

Fricker, P., R. Sandau, A.S. Walker, 1999. Digital photogrammetric cameras: possibilities and problems, *Photogrammetric Week 1999*, (Fritsch, D., R. Spiller, Eds.), Wichmann Verlag, pp. 71-82.

Fricker, P., A. Rohrbach, 2005. Pushbroom scanner provide highest resolution earth imaging information in multispectral bands, *Proceedings of the ISPRS Hannover Workshop, 17-20 May 2005*, unpaginated CD-ROM, 5 p.

Fricker, P., 2007. Raising the bar for the multi-band high-resolution airborne imagery, *Photogrammetric Week 2007,* (Fritsch, D., Ed.), Wichmann Verlag, pp.71-79.

Förstner, W., 1985. The reliability of block triangulation, *Photogrammetric Engineering & Remote Sensing,* 51(6): 1137-1149.

Förstner, W., 1995. Matching strategies for point transfer, *Photogrammetric Week 1995,* (Fritch, D., D. Hobbie, Eds.), Wichmann Verlag, pp. 173-183.

Förstner, W., B. Wrobel, 2004. Mathematical concepts of photogrammetry, *ASPRS Manual of Photogrammetry, 5th Edition,* (McGlone, J.C., E. Mikhail, J. Bethel, Eds.), American Society for Photogrammetry and Remote Sensing, pp. 15-180.

Förstner, W., B. Wrobel, F. Paderes, R. Craig, C. Fraser, J. Dolloff, 2004. Analytical photogrammetric operations, *ASPRS Manual of Photogrammetry, 5th Edition,* (McGlone, J.C., E. Mikhail, J. Bethel, Eds.), American Society for Photogrammetry and Remote Sensing, pp. 763-936.

Gonzalez, R.C., P. Wintz, 1987. *Digital image processing, 2nd Edition*, Addison-Wesley Publishing Company, 503 p.

Google Earth, 2008. http://earth.google.com/ (Last date accessed 29 April 2008).

Graham, R., A. Koh, 2002. *Digital aerial survey: theory and practice*, Whittles Publishing, Chaitness, 248 p.

Green, R.O., B. Pavri, 2001. AVIRIS Inflight calibration experiment measurements, analyses, and results in 2000, *AVIRIS Proceedings: 2001, JPL Publication 02-1* ftp://popo.jpl.nasa.gov/pub/docs/workshops/01_docs/2001Green_inflight_web.pdf (Last date accessed 29 April 2008), 14 p.

Gruber, M., R. Perko, M. Ponticelli, 2004. The all digital photogrammetric workflow: redundancy and robustness, *International Archives of Photogrammetry, Remote Sensing and Spatial Information Sciences*, 34(B1): 232-234.

Gruber, M., 2007. UltraCamX, the new digital aerial camera system by Microsoft photogrammetry, *Photogrammetric Week 2007,* (Fritsch, D., Ed.), Wichmann Verlag, pp. 137-145.

Grün, A., H.A. Beyer, 2001. System calibration through self-calibration, *Calibration and Orientation of Cameras in Computer Vision,* (Gruen, A., T.S. Huang, Eds.), Springler-Verlag Berlin, Heidelberg, pp. 164-193.

Hakkarainen, J., 1986. Resolving power of aerial photographs, *Surveying Science in Finland*, 1986, No. 2, pp. 8-59.

Hefele, J., 2006.Calibration experience with the DMC, *Proceedings of EuroSDR Commission I and ISPRS Working Group 1/3 Workshop EuroCOW*, 25-27 January 2006, unpaginated CD-ROM, 6 p.

Heier, H., 2001. Deploying DMC in today's workflow, *Photogrammetric Week 2001*, (Fritsch, D., R. Spiller, Eds.), Wichmann Verlag, pp. 35-45.

Heier, H., M. Kiefner, W. Zeitler, 2002. Calibration of Digital Modular Camera, *Proceedings of FIG XXII International Congress*, Washington D.C. USA, April 19-26.2002, unpaginated CD-ROM, 11 p.

Heipke, C., K. Eder, 1998. Performance of tie-point extraction in automatic aerial triangulation, *OEEPE official publication No. 35,* 185 p.

Heipke, C., K. Jacobsen, H. Wegmann, Ø. Andersen, B. Nilsen, 2002a. Test goals and test set up for the OEEPE test "Integrated sensor orientation", *OEEPE Official Publication* (Heipke, C., K. Jacobsen, H. Wegmann, Eds.), No. 43, pp. 11-18.

Heipke, C., K. Jacobsen, H. Wegmann, 2002b. Analysis of the Results of the OEEPE Test "Integrated Sensor Orientation", *OEEPE Official Publication* (Heipke, C., K. Jacobsen, H. Wegmann, Eds.), No. 43, pp. 31-49.

Hinz, A., 1997. Design concepts of digital phtogrammetric cameras, *Photogrammetric Week 1997,* (Fritsch, D., D. Hobbie, Eds.), Wichmann Verlag, pp. 43-48.

Hinz, A., 1999. The Z/I imaging aerial camera system, *Photogrammetric Week 1999*, (Fritsch, D., R. Spiller, Eds.), Wichmann Verlag, pp. 109-115.

Hinz A., C. Dörstel, H. Heier, 2000. Digital Modular Camera: System concept and data processing workflow, *International Archives of Photogrammetry and Remote Sensing*, 33(B2), unpaginated CD-ROM, 6 p.

Hinz, A., C. Dörstel, H. Heier, 2001. DMC – The digital sensor technology of Z/I-Imaging, *Photogrammetric Week 2001*, (Fritsch, D., R. Spiller, Eds.), Wichmann Verlag, pp. 93-103.

Honkavaara, E., 2000. Automatic tie point measurement: On properties of tie points, measurement methods and quality issues, Licentiate's Thesis. (92 pages)

Honkavaara, E., 2003. Calibration field structures for GPS/IMU/camera-system calibration, *The Photogrammetric Journal of Finland*, 18(2): 3-15.

Honkavaara, E., R. Ilves, J. Jaakkola, 2003. Practical results of GPS/IMU/Camera-system calibration, *Proceedings of International Workshop: Theory, Technology and Realities of Inertial/GPS Sensor Orientation*, Castelldefels, Spain, 22.-23.9.2003, unpaginated CD-ROM, 10 p.

Honkavaara, E., 2004. In-flight camera calibration for direct georeferencing. *International Archives of Photogrammetry, Remote Sensing and Spatial Information Sciences,* 35(B1): 166-171.

Honkavaara, E., L. Markelin, J. Marttinen, M. Vilander, 2004. External quality control of medium-scale orthophoto production – case Finnish Land Parcel Identification System. *The Nordic Journal of Surveying and Real Estate Research*, 1(2): 131-143.

Honkavaara, E., L. Markelin, R. Ilves, P. Savolainen, J. Vilhomaa, E. Ahokas, J. Jaakkola, H. Kaartinen, 2005. In-flight performance evaluation of digital photogrammetric sensors, *Proceedings of ISPRS Hannover Workshop 2005: High-Resolution Earth Imaging for Geospatial Information,* unpaginated CD-ROM, 6 p.

Honkavaara, E., J. Jaakkola, L. Markelin, J. Peltoniemi, E. Ahokas, S. Becker, 2006. Complete photogrammetric system calibration and evaluation in the Sjökulla test field – case study with DMC, *Proceedings of EuroSDR Commission I and ISPRS Working Group 1/3 Workshop EuroCOW 2006*, unpaginated CD-ROM, 6 p.

ISO 12233:1999. Photography. Electronic still-picture cameras. Resolution measurements.

Jaakkola, J., T. Sarjakoski, 1996. Experimental test on digital aerial triangulation, *OEEPE official publication*, No. 31, 155 p.

Jaakkola, M., W. Brindöpke, O. Kölbl, P. Noukka, 1985. Optimal emulsions for large-scale mapping - test of "Steinwedel" - Commission C of the OEEPE 1981-84, *OEEPE official publication,* No. 15, 102 p.

Janza, F.J, H.M. Blue, J.E. Johnston, 1975. *Manual of remote sensing, Volume 1, Theory, instruments and techniques, 1st Edition*, American Society of Photogrammetry, Falls Church, 867 p.

Kilpelä, E., 1981. Compensation of systematic errors of image and model coordinates, *Photogrammetria*, 37: 15-44.

Kocaman, S., V. Casella, M. Franzini, A. Gruen, 2007. The triangulation accuracy of ADS40 imagery over the Pavia testsite, *Proceedings of the 2007 Conference of the Remote Sensing and Photogrammetry Society*, Newcastle upon Tyne, 11-14 September, 2007, unpaginated CD-ROM, 6 p.

Kraus, K., 1993. *Photogrammetry, Volume 1: Fundamentals and standard processes, 4th Edition*, Dümmler, Bonn, 398 p.

Kraus, K., 1997. *Photogrammetry, Volume 2: Advanced methods and applications*, Dümmler, Bonn, 466 p.

Kröpfl, M., E. Kruck, M. Gruber, 2004. Geometric calibration of the digital large format camera UltraCamD, *International Archives of Photogrammetry, Remote Sensing and Spatial Information Sciences*, 34(B1): 42-44.

Kruck, E., 2006. Simultaneous calibration of digital aerial survey cameras, *Proceedings of EuroSDR Commission I and ISPRS Working Group 1/3 Workshop EuroCOW 2006*, unpaginated CD-ROM, 7 p.

Kuittinen, R., E. Ahokas, A. Högholen, J. Laaksonen, 1994. Test-field for aerial photography, *The Photogrammetric Journal of Finland*, 14(1): 53-62.

Kuittinen R., E. Ahokas, P. Järvelin, 1996. Transportable test-bar targets and microdensitometer measurements: A method to control the quality of aerial imagery, *International Archives of Photogrammetry and Remote Sensing*, 31(1): 99-104.

Kupfer, G., 1975. Improvement of analytical aerial triangulation by field calibration, Presented at the Conference of the Working Group on Image Geometry, Comm. I, ISP, Ottawa, 1975, pp. 51-67.

Kölbl, O., 2005. Transfer functions in image data collection, *Photogrammetric Week 2005,* (Fritsch, D., Ed.), Wichmann Verlag, pp. 93-104.

Leachtenauer, J.C., W. Malila, J.M. Irvine, L.P. Colburn, N.L. Salvaggio, 1997. General image-quality equation: GIQE, *Applied Optics*, 36(32): 8322-8328.

Leberl, F., M. Gruber, 2003. Flying the new large format digital aerial camera Ultracam, *Photogrammetric Week 2003,* (Fritsch, D., Ed.), Wichmann Verlag, pp. 67-76.

Leberl, F., M. Gruber, 2005. UltraCamD: Understanding some noteworthy capabilities, *Photogrammetric Week 2005,* (Fritsch, D., Ed.), Wichmann Verlag, pp. 57-68.

Leica Geosystems, 2008. http://www.leica-geosystems.com/corporate/en/ndef/lgs_57608.htm (Last date accessed 29 April 2008)

Light, D., 1992. The new camera calibration system at the U.S. Geological Survey, *Photogrammetric Engineering & Remote Sensing,* 58(2): 185-188.

Lillesand, T., R. Kiefer, 2000. *Remote sensing and image interpretation – 4th Edition,* John Wiley & Sons, Inc., 724 p.

Livingston, R.G., C.E.Berndsen, R. Ondrejka, R.M. Spriggs, L.J. Kosofsky, D. Van Steenbrugh, C. Norton, D. Brown, 1980. Aerial cameras, *Manual of Photogrammetry, 4th Edition*, (Slama, C.C., C. Theurer, S.W. Henriksen, Eds.), American Society of Photogrammetry, Falls Church, pp. 232-277.

Lowe, D.S, B. Kelly, H.I. McDevitt, G.T. Orr, H.W. Yates, 1975. Imaging and nonimaging sensors, *Manual of Remote Sensing*, *Volume 1, Theory, instruments and techniques, 1st Edition*, (Janza, F.J, H.M. Blue, J.E. Johnston, Eds.), American Society of Photogrammetry, Falls Church, pp. 367-397.

Markelin, L., E.Ahokas, E. Honkavaara, A. Kukko, J. Peltoniemi, 2005. Radiometric quality comparison of UltraCamD and analog camera, *Proceedings of ISPRS Hannover Workshop 2005: High-Resolution Earth Imaging for Geospatial Information*, unpaginated CD-ROM, 6 p.

Markelin, L., E. Honkavaara, J. Peltoniemi, J. Suomalainen, E. Ahokas, 2006. Radiometric evaluation of digital aerial cameras, *International Archives of Photogrammetry, Remote Sensing and Spatial Information Sciences*, 36 (B1), unpaginated CD-ROM, 6 p.

Martínez L., V. Palà, R. Arbiol, F. Pérez, 2007. Digital Metric Camera radiometric and colorimetric calibration with simultaneous CASI imagery to a CIE Standard Observer based colour space, *IEEE International Geoscience and Remote Sensing Symposium,* Barcelona, 23-27 July 2007, 4 p.

Meier, H.K., 1975. The effects of environmental conditions on distortion, calibrated focal length and focus of aerial survey camera, Presented at the Conference of Working Group on Image Geometry, Comm. I, ISP, Ottawa, 1975, 10 p.

Merchant, D.C., 1974. Calibration of the air photo system, *Photogrammetric Engineering & Remote Sensing*, 40(5): 605-617.

Merchant, D.C., R.L. Tudhope, 1989. Aerial photo systrem calibration over flat terrain, *Photogrammetric Engineering & Remote Sensing*, 55(12): 1755-1763.

Merchant, D.C, A. Schenk, A. Habib, T. Yoon, 2004. USGS/OSU progress with digital camera in situ calibration methods, *International Archives of Photogrammetry and Remote Sensing*, 35(2): 19-24.

Microsoft VirtualEarth, 2008. http://www.microsoft.com/virtualearth/ (Last date accessed 29 April 2008).

Mikhail, E.M., 1976, *Observations and Least-squares*, Thomas Y. Crowell, New York, 497 p.

Mikhail, E., J.S. Bethel, J.C. McGlone, 2001. *Introduction to modern photogrammetry*, John Wiley & Sons Inc., 479 p.

Morain A.S., M.V. Zanoni, 2004. Joint Isprs/Ceos-Wgcv task force on radiometric and geometric calibration, *International Archives of Photogrammetry and Remote Sensing*, 35(1): 354-360.

Moran, M.S., B.B. Ross, T.R. Clarke, J. Qi, 2001. Deployment and calibration of reference reflectance tarps for use with airborne imaging sensors, *Photogrammetric Engineering & Remote Sensing,* 67(3): 273-286.

Mostafa, M.M.R, J. Hutton, 2005. A fully integrated solution for aerial surveys; design, development and performance analysis, *Photogrammetric Engineering & Remote Sensing*, 71(4): 391-398.

Mugnier, C., W. Förstner, B. Wrobel, F. Paderes, R. Munjy, 2004. Mathematics of photogrammetry, *ASPRS Manual of Photogrammetry, 5th Edition,* (McGlone, J.C., E. Mikhail, J. Bethel, Eds.), American Society for Photogrammetry and Remote Sensing, pp. 181-316.

Nilsen, B. Jr, 2002a. Test field Fredrikstad and data acquisition for the OEEPE test "Integrated Sensor Orientation", Integrated Sensor Orientation – Test Report and Workshop Proceedings, *OEEPE Official Publication* (Heipke, C., K. Jacobsen, H. Wegmann, Eds.), No. 43, pp. 19-30.

Nilsen, B. Jr., 2002b. Can map compilation rely on GPS/INS alone? Integrated Sensor Orientation – Test Report and Workshop Proceedings, *OEEPE Official Publication* (Heipke, C., K. Jacobsen, H. Wegmann, Eds), No. 43, pp. 229-260.

Pacey, R.E., M. Scheidt, A.S Walker, 1999. Calibration of analogue and digital airborne sensors at LH Systems, *Proceedings of the 1999 ASPRS Annual Conference*, Portland, Oregon, pp. 950-956.

Pacey, R., P. Fricker, 2005. Forward motion compensation (FMC) – Is it the same in the digital imaging world, *Photogrammetric Engineering & Remote Sensing*, 71(11): 1241-1242.

Pagnutti, M., K. Holekamp, R. Ryan, S. Blonski, R. Sellers, B. Davis, V. Zanoni, 2002. Measurement sets and sites commonly used for characterizations, *International Archives of Photogrammetry and Remote Sensing*, 34(1), unpaginated CD-ROM, 6 p.

Pagnutti, M., R.E. Ryan, M. Kelly, K. Holekamp, V. Zanoni, K. Thome, S. Schiller, 2003. Radiometric Characterization of IKONOS multispectral imagery, *Remote Sensing of Environment*, 88(1): 53-68.

Paparoditis, N., J.P. Souchon, G. Martinoty, M. Pierrot-Deseilligny, 2006. High-end aerial digital cameras an their impact on the automation and quality of the production environment, *ISPRS Journal of Photogrammetry & Remote Sensing*, 60(6): 400-412.

Pellikka, P., 1998. Development of correction chain for multispectral airborne video data for natural resource assessment, *Fennia*, 176: 1, 110 p.

Peltoniemi, J.I., J. Piiroinen, J. Näränen, J. Suomalainen, R. Kuittinen, L. Markelin, E. Honkavaara, 2007. Bidirectional reflectance spectrometry of gravel at the Sjökulla test field, *ISPRS Journal of Photogrammetry & Remote Sensing*, 62(6): 434-446.

Perko, R., A. Klaus, M. Gruber, 2004. Quality comparison of digital and film-based images for photogrammetric purposes, *International Archives of Photogrammetry, Remote Sensing and Spatial Information Sciences*, 35(B1): 1136-1140.

Petrie, G. 2003. Airborne digital frame cameras, *Geoinformatics,* 7(6): 18-27.

Petrie, G. 2005. Airborne pushbroom line scanners, *Geoinformatics* 8(1): 50-57.

Petrie, G., 2006. Further advances in airborne digital imaging, *Geoinformatics*, 9(5): 16-23.

Pindyck, R.S., D.L. Rubinfeld, 1991. *Econometric Models and Economic Forecasts*, McGraw-Hill International Editions, 596 p.

Read, R.E., R.W. Graham, 2002. *Manual of Air Survey: Primary Data Acquisition*, Whittles Publishing, Caithness, 408 p.

Remodino, F., C. Fraser, 2006. Digital camera calibration methods: considerations and comparisons, *International Archives of Photogrammetry, Remote Sensing and Spatial Information Sciences*, 36(A5): 266-272.

Reulke, R., K-H. Franke, P. Fricker, T. Pomierski, R. Sandau, M. Schoenermark, C. Tornow, L. Wiest, 2000. Target Related Multispectral and True Color Optimization of the Color Channels of the LH Systems ADS40, *International Archives of Photogrammetry and Remote Sensing*, 33(B1): 244-250.

Reulke, R., S. Becker, N. Haala, U. Tempelmann, 2006. Determination and improvement of spatial resolution of the CCD-line-scanner system ADS40, *ISPRS Journal of Photogrammetry & Remote Sensing,* 60(2): 81-90.

Rosengarten, H., 2007. Intergraph's PhoWo Message, *Photogrammetric Week 2007,* (Fritsch, D., Ed.), Wichmann Verlag, pp. 19-25.

Ryan, R., B. Baldridge, R.A. Schowengerdt, T. Choi, D.L. Helder, S. Blonski, 2003. IKONOS spatial resolution and image interpretability characterization, *Remote Sensing of Environment*, 88(1): 37-52.

Salamonowicz, 1982. USGS aerial resolution targets, *Photogrammetric Engineering & Remote Sensing*, 48(9): 1469-1473.

Salmenperä, H., 1972. Camera calibration using a test field, *Photogrammetric Journal of Finland*, 6(1): 12-23.

Sandau, R., B. Braunecker, H. Driescher, A. Eckardt, S. Hilbert, J. Hutton, W. Kirchhofer, E. Lithopoulos, R. Reulke, S. Wicki, 2000. Design principles of the LH Systems ADS40 Airborne Digital Sensor, *International Archives of Photogrammetry and Remote Sensing*, 33(1): 258-265.

Schowengerdt, R.A., 1997. *Remote Sensing, models and methods for image processing*, *2nd Edition*, Academmic Press, Orlando, Florida, 522 p.

Schuster, R., B. Braunecker, 2000. Calibration of the LH Systems ADS40 airborne digital sensor, *International Archives of Photogrammetry and Remote Sensing*, 33(1): 288-294.

Schwarz, K.P, M.A. Chapman, M.W. Cannon, P. Gong, 1993. An integrated INS/GPS approach to the georeferencing of remotely sensed data, *Photogrammetric Engineering & Remote Sensing,* 59(11):1667-1674.

Shortis, M.R., S. Robson, 1998. Principal point behaviour and calibration parameter models for Kodak DCS cameras, *Photogrammetric Record,* 16(92): 165-186.

Slama, C.C, C. Theurer, S.W. Henriksen, 1980. *Manual of photogrammetry*, American Society of Photogrammetry, Falls Church, 1056 p.

Slater, P.N., 1975. Photographic systems for remote sensing, *ASPRS Manual of Remote Sensing,Volume 1, Theory, instruments and techniques, 1st Edition*, (Janza, F.J, H.M. Blue, J.E. Johnston, Eds.), pp. 235-323.

Souchon, J.-P., N. Paparoditis, O. Martin, C. Meynard, C. Thom, 2006. Is there an ideal digital aerial camera? *International Archives of Photogrammetry, Remote Sensing and Spatial Information Sciences*, 36(A1), unpaginated CD-ROM, 6 p.

Spiller, R.H., 1999. Z/I Imaging: A new system provider for photogrammetry and GIS, *Photogrammetric Week 1999,* (Fritch,. D., R. Spiller, Eds.), Wichmann Verlag, pp. 35-42.

Spreckels, V., A. Schlienkamp, K. Jacobsen, 2007. Model deformation – accuracy of digital frame cameras, *Proceedings of the ISPRS Hannover Workshop 2007: High-Resolution Earth Imaging for Geospatial Imaging*, unpaginated CD-ROM, 9 p.

Stensaas, G.L., 2007. U.S. Geological survey digital aerial mapping camera certification and quality assurance plan for digital imagery, *Photogrammetric Week 2007,* (Fritsch, D., Ed.), Wichmann Verlag, pp. 107-116.

Tang, L., Dörstel, C., Jacobsen, K., Heipke, C., Hinz, A., 2000. Geometric accuracy potential of the Digital Modular Camera, *International Archives of Photogrammetry and Remote Sensing*, 33(B4/3): 1051-1057.

Tayman, W.P., 1984. User guide for the USGS aerial camera report of calibration, *Photogrammetric Engineering & Remote Sensing*, 50(5): 577-584.

Tempelmann, U., A. Börner, B. Chaplin, L. Hinsken, B. Mykhalevych, S. Miller, U. Recke, R. Reulke, R. Uebbing, 2000. Photogrammetric software for the LH Systems ADS40 airborne digital sensor, *International Archives of Photogrammetry and Remote Sensing*, 33(B2): 553-559.

Tempelmann, U., L. Hinsken, U. Recke, 2003. ADS40 calibration & verification process, *Proceedings of International Workshop: Theory, Technology and Realities of Inertial/GPS Sesor Orientation*, Castelldefels, Spain, 22-23.9.2003, unpaginated CD-ROM, 6 p.

Thompson, M.M., H. Gruner, 1980. Foundations of photogrammetry, *Manual of Photogrammetry, 4th Edition*, (Slama, C.C., C. Theurer, S.W. Henriksen, Eds.), American Society of Photogrammetry, pp. 1-36.

Thomson, G.H., 2004. Analytical methods of assessing the image quality associated with digital and photographic imaging systems, *The Photogrammetric Record*, 19(107): 237-249.

Torlegård, K., 1989. Theory of image coordinate errors. *Non-topographic photogrammetry* (Karara, H.M., Ed.), Published by American Society for Photogrammetry and Remote Sensing, pp. 81-93.

Tölg, T., 2007. Newest technologies for compact digital aerial surevey cameras, *Photogrammetric Week 2007,* (Fritsch, D., Ed.), Wichmann Verlag, pp. 131-136.

UltraCamD, 2004. UltraCamD calibration report, UCD-SU-1-0005, Dec-01-2004, 57 p.

USGS, 2008. USGS digital aerial imaging quality assurance web-site. http://calval.cr.usgs.gov/digital_aerial_imaging_quality_assurance.php (Last date accessed 29 April 2008)

Vane, G., R.O. Green, T.G. Chrien, H.T. Enmark, E.G. Hansen, W.M. Porter, 1993. The airborne visible/infrared imaging Spectrometer (AVIRIS), *Remote Sensong of Environment*, 44(1993): 127-143.

Waldhäusl, P., 1986. Results of the Vienna Test of OEEPE Commission C*, OEEPE official publication No. 16,* 57 p.

Wegmann, H., K. Jacobsen, 2002. Image Orientation by Combined (A)AT with GPS and IMU, *International Archives of Photogrammetry, Remote Sensing and Spatial Information Sciences*, 34(B1): 279-284.

Wolf, P.R., B.A. Dewitt, 2000. *Elements of photogrammetry: with applications in GIS, 3rd Edition*, McGraw-Hill, 608 p.

Worton, F.J., 1977. Airborne camera environment, *Photogrammetric Record*, 9(50): 279-286.

Zebedin, L., A. Klaus, B. Gruber-Geymayer, K. Karner, 2006. Towards 3D map generation from digital aerial images, *ISPRS Journal of Photogrammetry & Remote Sensing*, 60(6): 413-427.

Appendix 1. Uniformity of permanent gravel targets

The uniformity of the permanent gravel targets with gravel diameter 8-16 mm (Figure A1-1) was analyzed by calculating standard deviations of DNs in images in image windows corresponding approximately 3 m x 3 m area in the object space. The image windows were selected interactively at the center of the targets. The white gravel was not evaluated because of clear degradation (**I**). Measurements were made on raw panchromatic and multispectral DMC images collected from 500 m and 800 m flying altitudes in 2005. From both flights three images were used where the targets were located close to image center. The targets had been in the field for 12 years practically without any maintenance.

The average standard deviations are shown in Figure A1-2. They were approximately 7%, 5%, and 2.5%, for the panchromatic images with GSDs 5 cm, 8 cm, and 25 cm, respectively. The average standard deviations were approximately 3.2% and 2.5% for the multispectral images with 22 cm and 38 cm GSD, respectively.

An accurate reflectance reference value can be obtained by using an average value calculated in a sufficiently large object space window, because the accuracy of the average value is inversely proportional to the square root of the number of observations (Eisenhart, 1963). The target size should be selected so that it consists of a sufficient number of data pixels, at least ("*standard deviation of object*"/"*desired standard deviation*")^2 and a border area which is disturbed by the point spread of the neighboring objects.

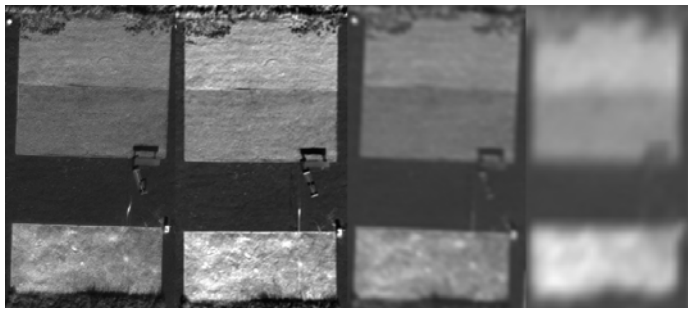

Figure A1-1. Permanent reflectance reference targets. Form top to down: gray, red, black, and white. GSDs from left to rigt: 4 cm, 8 cm, 25 cm, and 50 cm (panchromatic images).

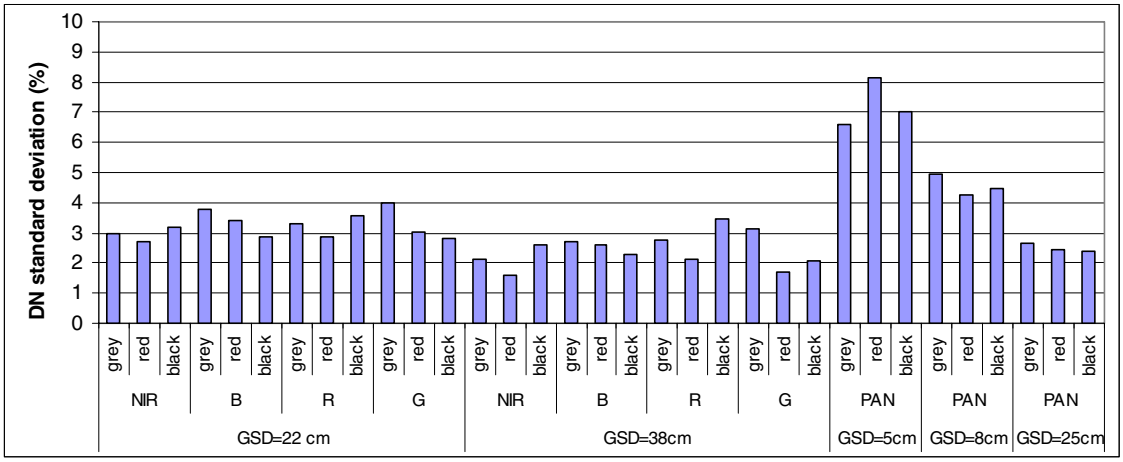

Figure A1-2. DN standard deviations of gray, red, and black gravel on images as % of DN.

Appendix 2. Accuracy of MTF determination

The precision of the MTF determination was assessed by calculating $\hat{\sigma}_0$ of the adjustment; statistics are given in Table A2-1. It appeared that $\hat{\sigma}_0$ was higher in the cross-flight direction (cf) than in the flight direction (f). The likely reason for this is the quality of the individual sectors (Figure A2-1). The sector pair indicated by cf is disturbed more by the nonuniformity of the target than the sector pair indicated by f. More non-uniform sectors were used for the MTF estimation in the cross-flight direction than in the flight direction, because most of the image strips were flown in north-south or south-north direction. The variability caused by target is visible in the MTF observations shown in Figure A2-2. However, because the maximum $\hat{\sigma}_0$ was 3.5% of the MTF and RMSEs were below 3%, the target non-uniformity should not seriously influence the analysis.

Table A2-1. RMSEs, minimums, maximums, and standard deviations of $\hat{\sigma}_0$ of the MTF adjustment in [%] of the MTF for the cross-flight direction (cf) and flight direction (f). N is the number of observations.

Block	N	cf				f			
		RMSE	MIN	MAX	σ_{RMSE}	RMSE	MIN	MAX	σ_{RMSE}
d1_g5	12	2.6	1.7	3.4	0.6	1.9	1.4	2.6	0.3
d1_g8a	19	2.6	1.3	3.1	0.4	2.0	0.9	3.2	0.7
d1_g8b	12	2.8	2.1	3.5	0.5	2.3	1.6	3.2	0.5

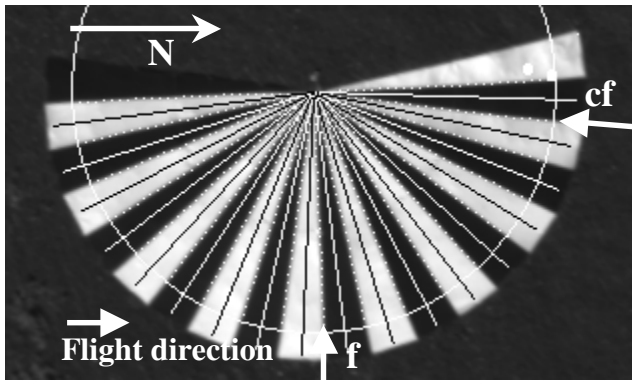

Figure A2-1. Spatial resolution evaluation from a Siemens star (image 2002) (f: resolution in flight direction, cf: resolution in cross flight direction).

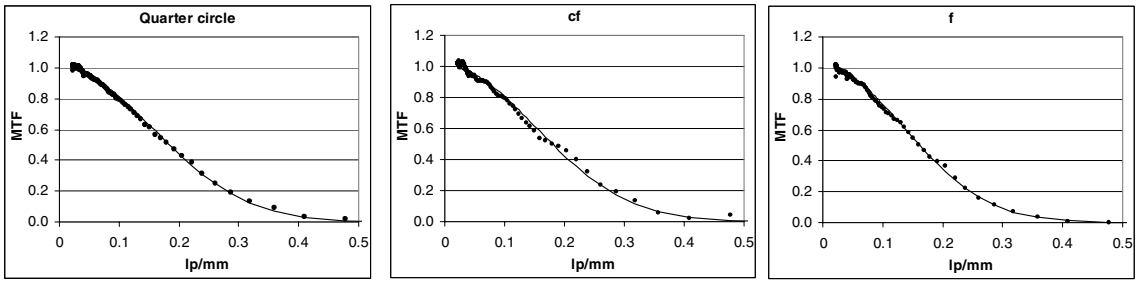

Figure A2-2. MTF adjustment to the observations (image 2002). The line shows the adjusted MTF and the dots show the scaled MTF observations. From left to right: quarter circle, cross-flight direction, and flight direction (**IV**).